ÉCOLE DE TECHNOLOGIE SUPÉRIEURE
UNIVERSITÉ DU QUÉBEC

MEMORANDUM PRESENTED TO
ÉCOLE DE TECHNOLOGIE SUPÉRIEURE

IN PARTIAL FULFILMENT
OF THE REQUIREMENTS FOR A MASTER'S DEGREE
IN MECHANICAL ENGINEERING
M.Eng.

BY
Antoine MOREAU

IMPLEMENTATION AND VALIDATION OF A METHOD FOR COMPUTING THE
INDUCED DRAG OF MULTIPLE LIFTING SURFACES AIRCRAFTS

MONTREAL, AUGUST 9 2011

ACKNOWLEDGMENT

IMPLEMENTATION AND VALIDATION OF A METHOD FOR COMPUTING THE INDUCED DRAG OF MULTIPLE LIFTING SURFACES AIRCRAFTS

Antoine MOREAU

ABSTRACT

The objective of this research is to implement and validate a method to compute the induced drag of multiple lifting surfaces aircraft configurations. The lifting line theory serves as a fundamental basis to calculate the induced drag. It was used by Laurendeau to develop a methodology to solve for the minimum induced drag lift distribution of three lifting surfaces aircrafts; equations that were used as a starting point for this work. Implementation is made such that non-planar wing and user-defined spanload distributions could be analyzed. A curve-fitting methodology is developed to adapt mathematics to the input spanload distribution, and a correction is applied to the induced drag results so that the lift over the fuselage is taken into account. Minimum induced drag lift distribution is also obtained as per Laurendeau's methodology. Results for wing-body-winglet configurations show good concordance with computational fluid dynamics (CFD) with a precision of more or less two drag counts. This shows that a lifting line approach, once corrected for the fuselage effect and dihedral, can provide accurate induced drag results. However, due to the absence of proper comparative data for two and three lifting surfaces aircraft configurations, an in-depth validation remains to be done for such aircraft designs. To do so, an approach to obtain the Oswald efficiency factor from Euler CFD results is proposed.

TABLE OF CONTENT

LIST OF FIGURES

Page

LIST OF ABBREVIATIONS AND ACRONYMS

6-DOF	Six Degrees-of-Freedom
ASW	Aft-Swept Wing
CFD	Computational Fluid Dynamics
c.g.	Center of Gravity
ESDU	Engineering Sciences Data Unit
FANSC	Full Aircraft Navier-Stokes code
FEM	Finite Element Method
FSW	Forward-Swept Wing
LLT	Lifting-Line Theory
MDO	Multi-Disciplinary Optimization
NL-LLT	Non-Linear Lifting-Line Theory
Spanload	Spanwise distribution of lift

LIST OF SYMBOLS AND UNITS

AoA Angle of Attack (degrees)

b Span of a Wing (adimensional)

CD Drag Coefficient (Drag Counts)

CDi Induced Drag Coefficient (Drag Counts)

CDo Zero-Lift Drag Coefficient (Drag Counts)

CDp Pressure Drag Coefficient (Drag Counts)

CL Lift Coefficient (adimensional)

D Drag Force (N)

e Oswald Efficiency Factor (adimensional)

h Stagger Distance Between Wings (adimensional)

L Lift Force (N)

η Adimensional Spanwise Coordinate (adimensional)

q Dynamic Pressure (psi)

σ Prandtl's Interference Factor (adimensional)

σ^* Kroo and Laurendeau's Interference Factor (adimensional)

y Bottock Line of the wing in *.spanload file (inches)

z Height of the wing in *.spanload file (inches)

INTRODUCTION

The quest for fuel efficient aircraft has led many researchers to orient their work on weight and drag reduction. As of today, the aerospace industry is likely to be reaching a state of maturation (ref. 51 to 54, ref. 74), which brings the problem of fuel consumption to the front line. Airliners have already started to adopt radical cost-cutting strategies to maintain their market position. While some investigations focus mainly on the potential gain of changing the aircraft configuration, lift will always remain a requirement to keep a fixed-wing aircraft in the air. Therefore, the lift-induced drag is a physical constraint in the design that engineers will have to deal with, since it can be minimized but not eliminated, no matter what the aircraft configuration is.

In 1921, the German engineer Ludwig Prandtl published the so called "*Prandtl Lifting-Line Theory*" (ref. 89) which linked the spanwise lift distribution of a finite wing to its respective induced drag. The fundamentals of this theory served as foundation for scientific research throughout the decades, leading to a large pool of works and publications on the subject. Using Prandtl's fundamental concepts, Kroo (ref. 32) developed a methodology to solve for the minimum induced drag spanloading of a 2 lifting surfaces system. This methodology was later extended by Laurendeau (ref. 108) for application on 3 lifting surfaces configurations.

Research Objectives and Limitations

In this present work, Laurendeau's equations (ref. 108) for the induced drag of a 3 lifting surfaces system serve as a starting point for the research. The objective of this work consists in computing the induced drag of an aircraft by implementing the latest method into a computer program, to adapt it so that a non-planar wing may be analyzed (while remain ing conscious that the solution is computed using a planar theory), to implement a correction to the resulting drag value so that the lift generated by the fuselage is taken into account and to validate the results with various literature and computational fluid dynamics (CFD) results.

Although a lot of research was made on the relative performances of 1, 2 and 3 lifting surfaces configurations, it is not in the scope of this work to evaluate the aerodynamic potential of such designs, as the primary objective remains a validation exercise of the theory and results. However, it was considered relevant to make a literature survey of the conclusions obtained by various authors.

Methodology

This research was performed in collaboration with Bombardier Aerospace's Advanced Aerodynamics department. Their support in knowledge and validation tools was essential for the progression of this work, which followed the following steps:

1. A literature survey on the induced drag of multiple lifting surfaces aircrafts configurations and on the evolution of the computation of spanwise lift distribution;
2. A detailed review of the theory used throughout this work;
3. A description of the implementation of the theory into a computer program;
4. A validation of the induced drag results by comparing with CFD and literature;
5. A discussion on the accuracy and limitations of the method;
6. Conclusions and recommendations.

Before starting to implement Laurendeau's method into a computer program, an investigation was performed to evaluate the robustness of the equations developed in his work (ref. 108). This was done in order to make sure that no mathematical or typographical errors could have slipped through correction.

The theory was implemented into a Matlab computer program called "LLT" and was first validated by comparing the drag results with a Bombardier in-house Multhopp (ref. 114) and non-linear vortex sheet (ref. 19) code named "CDI". It was later compared to Euler and Navier-Stokes CFD solutions obtained from a Bombardier's in-house code named "FANSC"

(ref. 83). Results show good concordance between theory and CFD, with an error of ±2 drag counts (1 count : Cd = .0001) for a single wing with dihedral, winglets and fuselage.

For multiple lifting surfaces configurations, LLT results were not validated since a robust source of comparison was not available. However, an investigation was performed about the validity of the minimum induced drag spanload for conventional two lifting surfaces configurations. Results have shown a good similitude with Iglesias and Mason's results (ref. 109) for minimum induced drag lift distribution. However, on a real production aircraft, the lift distribution tends to have a more triangular shape than the minimum drag spanload. The reasons for this situation are clarified in this work.

CHAPITRE 1

REVIEW OF THE LITTERATURE

1.1 Past Research on Multiple Lifting Surfaces Aircraft Configurations

A significant amount of research has been done on the induced drag and performances of one, two or three lifting surfaces aircrafts. The Wright Brothers started it all over 110 years ago; exercising what is now seen by some as a remarkable prescience: they put the pitch control surface of their aircraft at the front! One can suppose that to them, it would have seemed illogical when flying close to the ground to move part of the airplane down to make the rest of it move up. Where they right? Burns discusses the origin and resurrection of aircrafts with foreplanes in reference (ref. 71). However, at that time, Prandtl's Lifting line theory (ref. 89) and Munk's Biplane theory (ref. 100) were not yet available for the Wright brothers to understand completely the mutual interference in downwash velocities that occurs between two lifting surfaces. In his work, Munk explains how, when multiple lifting surfaces are located relatively close one to each other, the downwash induced by each surface affects all the other surfaces nearby. Using Munk's approach, Prandtl developed the equations for the induced drag of multiplanes. The developments of both Munk and Prandtl's equations are described in the "Theory" chapter of this work.

In 1978, Laitone (ref. 33) published a work in which he used Prandtl and Munk's theories to show that the minimum induced drag of a classical tail-aft aircraft was obtained when the lift on the tail was slightly positive. Such results were confirmed by Laurendeau (ref. 108). However, a trimmed aircraft using such concept would inherit a negative longitudinal stability. What is interesting in this conclusion is that it is actually possible for a designer to reduce the induced drag of a multiple lifting surfaces aircraft by properly distributing the lift on multiple wings. Starting from this concept, several authors started publishing results about the induced drag of multiplanes. Which configuration is the best? Canard? Tail-aft? Three surfaces? Summarizing all the available literature on this subject would represent an

exhaustive work and could constitute an entire thesis in itself. Nevertheless, I deemed appropriate to introduce the subject by a rapid overview of some results.

In reference (ref. 27), Kendall shows that a three-surfaces configuration can attain the minimum induced drag flight condition over a practical range of c.g. location while conserving a positive static stability, which confers this type of aircrafts a 10% higher cruise efficiency than a conventional tail-aft configuration. He also concludes that the pure canard is unstable at minimum induced drag center of gravity (c.g.) location. To attain stable flight conditions, the surface lift required to trim a canard configuration is more penalizing than on the tail-aft configuration.

However, Butler indicates a trend in (ref. 66) showing that for some applications where varying static stability is considered, the induced drag difference between three surfaces, tail-aft and canard may not be as significant as theory seems to indicate. These results are summarized in (ref. 30) by Kendall, which discusses this aspect more completely and concludes that a stable three-surfaces configuration can reach a potential induced drag saving up to 7% relative to a tail-aft design, and 15% relative to a stable canard. He also shows that a three-lifting-surfaces airplane configuration can fly at the minimum induced drag condition with varying c.g. location and be inherently stable, but that wind-tunnel tests were required to verify the theory.

Such tests were conducted one year later by Ostowari (ref. 20) on a Learjet-like model using tail-aft, canard and 3 lifting surfaces configurations in transonic flight conditions. He concluded that 3 surfaces have better lift and high-lift drag characteristics, but higher cruise drag. The induced drag in cruise flight is the highest for the canard and lowest for the tail-aft. He also states that a smaller stagger between the canard and the wing leads to better aerodynamics and stability characteristics, and a decrease in span of the canard surface gives better cruise drag and longitudinal stability characteristics. One could keep on going like this for dozens of pages but I consider more important in this study to state certain conceptual advantages of the three lifting surfaces configuration.

A true advantage of canard or three surfaces configurations is only revealed if the wing can be moved aft far enough so that it doesn't have to pass over or under the passenger's cabin. This gives an interesting option to the designers: to select a wing height more centered on the fuselage, allowing the main spar to go straight through the body. Such median wing allows for a reduction of the weight and drag of the wing-body junction and reinforces the rear pressure bulkhead. Depending of the aircraft configuration, it may also offer the opportunity to relocate the engines from the pylons to the wings, allowing for more weight savings. Another design option of a median wing is that the main landing gear can retract into the fuselage without the need for a belly fearing. The Piaggio P-180 Avanti is a good example of the use of multiple lifting surfaces to seek various design advantages. Reference (ref. 11) is a good source of information about the design of this aircraft.

Figure 1.1 Piaggio P-180 Avanti
Taken from « X-Plane » open source flight simulator

Other advantages of the canard and three lifting surfaces configurations have been found in the review of the literature:

1. A 3 surfaces configuration can set or change its static margin at any time by changing the ratio of the lift between the canard and the stabilizer. Therefore, the CG position can change significantly during the flight without influencing aircraft's behavior;

2. A 3 surfaces configuration can maintain minimum induced drag for all the duration of the flight;

3. On a canard aircraft, the canard can be designed to stall before the main wing, which greatly smoothes the stalls, or even prevents the main wing from stalling.

1.2   History of Spanload

The circulation theory of lift was one of the two major developments that energized theoretical aerodynamics at the beginning of the twentieth century. The second one being the development of the boundary layer concept around 1903 by Ludwing Prandtl, which allows calculation of the viscous drag. This same scientist published in 1921 (ref. 89) the so called "*Prandtl Lifting-Line Theory*", which is a by-product of the circulation theory. This new model linked together the spanwise distribution of lift (spanload) and the induced drag of a finite wing. Throughout the ages, various scientists and practicing aerodynamicists have articulated their work around this method to improve aircraft performances, as it is still used in today's industry. The following chapter underlines a few of the major breakthroughs that emerged from the development of this fundamental approach, as it is also the source of the theory used in this work.

In his work, Prandtl obtained a general solution to calculate the induced drag of a finite wing. He concluded that an elliptical spanload would minimize lift-induced drag. The following figures were taken from his report.

(a)   (b)
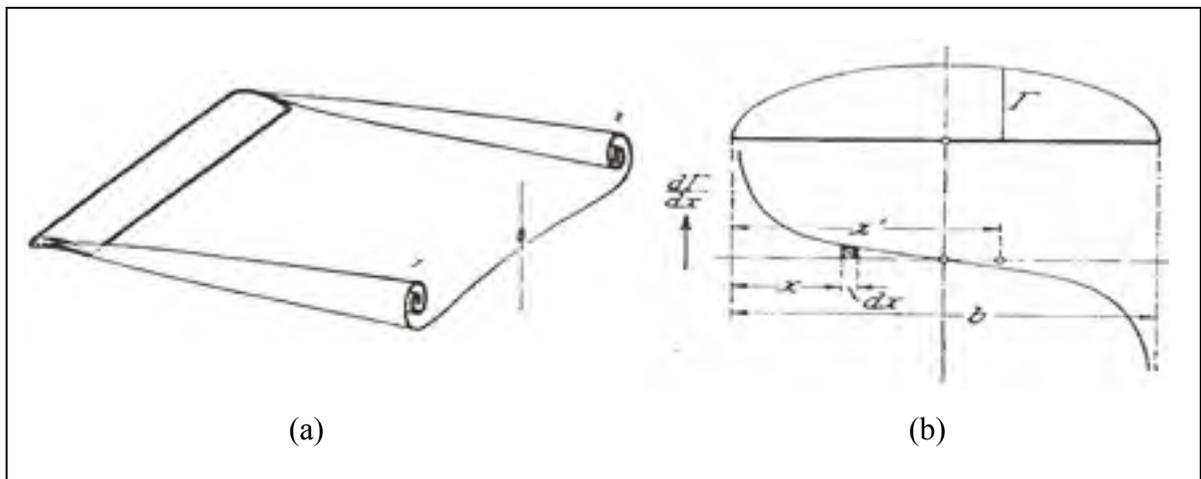
Figure 1.2 Prandtl's « vortex ribbons » (a) and ideal elliptical spanloading (b)
Taken from reference 89 (1921, p. 27 and 29)

The original theory developed by Prandtl was extended to multiple airfoils by Marx Munk in 1922 (ref. 100) and became what is referred to as "*The Biplane Theory*". In his work, Munk introduced the fact that two lifting surfaces will interfere within each others, as one wing will be affected by the downwash of the other one. Therefore, he divided the induced drag equation for two lifting surfaces into four terms: two terms for the individual drag of each surface, and two more for their mutual interference. Finally, he proved that the mutual drag terms are equal. He also applied his theoretical methodology to assess the effect of sweep angle on spanloading in reference (ref. 93) in 1923. A year later, Prandtl published "*Induced Drag of Multiplanes*" (ref. 92), in which he applied the theory developed by Munk to systems of two and three elliptically loaded lifting surfaces. The resulting solution was a simple, lightweight equation using sigma (σ) factors that allowed designers to quickly estimate the induced drag on any two or three wings aircraft configuration. At this point, it seemed understood and accepted that an elliptical lift distribution could minimize the induced drag of a lifting surface. The downwash of an ideal spanloading could be defined as a Y = C function. However, the design of an aircraft is a compromise between multiple disciplines, and Prandtl noted in his work that the structural weight associated with the elliptical spanloading (see spanload "a" on next figure) was not necessarily the optimum distribution. He proposed in 1932 (ref. 35) a solution to obtain the ideal spanloading of a wing with a constrained root bending moment. His conclusions were that the ideal wing would have a 22% increase in span with an 11% induced drag reduction. As for the ideal spanloading, its shape was more triangular than elliptical (**b** and **c**).
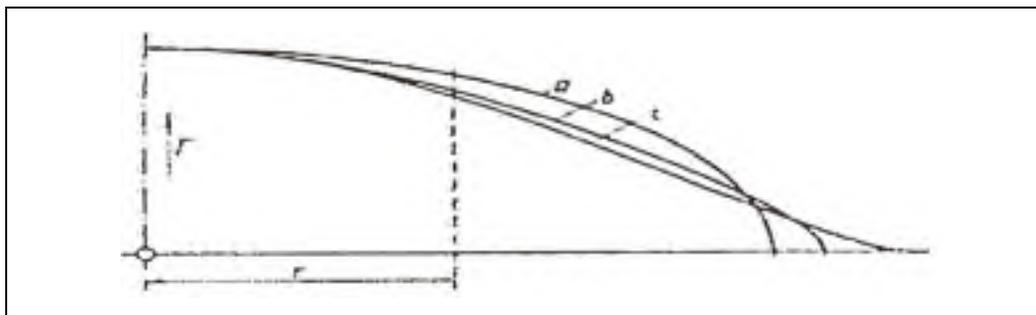
Figure 1.3 Prandtl's ideal spanload for a constrained root bending moment
Taken from reference 35 (2006, p. 7)

During and after World War II, from 1940 to 1955, the Horten brothers used Prandtl's latest spanload work to develop their flying wings designs. They introduced concepts such as the induced thrust at tips and the "Mitteleffekt" (ref. 35). They eventually solved for an ideal spanload constrained for root bending moment and stability requirements, which is referred to as the "*Bell Shaped*" spanload.
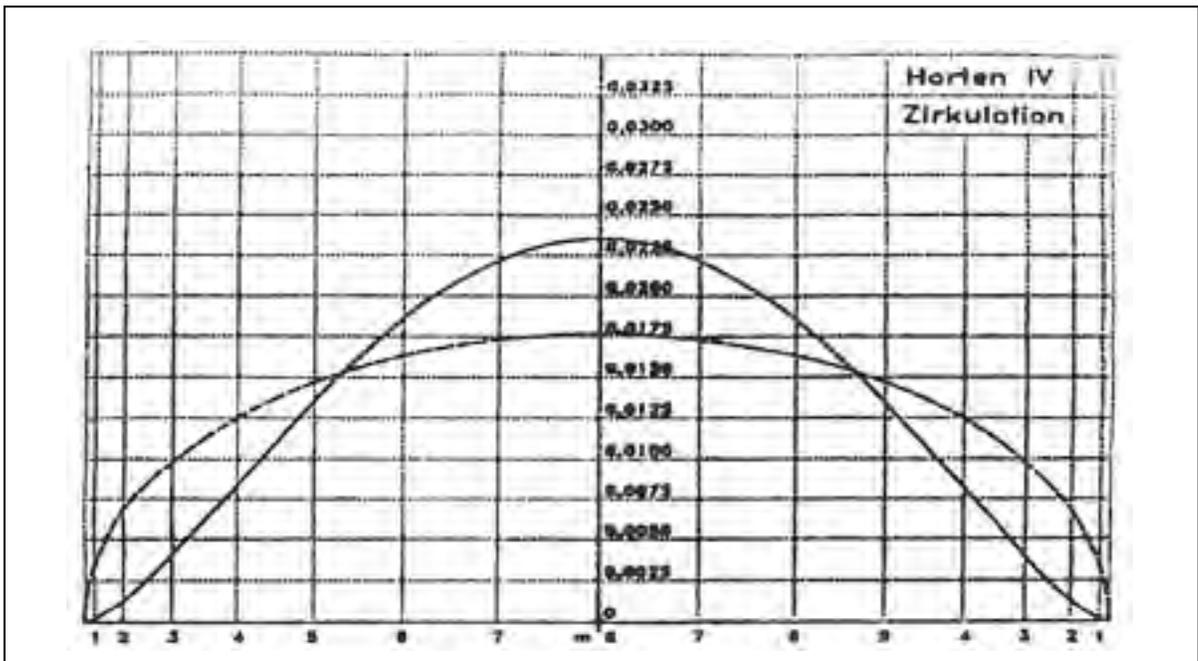
Figure 1.4 Horten brother's "Bell Shaped" spanloading for flying wing
Taken from reference 35 (2006, p. 8)

In 1950, Jones published a work (ref. 101) in which he solved for an ideal spanloading with constraints on lift and bending moment. However, his calculation of the root bending moment is less general than Prandtl's. He concluded that a 15% reduction of induced drag was possible with a 15% increase in span as compared to an elliptically loaded wing of equal lift and bending moment. Just like Prandtl, the resulting spanload is more triangular. Nevertheless, even if the drag reductions predictions differ from Prandtl to Jones, one can notice an obvious similarity in the spanload shapes.
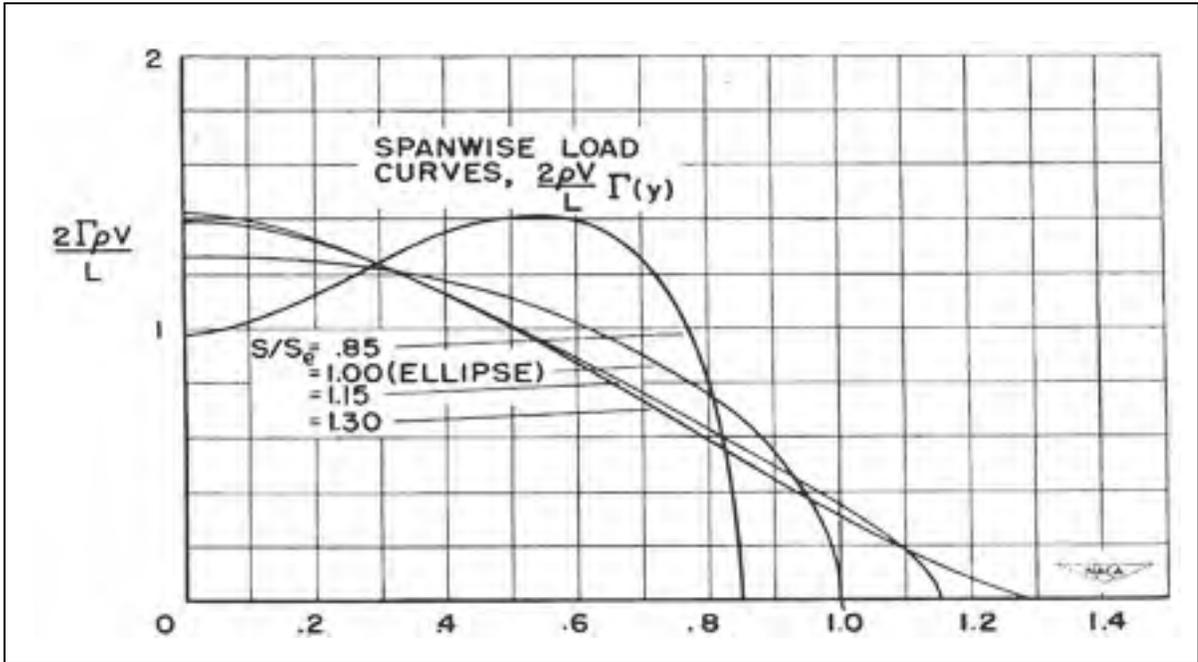
Figure 1.5 Jones's ideal spanloading with constrained root bending moment
Taken from reference 101 (1950, p.14)

In 1967, Lundry (ref. 34) performed an investigation to solve for the minimum induced drag spanloading while constraining the lift and span of a swept wing to achieve zero pitching moment. This work was, in most point, very similar to the Horten's work, with the fundamental difference that Lundry was trying to quantify the drag penalty of trimming the aircraft by shaping the spanload. It is however very interesting to see that he obtained the same "bell shaped" distribution that the Horten's.
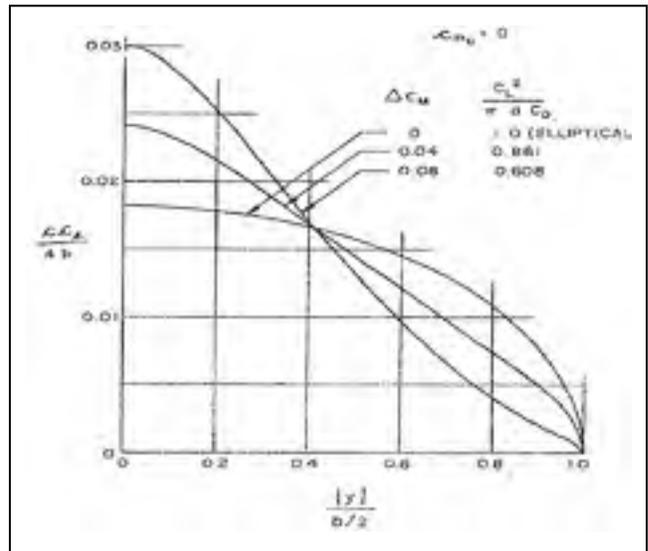
Figure 1.6 Lundry's ideal spanloading
Taken from reference 34 (1967, p. 2)

The work done by Prandtl, Horten, Jones and Lundry introduced a new dimension in spanload optimization, as the ideal downwash distribution was now defined as a $Y = BX + C$ function. Several years later, in 1975, Klein and Viswanathan (ref. 65) performed an investigation to solve for the ideal spanload of a wing with constrained structural weight, including bending moments and shear stresses. They concluded that a 7% reduction of induced drag was possible with a 16% increase in span compared with an elliptically loaded wing of equal weight.
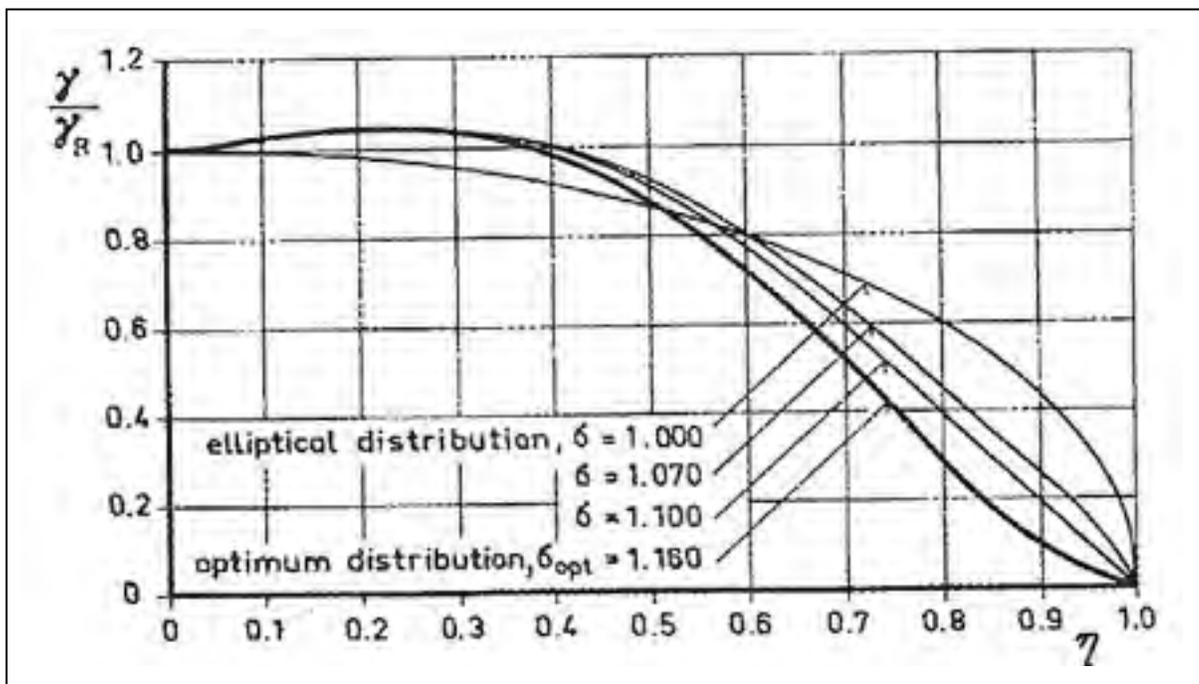
Figure 1.7 Klein and Viswanathan's ideal spanload for constrained wing weight
Taken from reference 65 (1975, p. 3)

This work defined the ideal downwash distribution as a parabolic function $Y = AX^2 + BX + C$. For the reader who would like to seek more details about the approaches mentioned herein, Jones published a summary in 1979 (ref. 35). Up until this time, most of the research done on spanloading was focused on the assessment of ideal lift distribution over a single planar wing. In 1980, Jones and Lasinski (ref. 103) obtained an analytical solution for the ideal spanload of wings with winglets by constraining the area under the bending moment curve; the same approach used by Prandlt. They observed that for an ideal wing shape,

similar reductions of induced drag can be achieved by either horizontal or vertical tip extensions.
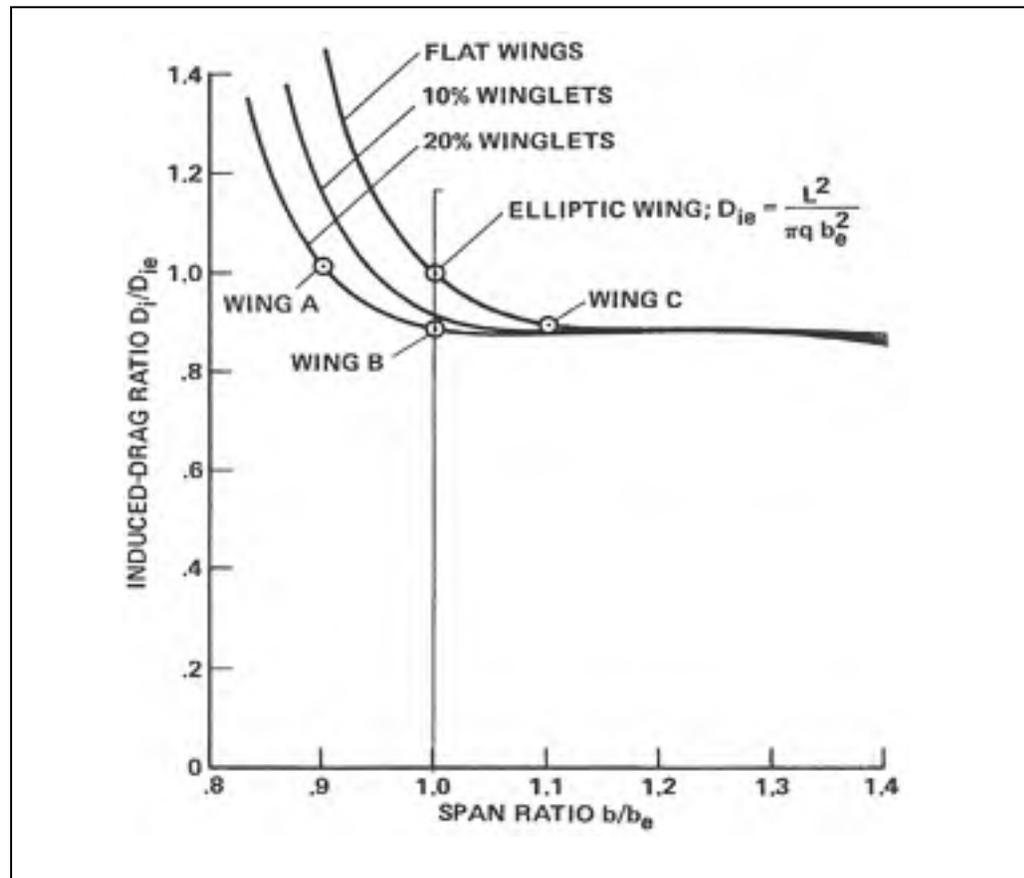
Figure 1.8 Jones and Lasinski's drag reduction with winglets
Taken from reference 103 (1980, p. 21)

At this point, the lift distribution optimization was now assessing non-planar lifting surfaces. However, since the foundation of the solution was still based on Prandtl's lifting line theory, the induced drag was computed in a planar manner. During the same period of time, Kroo proposed a method in (ref. 26) that allowed to solve for the ideal spanload distribution that minimizes the induced drag of any biplane configuration. His approach was based on Prandtl's work "*Induced Drag of Multiplanes*" cited previously. By considering an elliptical lift distribution over the second lifting surface (canard or tail), the minimum drag spanload over the wing can be obtained. He also proposed a general equation very similar to the one

published by Prandtl in 1924, with the simple addition of sigma* (σ*) factors, which can be calculated or extracted from graphics. No structural calculations were included into this work.

Kroo's method was later extended to three lifting surfaces configurations by Laurendeau in 1990 (ref. 108). The same assumption of elliptical spanloading on the secondary and tertiary surfaces was used. The method allows to solve for the minimum induced drag spanloading over the wing and new sigma* (σ*) factors are determined. Laurendeau's approach offers an analytical solution for the induced drag of multiple lifting surfaces aircrafts that seems appropriate for actual needs. However, since it is based on the lifting-line theory, the drag calculation is done like if the wing was planar, without consideration for the sweep or dihedral. Even so, recent literature let believe that fairly good accuracy can be expected from it. To mention a few, the following authors have used linear and non-linear lifting-line approaches (NL-LLT) in their work for various applications and managed to obtain satisfactory precision for conceptual design purposes.

Chi (ref. 88) uses numerical lifting-line for icing simulation and compares with CFD. He obtains results that are within 2-5% error. Cheng (ref. 84) applies the same method on forward-swept wings (FSW) and concludes that such wings performances can be properly estimated using simple correlations with aft-swept wings (ASW). Owens (ref. 85) investigates numerical NL-LLT as a tool to be used for aircraft design and obtains good results according to data. In ref (ref. 86), Funk implemented a similar approach into a six degree-of-freedom (6-DOF) model to simulate stall departure of a Cessna. Results compare well to flight data on general aviation aircraft. Ariyur (ref. 87) uses numerical lifting-line to model ground effect and compares with a Gulfstream V. Results are satisfactory and the author suggests ways to improve accuracy.

This concludes the review of the literature for this work. All theoretical bases employed for the development Laurendeau's method and LLT software are detailed next.

CHAPITRE 2

THEORY

2.1   The Biot-Savart Law and Kutta-Joukowski Principle

Before starting any development on Prandtl's lifting-line theory, it seems appropriate to quickly introduce the two fundamental principles on which it is based: the Biot-Savart law and the Kutta-Joukowski principle.

The Biot-Savart law is used to calculate the velocity "V" at a given point "P" located at a certain distance "r" from a segment "dl" located on an infinite vortex filament of strength "Γ". To make an analogy with electromagnetism, the vortex filament would be an electric wire carrying an electrical current "Γ" and the resulting magnetic field at point "P" would represent the velocity induced by this filament. For application to aerodynamic, the Biot-Savart law goes as following:

$$V = \int_{-\infty}^{\infty} \frac{\Gamma}{4\pi} \frac{dl \times r}{|r|^3} \tag{2.1}$$

This fundamental principle applies for any vortex filament. However, the lifting-line theory uses only semi-infinite straight filaments as illustrated on the next figure.
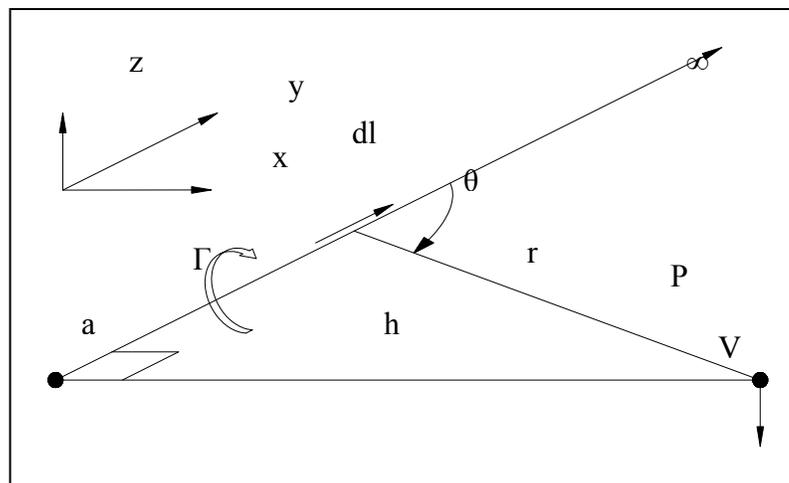
Figure 2.1 Velocity induced at point P by a semi-infinite straight vortex filament

The application of Biot-Savart law to this simplified system reduces to:

$$V = \frac{\Gamma}{4\pi}\int_0^\infty \frac{\sin\theta}{r^2}dl = -\frac{\Gamma}{4\pi h}\int_{\pi/2}^0 \sin\theta d\theta = \frac{\Gamma}{4\pi h} \tag{2.2}$$

Thus, the velocity induced at a given point "P" by a semi-infinite, straight vortex filament at a perpendicular distance "h" from "P" is simply $\Gamma/4\pi h$.

The second fundamental principle used by Prandtl is the Kutta-Joukowski principle. This principle defines lift force "L" as a function of the strength "Γ" of a vortex filament, or circulation.

$$L = \rho V\Gamma \tag{2.3}$$

This result underscores the importance of the concept of circulation, as it links together the strength of a vortex to the generation of lift. Its fundamental meaning is that the lift per unit span is directly proportional to the circulation around the body. Now that the basics are well established, the lifting-line theory can be developed.

2.2 Prandtl's Lifting Line Theory

Prandtl had understood that the very low pressures over a finite wing would force the air to roll around the tip, pushing the flow over the wing to move inboard, and similarly, forcing the air under the wing to move outward. The resulting difference in spanwise velocity causes the air to roll up into a several streamwise vortices, influencing the lift force along the span.
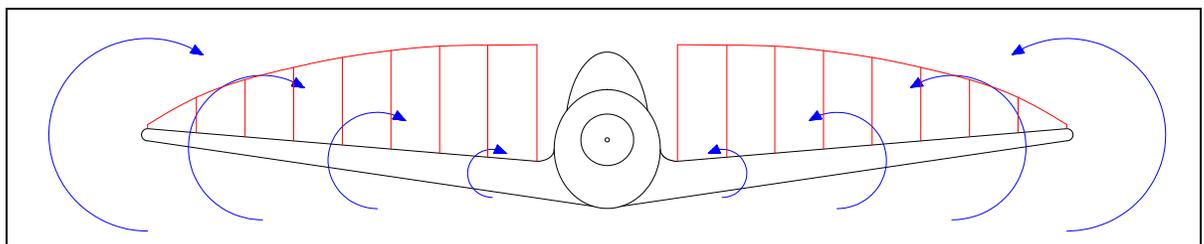
Figure 2.2 Streamwise vortices and spanwise lift force distribution

In his lifting-line theory, Prandtl modeled these streamwise vortices using Biot-Savart law as vortex model, and linked vortices from both sides of the plane together with a bound vortex of equal strength; creating what is called a horseshoe vortex. The figure below illustrates a single horseshoe vortex on a finite wing.
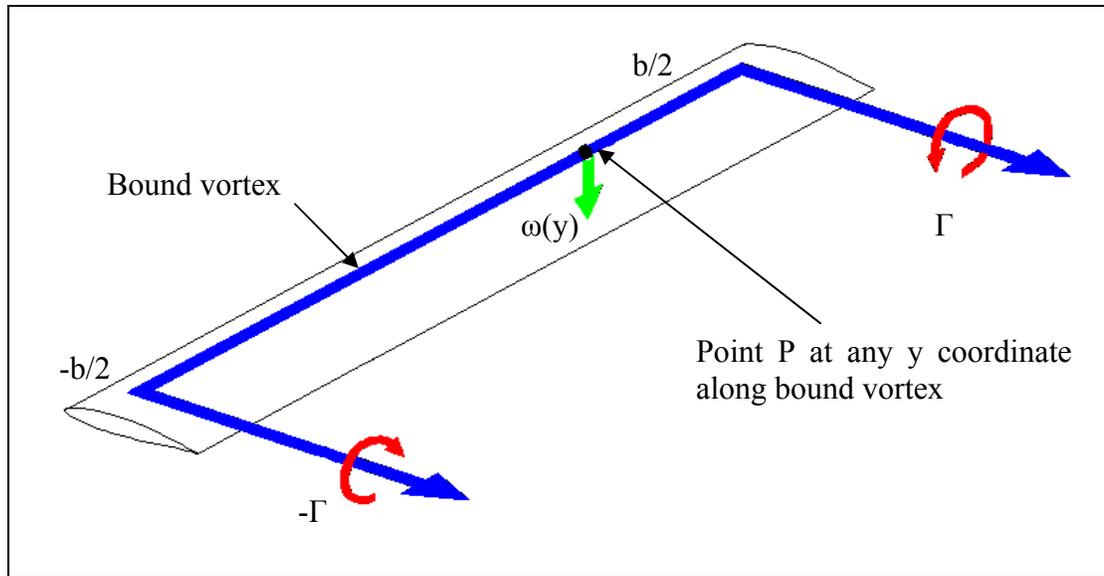
Figure 2.3 Single horseshoe vortex over a finite wing

Using Biot-Savart law, the velocity at point P at a given spanwise coordinate "y" on a wing of span "b" induced by the free-trailing vortices can be calculated as following.

$$\omega(y) = -\frac{\Gamma}{4\pi(b/2+y)} - \frac{\Gamma}{4\pi(b/2-y)} = -\frac{\Gamma}{4\pi}\frac{b}{(b/2)^2 - y^2} \tag{2.4}$$

This downward velocity "$\omega(y)$" induced at point "P" by the trailing vortices is called *downwash*, and changes the local effective angle of attack of this particular wing section. The lift force generated at this coordinate is therefore diminished and inclined backward. Thus, the local effective lift of this wing section has a component of force parallel to the undisturbed freestream flow. This drag force is a consequence of generating lift on a finite wing and is called induced drag, or vortex drag.
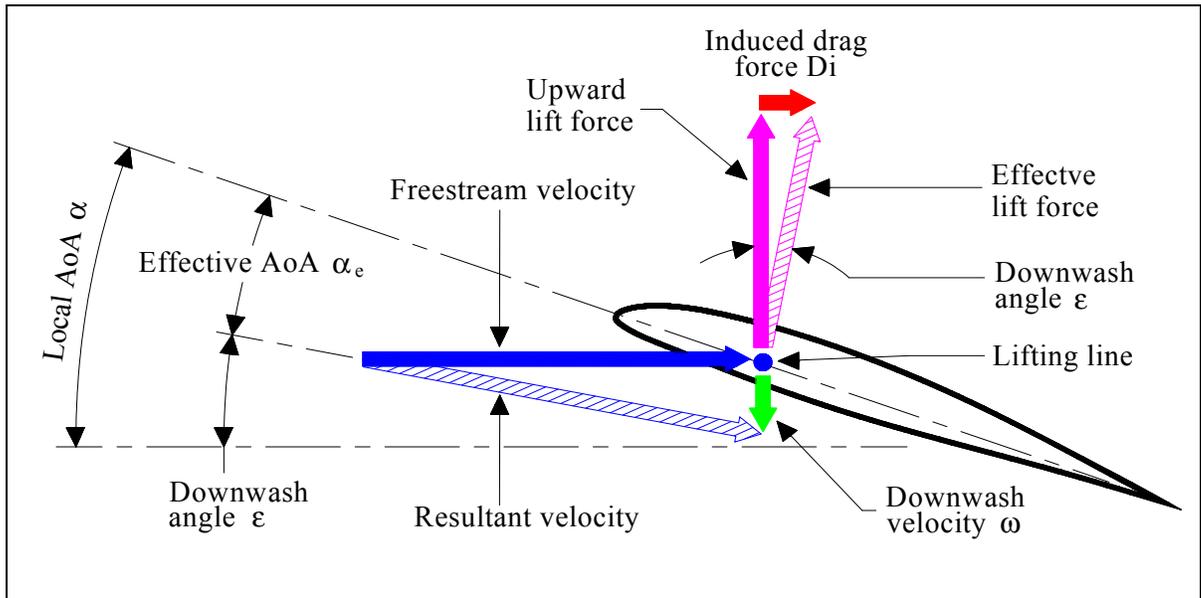
Figure 2.4 Induced flow over a wing section

To determine the spanwise lift distribution and the induced drag of a complete finite wing, Prandtl superposed an infinite number of horseshoe vortices along the lifting line. Each of these vortices has a vanishingly small strength "$d\Gamma$" corresponding to an infinitesimally short segment of the lifting line "dy". Let us single out a segment "dy" located at "y" having a circulation "$\Gamma(y)$" and a change of circulation along the segment "$d\Gamma$". Therefore:

$$d\Gamma = \frac{\partial \Gamma}{\partial y} dy \qquad (2.5)$$

Substituting the latest into (2.2), the downwash variation induced by this segment on any point P located arbitrary at a coordinate y_0 along the lifting line is:

$$\partial \omega = -\frac{(\partial \Gamma / \partial y)\, dy}{4\pi (y_0 - y)} \qquad (2.6)$$

To compute the total velocity induced at the spanwise coordinate y_0 by the entire trailing vortex sheet, equation (2.6) is integrated from one tip to the other.

$$\omega(y_0) = -\frac{1}{4\pi}\int_{-s}^{s}\frac{(\partial\Gamma/\partial y)\partial y}{y_0 - y} \qquad (2.7)$$

Note that the integration boundaries for the tips are not defined as b/2 and –b/2, as they have been replaced to take into account the dihedral angle and winglets. The integration is then performed as a line integral along the wingspan, like if a non-planar wing was unfolded into an equivalent planar surface.
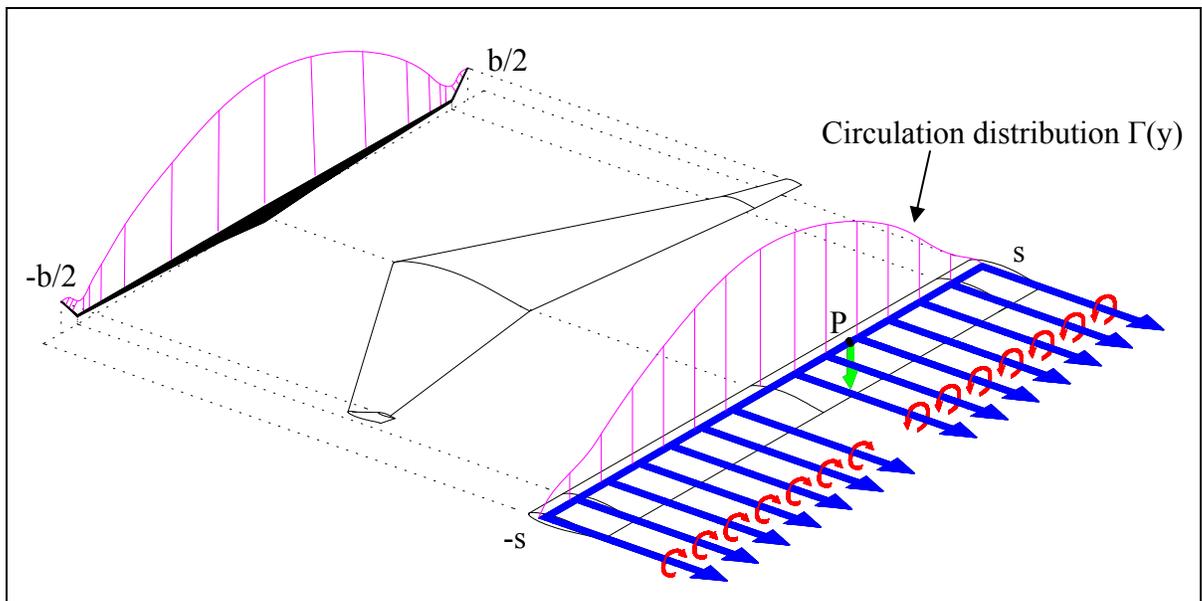
Figure 2.5 Induced velocity at point P by superposition of horseshoe vortices along a lifting line representing a non-planar lifting surface

From (2.7), the local downwash angle $\varepsilon(y_0)$ can be obtained from trigonometry.

$$\varepsilon(y_0) = \tan^{-1}\left(\frac{\omega(y_0)}{V}\right) \approx -\frac{\omega(y_0)}{V} \qquad (2.8)$$

Where V is the freestream velocity. From figure 2.5, the local induced drag at point P located at coordinate y_0 from the center of the wing follows.

$$Di(y_0) = L(y_0)\sin(\varepsilon(y_0)) \qquad (2.9)$$

In (2.9), the local lift L(y$_0$) at point P is obtained from the Kutta-Joukowski principle (2.3). The substitution of this principle into (2.9) reduces to:

$$Di(y_0) = \rho \omega(y_0)\Gamma(y_0) \tag{2.10}$$

By integrating (2.3) and (2.10) over the entire unfolded span, the wing's total lift force and corresponding induced drag can be obtained.

$$L = \int_{-s}^{s} \rho V \Gamma(y)dy \tag{2.11}$$

$$Di = \int_{-s}^{s} \rho \omega(y)\Gamma(y)dy \tag{2.12}$$

Prandtl extended his research to solve for the circulation distribution that would minimize the induced drag of a finite wing: the elliptical spanloading. However, there is no need to detail this part of his work as it is not used for further development in this report. The demonstration of this solution is frequently detailed in books such as the ones published by Anderson (ref. 110) or Bertin (ref. 111). The only relevant equation for this work concerning the elliptical lift distribution is the following, concluding this section on the lifting-line theory.

$$Di_{Elliptical} = \frac{L^2}{\pi q b^2} \tag{2.13}$$

2.3   Munk's Biplane Theorem

Munk used Prandtl's lifting-line theory and the Biot-Savart law to assess the fundamental principles related to systems of multiple lifting surfaces. The details of his approach are available in (ref. 100). However, for the purpose of this work, it does not seem necessary to go through the whole theoretical process as only the conclusions will be used for further developments.

Using the Biot-Savart law, Munk obtained a solution for the downwash velocity induced on a given wing element by a second wing. The following figure illustrates in a visual manner the influence of the circulation over a wing influencing the downwash velocity on another nearby lifting surface.
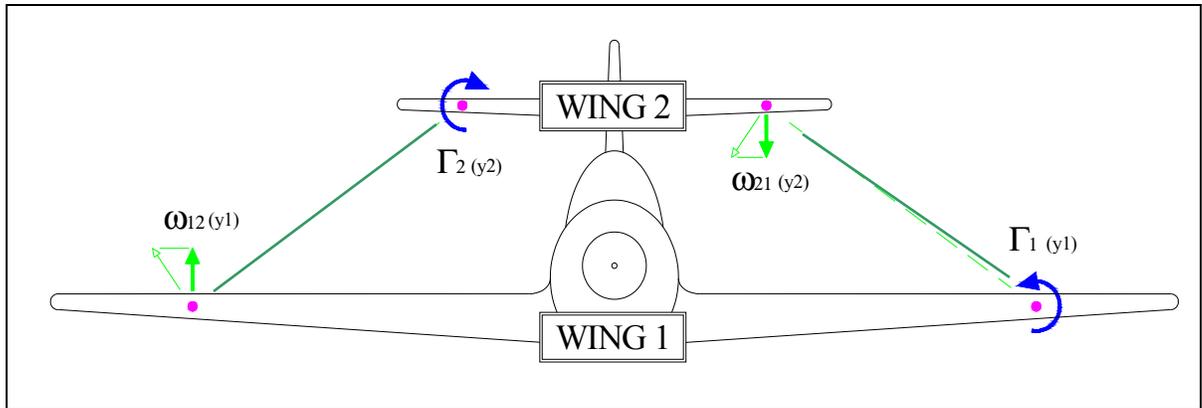
Figure 2.6 Mutually induced downwash velocities on two lifting surfaces

Recalling Prandtl's equation (2.10), the induced drag at a point y, located on wing 2, generated by wing 1 is quantified as following:

$$Di_{12}(y) = \rho \omega_{12}(y)\Gamma_2(y) \tag{2.14}$$

He also understood that if the circulation around wing 1 had influence over the second wing, then the circulation around the second wing would also influence the first one.

$$Di_{21}(y) = \rho \omega_{21}(y)\Gamma_1(y) \tag{2.15}$$

The integration of these equations, in the same way done by Prandtl from (2.10) to (2.12), allows defining the total drag of the system as a summation of four terms.

$$Di_{system} = Di_1 + Di_{12} + Di_{21} + Di_2 \tag{2.16}$$

A proper assessment of the mutual downwash velocities ω_{12} and ω_{21}, which are not constant along the span, is required to obtain a solution. Throughout his developments, Munk stated two fundamental theorems that will be of assistance in what follows.

> *"Any system, as regard its total induced drag, is equivalent to a simpler system having the same front view, in which the centers of pressure of all the constituent wing surfaces, while maintaining the same lift distribution, are shifted into one and the same plane, at right angles to the direction of flight."* (M. Munk, ref. 100).

> *"In an unstaggered wing system, the drag D_{12}, induced by wing1 on wing 2, equals the drag D_{21} induced by wing 2 on wing 1."* (M. Munk, ref. 100).

From these theorems, equation (2.16) may be simplified.

$$Di_{system} = Di_1 + Di_{mutual} + Di_2 \tag{2.17}$$

Where Di_{mutual} is the double of the interference drag induced by a single wing to another.

$$Di_{system} = Di_1 + 2Di_{12} + Di_2 = Di_1 + 2Di_{21} + Di_2 \tag{2.18}$$

2.4   Prandtl's Equation for Multiplanes

As mentioned in the previous section, to properly evaluate the total induced drag of a system containing multiple lifting surfaces, it is necessary to have an appropriate calculation of the spanwise downwash velocity profile $\omega_{xx}(y)$ of the wings. To assess that, Prandtl (ref. 92) used a graphic representing the spanwise downwash velocities (here called "z") induced by a flat plate for several vertical distances (gap "G"), expressed as a fraction of the span ($b1$).
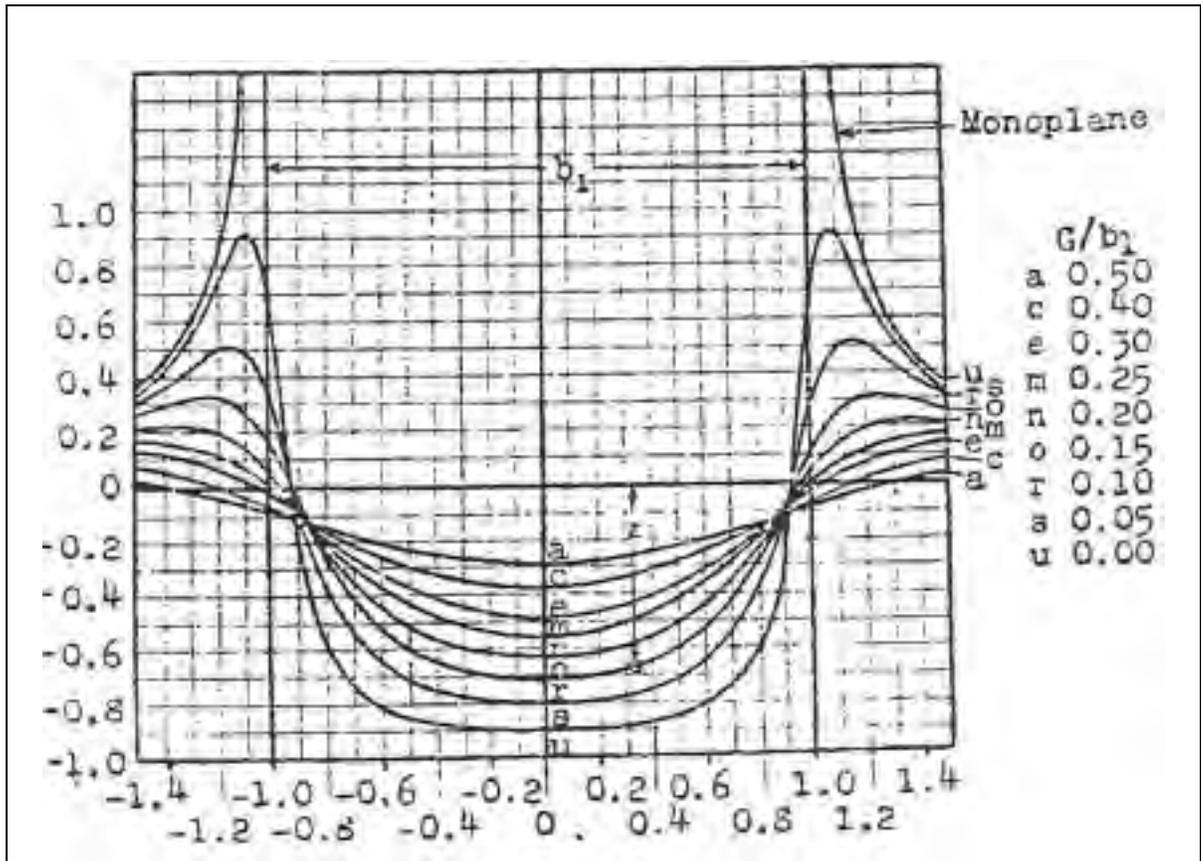
Figure 2.7 Spanwise downwash velocities ω(y) for various gaps
Taken from reference 92 (1965, p. 20)

This flat plate analysis was originally proposed by Munk and the test results were performed by Wr. K. Fohlhausen. To simplify the use these curve, equation (2.14) is adapted using the Kutta-Joukowski principle and the term $\rho\Gamma_2$ is replaced by $\delta L_2/V$. The interference drag can be obtained by integrating from tip to tip according to lifting-line theory (2.12).

$$Di_{12} = -\int_{-s}^{s} \frac{\omega_{12}(y)}{V} \delta L_2(y) \tag{2.19}$$

Prandtl makes a final adaptation to the $\omega_{12}(y)$ term, since both wings 1 and 2 might not have the same span and lift.

$$\omega_{12}(y) = \frac{2L_1}{\pi V b_1^2} z(y) \qquad (2.20)$$

The z(y) term is directly obtained from the preceding figure, and the drag induced by wing 1 on wing 2 can now be calculated by solving the integration (2.19). This integral was evaluated at the time using planimetry for various span ratios b2/b1 and different values of the gap G/b1 on the assumption the lift distribution over wing 2 is elliptical. The result makes use of an interference factor "σ" which can be obtained graphically.

$$Di_{mutual} = 2Di_{12} = 2Di_{21} = \frac{2L_1 L_2 \sigma}{\pi q b_1 b_2} \qquad (2.21)$$

The total induced drag of any biplane configuration can now be obtained by the substitution of (2.21) and (2.13) into (2.17). This relation is known as *The Biplane Equation*.

$$Di_{Biplane} = \frac{L_1^2}{\pi q b_1^2} + \frac{2L_1 L_2 \sigma}{\pi q b_1 b_2} + \frac{L_2^2}{\pi q b_2^2} \qquad (2.22)$$

The biplane equation was reworked in 1980 by Laitone (ref. 28), who added Oswald efficiency factor "e" to each terms of (2.22). It was later extended to three lifting surfaces configurations by Kendall in 1985 (ref. 27). The resulting induced drag for the system is:

$$Di_{Triplane} = \frac{L_1^2}{\pi q b_1^2} + \frac{2L_1 L_2 \sigma_{12}}{\pi q b_1 b_2} + \frac{L_2^2}{\pi q b_2^2} + \frac{2L_3 L_2 \sigma_{32}}{\pi q b_3 b_2} + \frac{L_3^2}{\pi q b_3^2} + \frac{2L_1 L_3 \sigma_{13}}{\pi q b_1 b_3} \qquad (2.23)$$

The sigma (σ) factors required to use these equations can be obtained from the following figure where the x axis is the span ratio b/b_{wing} and r is the vertical gap between each lifting surfaces expressed as $r = 2Gap/ b_{wing}$.
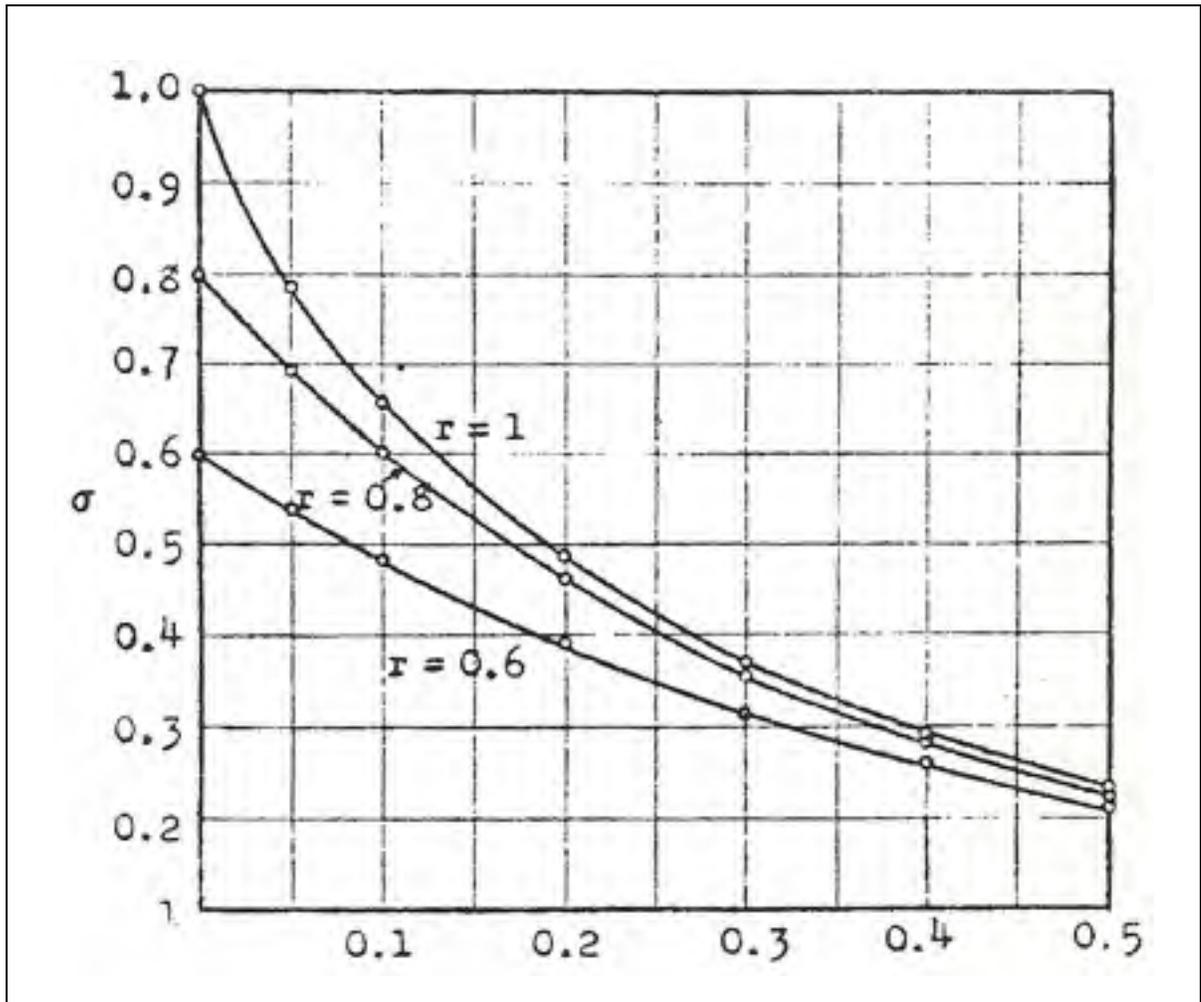
Figure 2.8 Prandtl's interference factor σ
Taken from reference 92 (1965, p. 20)

Of course, using this approach means that we recognize and accept Prandtl's methodology, which considers elliptical lift distribution over all lifting surfaces, which is not always the case.

In order to be able to compute the induced drag of non-elliptical lift distribution, the following chapter introduces an approach to define analytically any spanload distribution over a wing so that it can be used in the methods defined earlier.

2.5   Technique for General Spanwise Circulation Distribution

The technique for general spanwise circulation distribution consists in representing the circulation by a Fourier sine-series composed on "n" terms. A detailed development of the method is available in Anderson (ref. 110) and Bertin (ref. 111). Figure 2.9 represents the behavior of the circulation distribution as the Fourier series is modified.
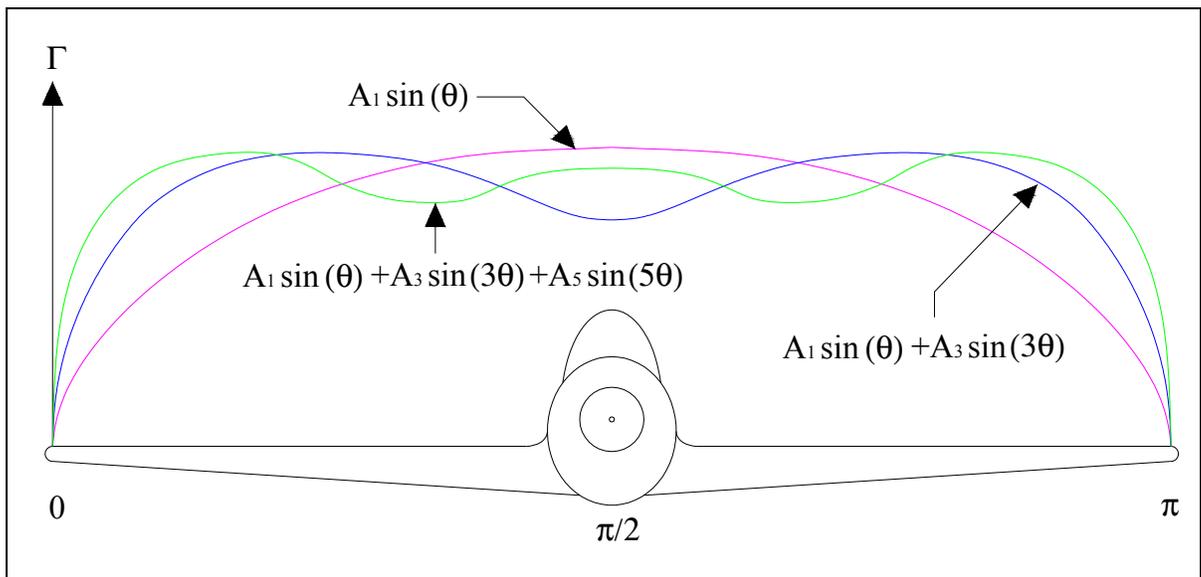
Figure 2.9 Circulation distribution represented by Fourier series

As illustrated on the figure above, adding terms to the series increases the "flexibility" of the curve. If only one term is considered, the distribution is elliptical. By altering the An Fourier coefficients, it is possible, if the series is composed of a sufficient amount of terms, to model about any shape of spanwise circulation distribution over a wing. Only odd terms (1,3,5…) are used to model the spanloading since they assure a symmetrical behavior of the curve from one tip to the other. However, since Fourier series are simpler to use in a polar coordinate system, it is convenient to replace the Cartesian spanwise coordinates (y) by the equivalent polar (θ) coordinate. Consider the transformation:

$$y = -s\cos(\theta) \tag{2.24}$$

In the latest equation, one must remember that the "s" variable represents the "unfolded" spanwise coordinate as illustrated in figure 2.5. Any circulation distribution over a wing can be defined by the following Fourier series with n = 1, 3, 5 and θ being the spanwise location.

$$\Gamma(\theta) = 4sV \sum_{1}^{N} A_n \sin(n\theta) \qquad (2.25)$$

The lift force corresponding to this distribution can be obtained by applying the coordinate system transformation (2.24) to the lift equation (2.11) defined in the lifting-line theory, and by substituting (2.25) into it.

$$L = \int_{-s}^{s} \rho V \Gamma(y) dy = 4\rho V^2 s^2 \int_{0}^{\pi} \sum_{odd} A_n \sin(n\theta) \sin(\theta) d\theta \qquad (2.26)$$

The same approach is repeated with (2.12) for the induced drag calculation.

$$Di = \int_{-s}^{s} \rho \omega(y) \Gamma(y) dy = 4\rho V^2 s^2 \int_{0}^{\pi} \sum_{odd} nA_n \sin(n\theta) \sum_{odd} A_n \sin(n\theta) d\theta \qquad (2.27)$$

These two integrals can be solved and reduced to very simple relations.

$$L = 4\pi q s^2 A_1 \qquad (2.28)$$

$$Di = \frac{L^2}{\pi q b^2} \sum_{odd} n \left(\frac{A_n}{A_1} \right)^2 \qquad (2.29)$$

Therefore, the lift generated by a given Fourier distribution over a wing can be computed from the A_1 coefficient only. As for the induced drag, there is an obvious similarity with Prandtl's elliptical spanload equation (2.13), with the only addition of the summation term. The following section details how Fourier distributions can be used into Prandtl's equation for multiplanes.

2.6 Kroo's Method

Kroo proposed in 1982 (ref. 26) a method to solve for the minimum induced drag spanload over a wing influenced by a secondary elliptically loaded lifting surface. Summarizing his approach, the Fourier series technique explained in the previous section was used to define the circulation distribution over the primary wing. To describe the downwash velocities ω_{12} induced by a secondary lifting surface on the wing, an analytical methodology given by von Kármán and Burgers (ref. 112) was applied. The induced drag equation for a biplane (2.22) was then rewritten to accommodate the non-elliptical loading on the wing. By derivation of this newly adapted formulation, the Fourier coefficients An that define the minimum induced drag spanloading were obtained by the derivation $\delta D_i / \delta A_n = 0$.

Once again, the key in this solution is to properly evaluate the downwash velocities induced by one wing on another. The method proposed by von Kármán and Burgers is a mathematical representation that approaches the velocity fields used by Prandtl on Figure 2.7. To clarify the upcoming developments and the ones that will follow in further sections, the reader may consider indices 1 and 3 to represent the secondary lifting surfaces (canard or stabilizer) as indices 2 refers to the main wing. The local downwash velocity induced on a given segment of the main wing by a secondary lifting surface is defined as following.

$$\frac{\omega_{12}}{\omega_{01}} = 1 - \mathrm{Re}\left(\frac{\xi}{\sqrt{\xi^2 - 1}}\right) \qquad (2.30)$$

In this equation, the local induced downwash velocities ω_{12} on the wing are expressed as a ratio of the ω_{01}, which represents the downwash velocity at the root of the secondary lifting surface. The term ξ is obtained from:

$$\xi = \frac{2y}{b_1} + i\frac{2h}{b_1} \qquad (2.31)$$

where b_1 is the span of the secondary lifting surface, h the vertical separation between the wings and y the spanwise coordinate on the main wing. The term ω_{01} can be expressed by:

$$\omega_{01} = \frac{L_2 V}{\pi q b_2^{\,2}} \qquad (2.32)$$

From these equations, the downwash velocities mutually induced between two lifting surfaces can be obtained. The figure below illustrates these velocities for various vertical gaps between a wing and a secondary lifting surface of span $b_1 = 0.625\ b_2$, which is exactly the same figure used by Prandtl (see Figure 2.7), with the only difference that he quantified the gap as a function b_1.
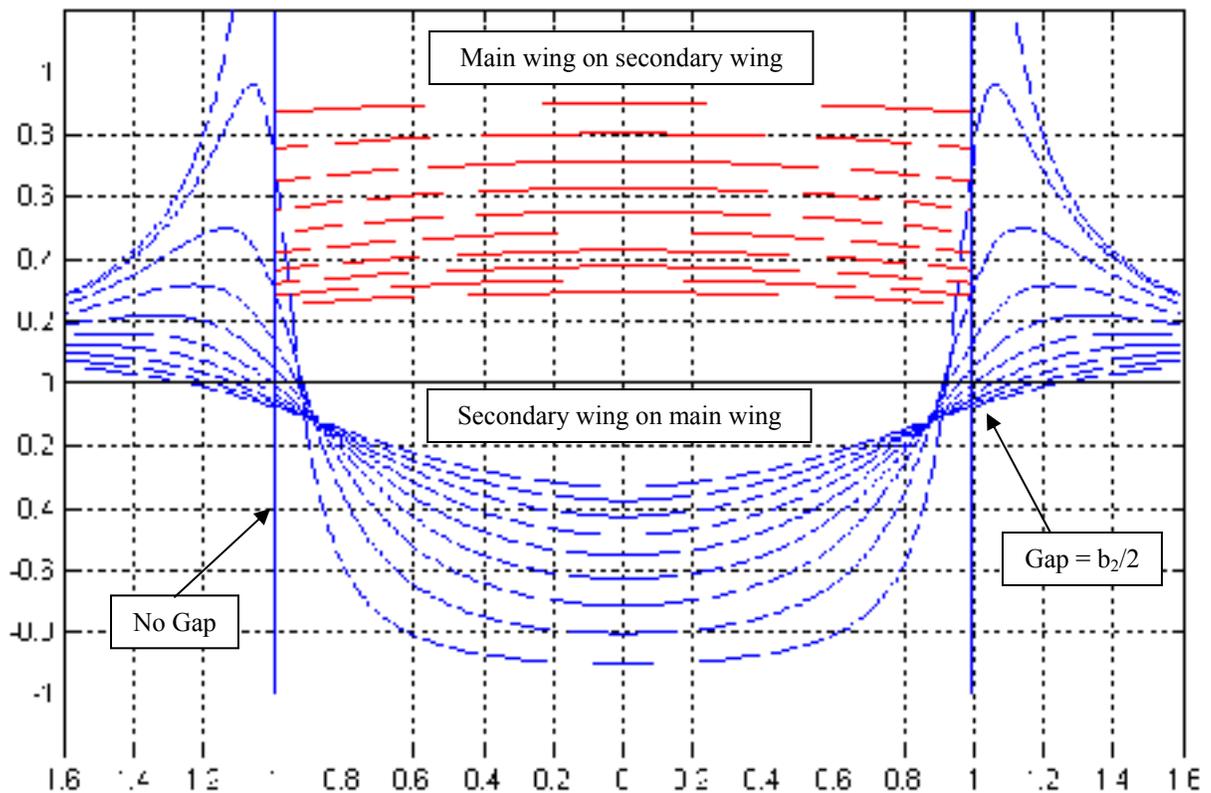
Figure 2.10 Induced downwash velocities on surfaces 1 and 2 for various vertical gaps

Recalling (2.17), the total induced drag of the system is the summation of the individual drag of each lifting surface and the mutual drag resulting from their interference. The drag of the main wing and the secondary lifting surface are calculated respectively using (2.29) and (2.13). The mutual drag is twice the drag induced by one wing on the other and is calculated by solving (2.12).

$$Di_{mutual} = 2Di_{12} = 2\rho \int_{-s}^{s} \omega_{12}(y)\Gamma_2(y)dy \tag{2.33}$$

The circulation distribution over the wing $\Gamma_2(y)$ is defined by Fourier series in polar coordinates and the downwash velocity field ω_{12} is obtained from von Kármán and Burgers equations. By substituting these terms into the integration, we have:

$$Di_{mutual} = \frac{4L_1L_2}{\pi^2 q b_2^{\,2}} \int_{\pi}^{0} \left(\frac{\omega_{12}}{\omega_{01}}\right) \sum_{odd} \left(\frac{A_n}{A_1}\right)^2 \sin(n\theta)d\theta \tag{2.34}$$

The coordinate system transformation (2.24) can be reversed by posing:

$$\overline{y} = \frac{y}{-s} = \cos\theta \tag{2.35}$$

The total drag of the system is therefore defined by:

$$Di_{Biplane} = \frac{L_1^{\,2}}{\pi q b_1^{\,2}} + \frac{2L_1L_2\sigma_1}{\pi q b_1 b_2} + \frac{L_2^{\,2}\sigma_2}{\pi q b_2^{\,2}} \tag{2.36}$$

with

$$\sigma_2 = \sum n\left(\frac{A_n}{A_1}\right)^2 \tag{2.37}$$

$$\sigma_1 = \frac{4b_2}{\pi b_1} \sum_{odd} \left(\frac{A_n}{A_1} \right) I_{12(n)}$$ (2.38)

and

$$I_{12(n)} = \int_0^1 \left(\frac{\omega_{12}}{\omega_{01}} \right) \sin \left[n(\cos^{-1} \overline{y}) \right] d\overline{y}$$ (2.39)

Therefore, the induced drag of a biplane, for which the circulation distribution over the wing is defined by several Fourier coefficients A_n, can be obtained. Kroo proposes a method to solve for the A_n coefficients that will minimise the induced drag of the system by derivation of (2.36).

$$\frac{\partial Di}{\partial A_n} = 0$$ (2.40)

The A_n coefficients for minimum induced drag can be isolated from the solution of this derivation.

$$\frac{A_n}{A_1} = -4 \frac{(L_1 / L_2) I_{12(n)}}{\pi n (b_1 / b_2)^2}$$ (2.41)

The A_1 coefficient determines the lift of the wing and is obtained from (2.28). By substitution of this latest equation into (2.37) and (2.38), the sigma (σ) factors for minimum induced drag are obtained. Equation (2.36) can finally be reduced to:

$$Di_{BiplaneMin} = \frac{L_1^2 \sigma^*}{\pi q b_1^2} + \frac{2 L_1 L_2 \sigma}{\pi q b_1 b_2} + \frac{L_2^2}{\pi q b_2^2}$$ (2.42)

$$\sigma = \frac{4 I_{12(1)}}{\pi (b_1 / b_2)}$$ (2.43)

$$\sigma^* = 1 - \frac{16}{(\pi b_1 / b_2)^2} \sum_3^N \frac{I_{12(n)}^2}{n}$$ (2.44)

The σ factor obtained by Kroo is the same as Prandtl's interference factor illustrated in figure 2.8. However, its calculation is now completely analytical, which saves us the trouble of having to rely on planimetry! As for the σ* factor, its use in conceptual design allows to quickly assess the minimum induced drag achievable by any biplane configuration. The following figure illustrates the σ (blue curves) and σ* (red curves) interference factors in function of the gap between the wings and the ratio of their span.
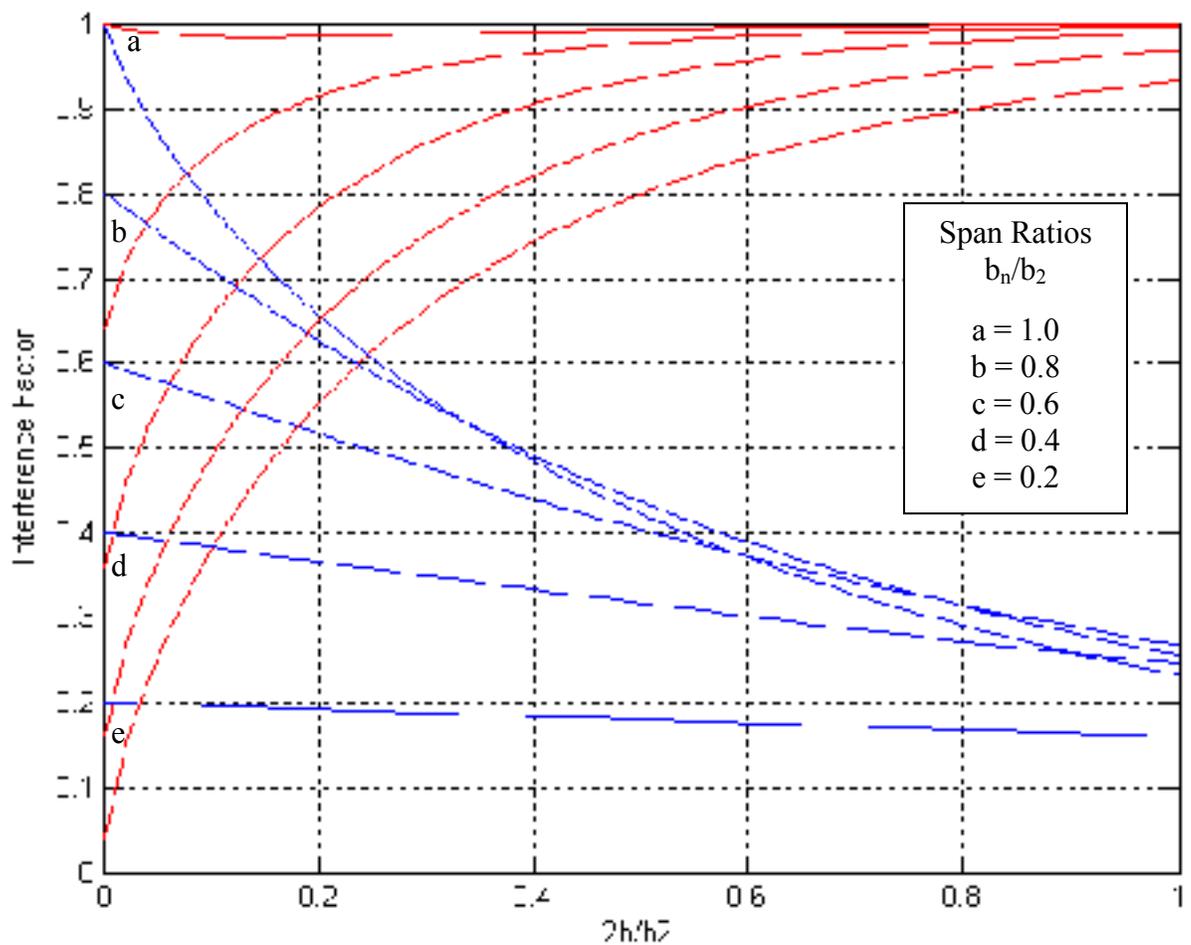
Figure 2.11 Prandtl and Kroo interference factors

This concludes the theory behind Kroo's method. The last theoretical concept required for the future developments of this work is introduced in the following section.

2.7   Laurendeau's Method

Laurendeau proposed in 1990 (ref. 108) an extension to the method developed by Kroo by adding a third lifting surface to the system. This third wing is considered elliptically loaded, which is the same assumption used by Kroo for his secondary lifting surface. By derivation of the induced drag equation for the complete system, the A_n coefficients defining the minimum induced drag spanloading of any three lifting surfaces configuration can be solved, and the corresponding σ factors are obtained.

Recalling Prandtl, the total induced drag of a system composed of multiple lifting surfaces will contain one term for the induced drag of each individual wing, and one mutual drag term for each pair of wings. For a three lifting surface configuration, the induced drag equation will therefore be composed of six terms as showed in (2.23).

$$Di_{Triplane} = Di_1 + Di_2 + Di_3 + Di_{12} + Di_{32} + Di_{13} \qquad (2.45)$$

Once again, indices 2 refer to the main wing, as indices 1 and 3 are used for the canard and stabilizer. In this latest expression, the terms Di_1 and Di_3 are evaluated using (2.13) since both surfaces are elliptically loaded. As for the drag of the main wing, it is obtained using (2.29), which is exactly the same thing as using (2.13) multiplied by the σ_2 factor described by (2.37). The mutual drag terms Di_{12} and Di_{32} are assessed in the exact same way as in the previous section. Recall the integration (2.34), the equation for the mutual drag of any secondary surface k interfering with the primary wing is defined as following.

$$Di_{k2} = \frac{2L_k L_2 \sigma_{k2}}{\pi q b_k b_2} \qquad (2.46)$$

Where σ_{k2} is obtained from (2.38). The only missing term is the mutual interference drag between the two secondary surfaces. Relation (2.46) can be reworked to allow the calculation of Di_{13}.

$$Di_{13} = \frac{2L_1L_3\sigma_{13}}{\pi q b_1 b_3} \tag{2.47}$$

To obtain the σ_{13} factor, the development of equation (2.38) is applied to elliptically loaded surfaces only and reduces to;

$$\sigma_{13} = \frac{4I_{13}}{\pi(b_1/b_3)} \tag{2.48}$$

with

$$I_{13} = \int_0^1 \left(\frac{\omega_{13}}{\omega_{01}}\right) \sin(\cos^{-1}\overline{y})d\overline{y} \tag{2.49}$$

$$\frac{\omega_{13}}{\omega_{01}} = 1 - \text{Re}\left(\frac{\xi}{\sqrt{\xi^2 - 1}}\right) \tag{2.50}$$

$$\xi = \frac{2y_3}{b_1} + i\frac{2h_{13}}{b_1} \tag{2.51}$$

Regrouping all six terms, equation (2.45) can be rewritten.

$$Di_{Triplane} = \frac{L_1^2}{\pi q b_1^2} + \frac{2L_1L_2\sigma_{12}}{\pi q b_1 b_2} + \frac{L_2^2\sigma_2}{\pi q b_2^2} + \frac{2L_3L_2\sigma_{32}}{\pi q b_3 b_2} + \frac{L_3^2}{\pi q b_3^2} + \frac{2L_1L_3\sigma_{13}}{\pi q b_1 b_3} \tag{2.52}$$

Following Kroo's approach, Laurendeau applies derivation (2.40) to obtain the A_n coefficients corresponding to the minimum induced drag of the system.

$$\frac{A_n}{A_1} = -4\left[\frac{(L_1/L_2)I_{12(n)}}{\pi n(b_1/b_2)^2}\right] - 4\left[\frac{(L_3/L_2)I_{32(n)}}{\pi n(b_3/b_2)^2}\right] \tag{2.53}$$

This result is then inserted into the calculation of the multiples σ factors. Equation (2.52) is modified to include Kroo's σ* factors for minimum induced drag.

$$Di_{TriplaneMin} = \frac{L_1^2 \sigma_1^*}{\pi q b_1^2} + \frac{2L_1 L_2 \sigma_{12}}{\pi q b_1 b_2} + \frac{L_2^2}{\pi q b_2^2} + \frac{2L_3 L_2 \sigma_{32}}{\pi q b_3 b_2} + \frac{L_3^2 \sigma_3^*}{\pi q b_3^2} + \frac{2L_1 L_3 \sigma_{13}^*}{\pi q b_1 b_3}$$

(2.54)

In this last relation, the σ factors are Prandtl's interference factors and are obtained using (2.43). As for the σ_k^* factors, they can be obtained from (2.44) and Laurendeau proposes a solution for the σ_{13}^* factor, expressing the interference between the canard and stabilizer.

$$\sigma_{12} = \frac{4 I_{12(1)}}{(\pi b_1 / b_2)}$$

(2.55)

$$\sigma_{32} = \frac{4 I_{32(1)}}{(\pi b_3 / b_2)}$$

(2.56)

$$\sigma_1^* = 1 - \frac{16}{(\pi b_1 / b_2)^2} \sum_3^N \frac{I_{12(n)}^2}{n}$$

(2.57)

$$\sigma_3^* = 1 - \frac{16}{(\pi b_3 / b_2)^2} \sum_3^N \frac{I_{32(n)}^2}{n}$$

(2.58)

$$\sigma_{13}^* = \frac{4 I_{13}}{(\pi b_1 / b_3)} - \frac{16}{((\pi^2 b_1 b_3) / b_2^2)} \sum_3^N \frac{I_{12(n)} I_{32(n)}}{n}$$

(2.59)

This concludes the overview of the theory used throughout this work. The following sections of this chapter are meant to verify the robustness of Kroo's and Laurendeau's equations.

2.8   Theory Robustness

2.8.1   The "Zero - Gap" Cases

The use of Prandtl's equations for the analysis of multiple lifting surfaces aircrafts results to a numerical problem: the Biot-Savart law, on which Prandtl's theory is based-on, has a singularity in the center of a vortex; singularity that occurs at the tip of a lifting surface. In the case of a multiplane with no stagger between lifting surfaces, a mathematical discontinuity occurs at the tip of each lifting surfaces having a smaller span than the main wing. Recalling figure 2.10, a "zero-gap" configuration results in a mutually induced downwash tending to infinity at the tip of the shortest lifting surface. This is due to the fact that a singularity occurs in the calculation of the induced downwash velocity defined by (2.30) :

$$\frac{\omega_{12}}{\omega_{01}} = 1 - \mathrm{Re}\left(\frac{\xi}{\sqrt{\xi^2 - 1}}\right) \qquad (2.60)$$

In this equation, the value of ζ equals zero for zero-gap cases, which results in an infinite downwash velocity and numerical error. Therefore, in the implementation of the "LLT" program, a special case was added for zero-gap conditions, replacing $\zeta = 0$ by $\zeta = 10^{-7}$. This small induced imperfection has shown not to provoke any computation errors up-to seven digits after zero and insures robustness of the computational process.

The singularity in Biot-Savart equation also induces a computational difficulty in the calculation of the σ and σ^* factors for near-zero gap conditions. The exact solution of integration (2.39) has been solved into the following interference factors:

$$\sigma = b_1/b_2 \qquad (2.61)$$
$$\sigma^* = (b_1/b_2)^2 \qquad (2.62)$$

In order to attain such results numerically and assuming a linear discretisation of the span, one should consider using 1000 wing section cuts semi-spanwise to solve the (2.39) integration numerically and obtain proper computation of the σ and σ* factors to within 10^{-7}.

2.8.2   Interchangeability Front - Rear

This validation test is made to make sure that Kroo's and Laurendeau's equations are correct and that no typological errors have slipped through correction. As a first experiment, the interchangeability of wings 1 and 2 in the equations is investigated. Since the induced drag calculation is done independently of the depth of each lifting surface, the drag result should not vary when wing's identification number is changed in the equation.
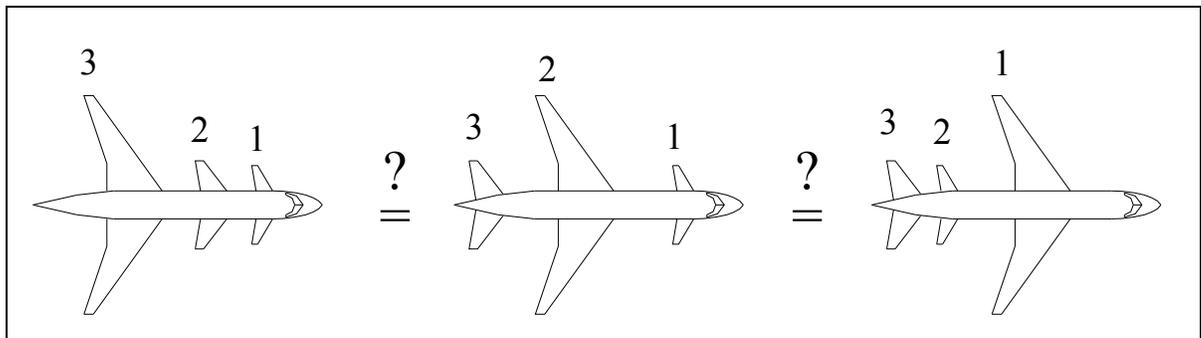
Figure 2.12 Validation of Front-to-Rear Interchangeability in the Equations

Subsequent to a mathematical verification, it was determined that the equations are robust and consistent in term of front-to-rear interchangeability as long as the main wing has a larger span than the two other lifting surfaces. Consequently, one should clearly predetermine the numerical indices relating to each lifting surfaces. For the remaining part of this work, the indices "2" will represent the main wing, having the largest span. The wingspan of the other lifting surfaces is therefore expressed as a fraction of the main span. In no case wings number 1 and 3 can have a larger wingspan than wing number 2, since the fundamental theory concerning the mutual downwash equations will no longer be functioning.

2.8.3   Interchangeability Top - Bottom

In the same train of thought than for the previous section, the top-to-bottom interchangeability of the equations was investigated. Once again, induced drag results should not vary with the identification of the lifting surfaces since the aircraft configuration is the same.
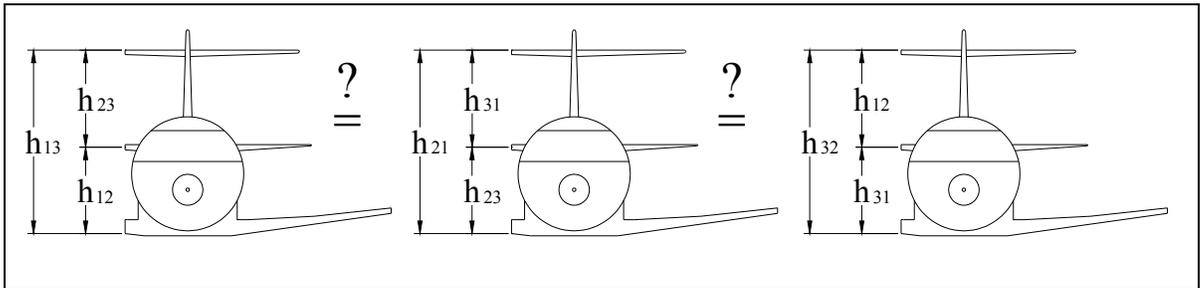
Figure 2.13 Validation of Top-to-Bottom Interchangeability in the Equations

An analytical verification shows that the equations are robust and consistent as long as the value of the gaps between various lifting surfaces are **positive** and expressed as a fraction of the main wingspan. Therefore, if one supposes an aircraft having a reference wingspan of 100 feet, a tailspan of 30 feet and a stagger height of 20 feet, the aircraft definition for use in the equations goes as following:

$$b_2 = 1$$
$$\overline{b_{12}} = b_1 / b_2 = 0.3$$
$$\overline{h_{12}} = 2h_{12} / b_2 = 0.4$$

The theory is now ready to be implemented into a computer program.

CHAPITRE 3

IMPLEMENTATION

3.1   Software Description

In order to asses the induced drag of multiple lifting surfaces aircraft configurations, the various theories summarized in the previous chapter were implemented into a program called LLT. The software was written in Matlab and can compute the induced drag of any one, two or three lifting surfaces configuration in less than 0.10 seconds on an average dual-core PC. The necessary inputs and resulting outputs are described below.

LLT inputs:

- An input file, in text format, containing various geometry and lift coefficients for the canard, stabilizer and wing;

- If specified by the user, a spanload file, in text format, detailing the discretisation of the wing. It contains the height and spanwise coordinates for every wing element and the related adimensionalized normal force coefficient.

LLT Internal Operations:

- Calculation of the An coefficients corresponding to the input spanload distribution;

- Induced drag calculation for the main wing with winglets;

- Correction of the main wing's induced drag to include the fuselage effect;

- Calculation of the total induced drag of the aircraft.

LLT Outputs:

- Exports an induced drag report in text format;

- Displays a figure of the various lift distributions;

- Writes a spanload sheet for the minimum induced drag spanloading.

3.2 Main Wing Induced Drag Calculation

As a first step to the development of LLT, the induced drag of a single wing-winglet-body was implemented. The dihedral and spanload distribution are defined by the coordinates in the spanload sheet; coordinates that are expressed in the non-planar "η" coordinate system. Let us pose the following axis systems, which will be used throughout the implementation.
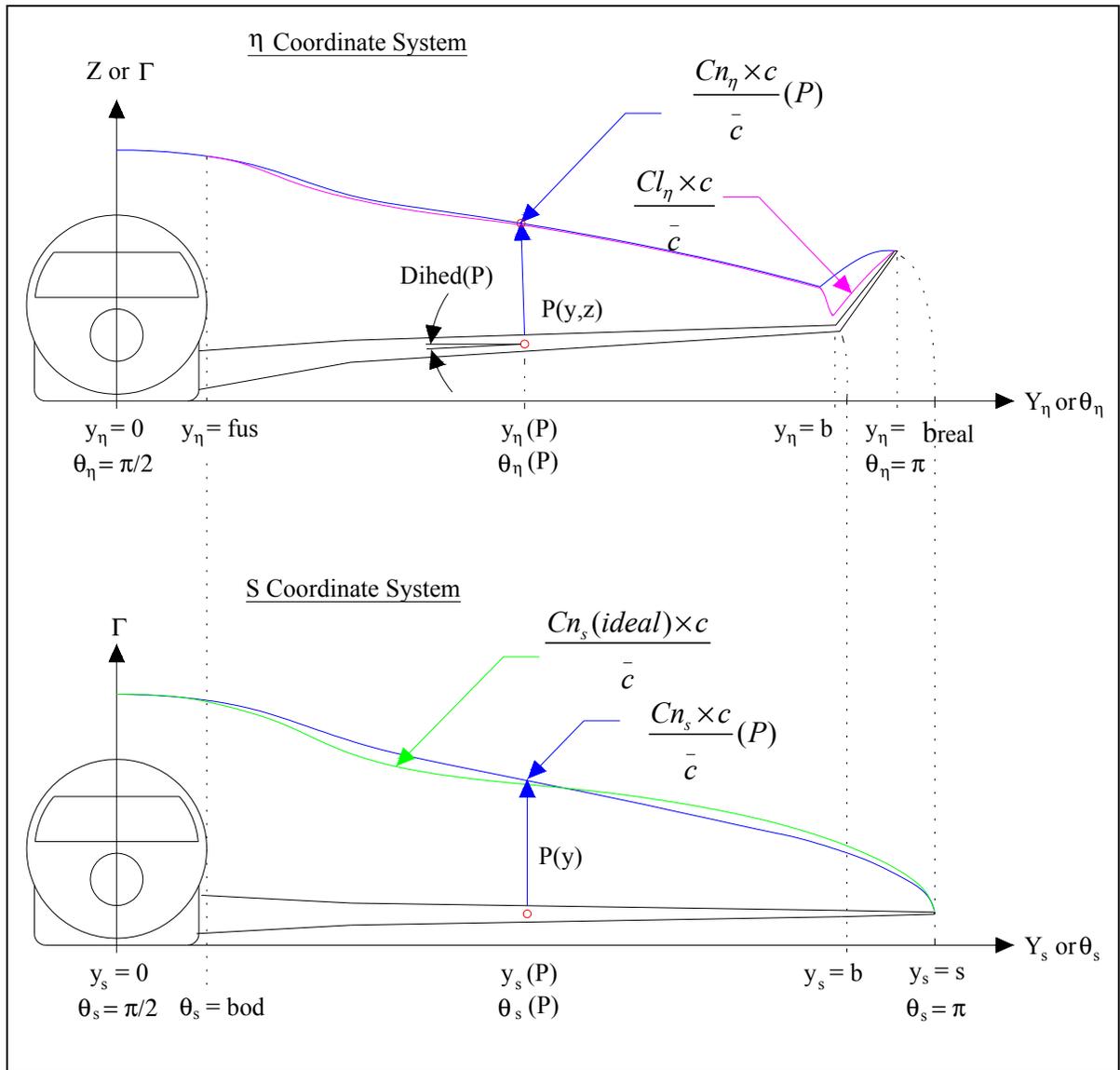
Figure 3.1 Coordinate systems

According to the lifting line theory, the induced drag of a circulation distribution given by a spanload sheet, without considering the fuselage, can be calculated from :

$$Di = \int_{-s}^{s} \rho \omega(y_s)\Gamma(y_s)ds = 8\rho V^2 s^2 \int_{\pi/2}^{\pi} \sum nA_n \sin(n\theta_s) \sum A_n \sin(n\theta_s)d\theta_s \qquad (3.1)$$

To solve this, the normal force coefficients $Cn_y \cdot c/\bar{c}$ given for various span locations by the spanload sheet have to be converted into the "s" planar coordinate system. The length "ds" of a spanwise element "I" in the "s" coordinate system can be defined by:

$$ds(i) = \sqrt{(Y(i+1)-Y(i))^2 + (Z(i+1)-Z(i))^2} \qquad (3.2)$$

or also

$$ds(i) = \frac{Z(i+1)-Z(i)}{\cos(\delta(i))} \qquad (3.3)$$

and $\delta(i)$ being the dihedral of this wing element.

Once the spanload sheet data's have been converted to a planar coordinate system, the corresponding A_n Fourier coefficients can be obtained by curve-fitting a Fourier series over the data. Section 3.2.3 proposes an approach to curve-fit a spanload distribution over input data. However, before this can be done, some adjustments need to be made on the input spanload data concerning the fuselage and the wing tip. As it can be observed on figure 3.2, the data obtained from a spanload sheet is incomplete over the fuselage and tip regions.
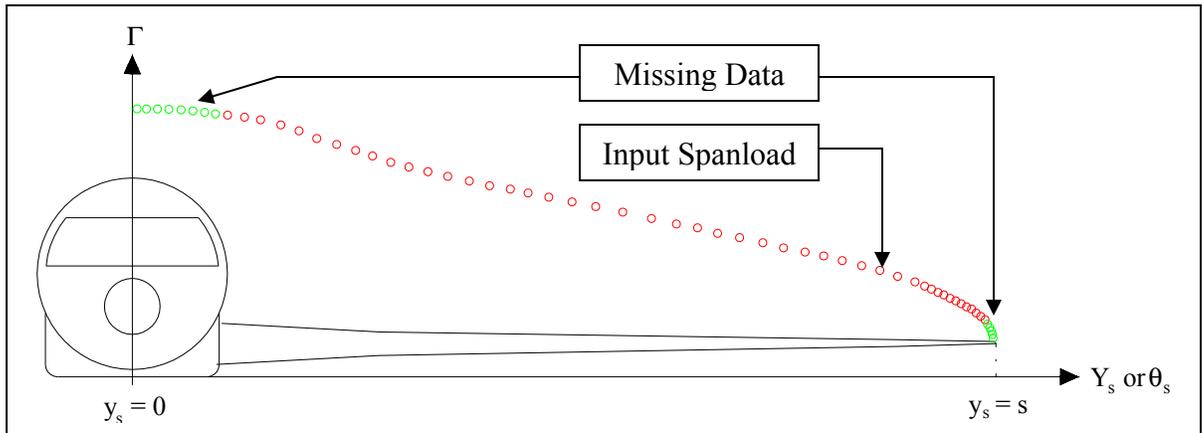
Figure 3.2 Spanload definition by imported and created data points

These missing data points are due to the fact that the spanload sheets are generated from several cut planes over the wing on a CFD solution (red points). Therefore, the extrapolated tip loads and exact tip coordinate "s" are unknown, and some realistic data points (green points) need to be added over the fuselage and the tip regions before proceeding to curve-fitting the Fourier series.

3.2.1 Adding Fuselage Data Points

The missing data over the fuselage was created by using a 2nd order polynomial following an approach developped by Bombardier Aerospace. Figure 3.3 gives a visual example of the created fuselage data points using this methodology. The equation 3.4 defines these points.
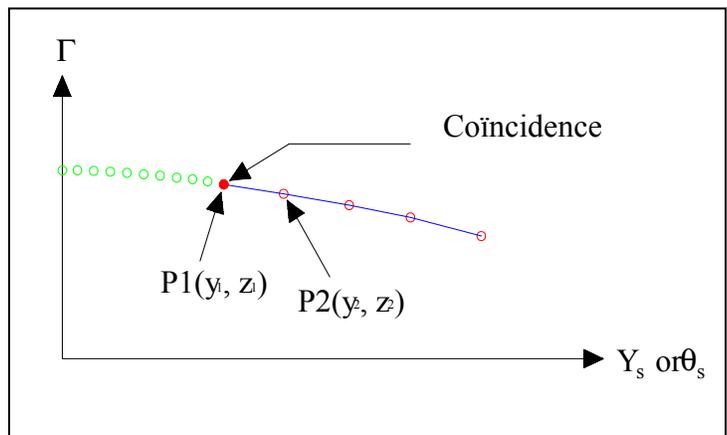
Figure 3.3 Fuselage data completion

$$(Cn \times c / \bar{c})_{ys} = A y_s^2 + B y_s + C \qquad\qquad (3.4)$$

Bombardier's methodology allows to determine the value of the A, B and C coefficients so that the missing lift data over the fuselage represents accurately what it should normally be. This methodology was developped through CFD and wind-tunel testing.

In most cases, this 2nd order approach allows generating fuselage lift data that is very close to the expected values. However, in some irregular cases, a small error can be observed between generated lift data and what should be obtained by an equivalent Fourier distribution. Usually, this error is observed when the lift distribution is constituted of a double curvature, close to the fuselage, which is often the case for canard configuration.
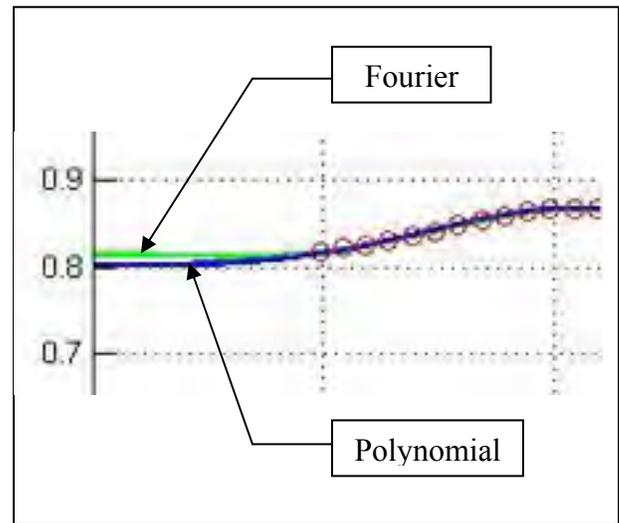
Figure 3.4 Fuselage data error

3.2.2 Adding Tip Data Points

Completing the missing data over the tip was much more complicated than for the fuselage. This is due to two major causes. First: the exact location of the wing tip "s" is unknown from the spanload sheet and has to be estimated. The precision of the "s" span is of primary importance, as it has a great influence on the precision of the drag results. Second: the quality of the fit over the generated data needs to be as realistic as possible. Depending on how much points are created, the fitting of the Fourier curve in the tip region will not be the same. This is also more of a problem since the spanload datas seam to be less consistant approaching wingtip. Since the variation of circulation $(\partial\Gamma / \partial y)\, dy$ is large in this region, a slight variation in the curve-fitting changes the drag results by several drag counts. The method to

complete the missing tip data needs to be robust, so that the drag solution can be trusted without hesitation. However, in this case, robustness usualy means reduced precision. A compromise between precision and robustness has to be made. Five different approaches were investigated individualy and in various combinaitions.

A linear extension of the slope between the last two data points was experiemented in case 1. This approach showed very poor precision, as a very small variation of the slope would influence greatly the s span. Also, some cases have been seen where the slope was positive, which caused result divergence. To counter that effect, a 2nd order polynomial was used in case 2 to force the slope to near infinity at s. The drag results obtained from this method were excellent in some cases, and poor in others, as the quality of the curve-fitting was case-dependant. Since robustness of the resutls could not be taken for granted, this solution was put aside and a third

Figure 3.5 Tip data : Linear extension
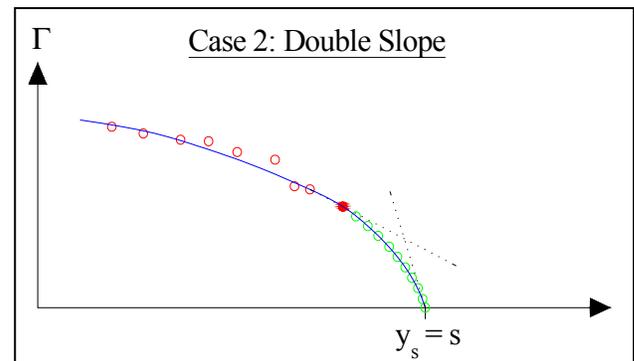
Figure 3.6 Tip data : Double slope

approach was experimented in case 3. The idea here consists in simply duplicating many times the last spanload data point to increase its weight, while approximating s span to the value of the last data point. Drag results were average, within 2 drag counts of the exact solution, with great robustness.
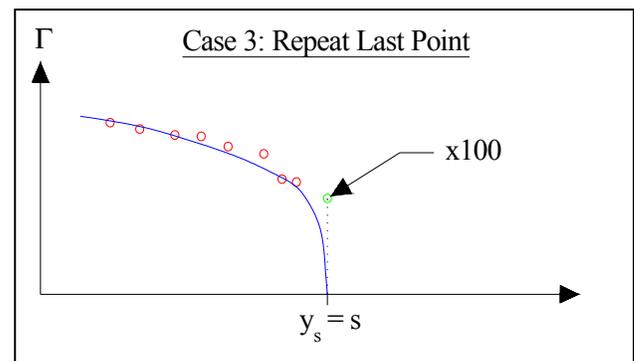
Figure 3.7 Tip data : Last point duplication

The case 4 was investigated by creating additionnal control points in between the few last data points. This approach only returned good results when the last datas were relatively well aligned within each others. As a 5th case, it was

Figure 3.8 Tip data : Add spanload data

experimented to impose the value of the s span and duplicate the last data (s, 0) as in the third approach. This gave good results as long as the span estimation was well made, which is not necessirely easy. As in case 3, the robustness of the fit is excellent. However, the precision of the value of s settles the quality of the drag results. Several combinations of these methods were tried to find the

Figure 3.9 Tip data : Impose span

best compromise between the precision of the drag results and the robustness of the code, notably: case 4 + case 3, case 4 + case 1, case 4 + case 2, case 4 + case 5... It was established through trial and error on various spanload data that the case 3 was a good compromise. It allows for good robustness of the fit and the precision of drag results, which is usually within ±2 drag counts, is satisfactory for conceptual design purposes. The robustness of the curve-fittings is good, as shown on various problematic tip load data in figure 3.10.

Figure 3.10 Tip spanload distribution for various wings (Y axis confidential)

3.2.3   Curve-Fitting the Data

Once the lift distribution data points have been obtained for the whole wing span, a method based on the minimization of the Chi-square (X^2) is used to find the An Fourier coefficients that will fit best the lift data. Since the actual coordinate system is planar, the total normal force over the unfolded wing can be defined by Kutta-Joukowski.

$$\frac{N_s \times c}{\bar{c}}(\theta_s) = \rho v \Gamma(\theta_s) = 4\rho v^2 s \sum A_n \sin(n\theta_s)$$

(3.6)

By making the following substitution into (3.6):

$$N_s = \frac{1}{2}\rho V^2 S_{ref} \times Cn_s$$

(3.7)

the equation of the normal force coefficients is obtained.

$$\frac{Cn_s \times c}{\bar{c}}(\theta_s) = \frac{8s}{\bar{c}} \sum A_n \sin(n\theta_s)$$

(3.8)

The Chi "X" can be defined by the local error between a given function $f(An, \theta_s)$ and its target values, as illustrated on the following figure.
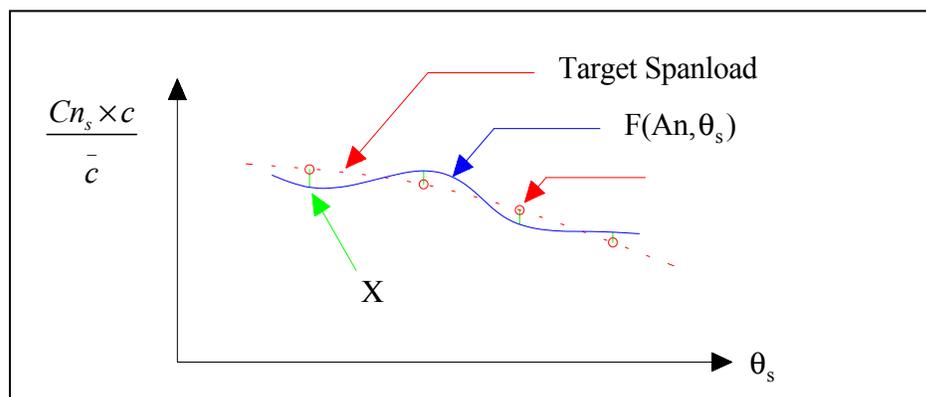
Figure 3.11 Chi (X) of a function to its related data

Therefore, for a given number of data points i, the An Fourier coefficients that fit best the target data are the one that minimizes the total value of X^2 for the whole spanload.

$$X^2 = \sum_i \left(\frac{Cn_s \times c}{\bar{c}}(\theta_i) - F(A_n, \theta_i) \right)^2 = \text{minimum} \tag{3.9}$$

and X^2 is minimum when

$$\frac{\partial X^2}{\partial A_n} = 0 \tag{3.10}$$

By substitution of (3.8) and (3.9) into (3.10), we have

$$\frac{\partial X^2}{\partial A_n} = 0 = 2 \sum_i \left[\sum_n \left(C_{N(\theta_i)} - \frac{8s}{\bar{c}} A_n \sin(n\theta_i) \right) \cdot \sum_m \sin(m\theta_i) \right] \tag{3.11}$$

and the An Fourier coefficients can be isolated.

$$\sum_i \left(\sum_n (\sin(n\theta_i)) C_{N(\theta_i)} \right) = \sum_i \left[\sum_n \left(\frac{8s}{\bar{c}} \sin(n\theta_i) \right) \cdot \sum_m (\sin(m\theta_i)) \right] \cdot A_n \tag{3.12}$$

In the latest equation, m and n = 1,3,5... up to the number of An Fourier coefficients defining the series. (3.12) can therefore be rewritten in matrix format:

$$
\begin{bmatrix}
\sum_i (\sin(1\theta_i)) C_{N(\theta_i)} \\
\sum_i (\sin(3\theta_i)) C_{N(\theta_i)} \\
\sum_i (\sin(5\theta_i)) C_{N(\theta_i)} \\
...
\end{bmatrix}
=
\begin{bmatrix}
\frac{8s}{\bar{c}} \sum_i (\sin(1\theta_i)^2) & ... \\
\left(\frac{8s}{\bar{c}} \sum_i \sin(3\theta_i) \right) \cdot \sin(1\theta_i) & ... \\
\left(\frac{8s}{\bar{c}} \sum_i \sin(5\theta_i) \right) \cdot \sin(1\theta_i) & ... \\
... & ...
\end{bmatrix}
\times
\begin{bmatrix}
A_1 \\
A_3 \\
A_5 \\
...
\end{bmatrix}
$$

This equation has the [A] = [B] × [X] format, with [B] being a Vandermonde matrix. The value of matrix [X], containing the An coefficients, can be solved using a matrix inversion:

$$[X] = [A]^{-1} \times [B]$$

<div align="right">(3.13)</div>

This concludes the curve-fitting methodology. The [X] matrix contains a single column of A1, A3, A5... An coefficients defining the best possible fit of a Fourier series on the spanload data using a least-square method.

The quality of the resulting fit varies depending on the number of An coefficients to fit. The more An coefficients there is, the more flexible the curve becomes. The number of coefficients cannot exceed the number of data points. However, it is not necessarily a good thing to use too much An coefficients since the resulting curve may become too sensitive and diverge on a single point as seen at y=0.98 on figure 3.12.
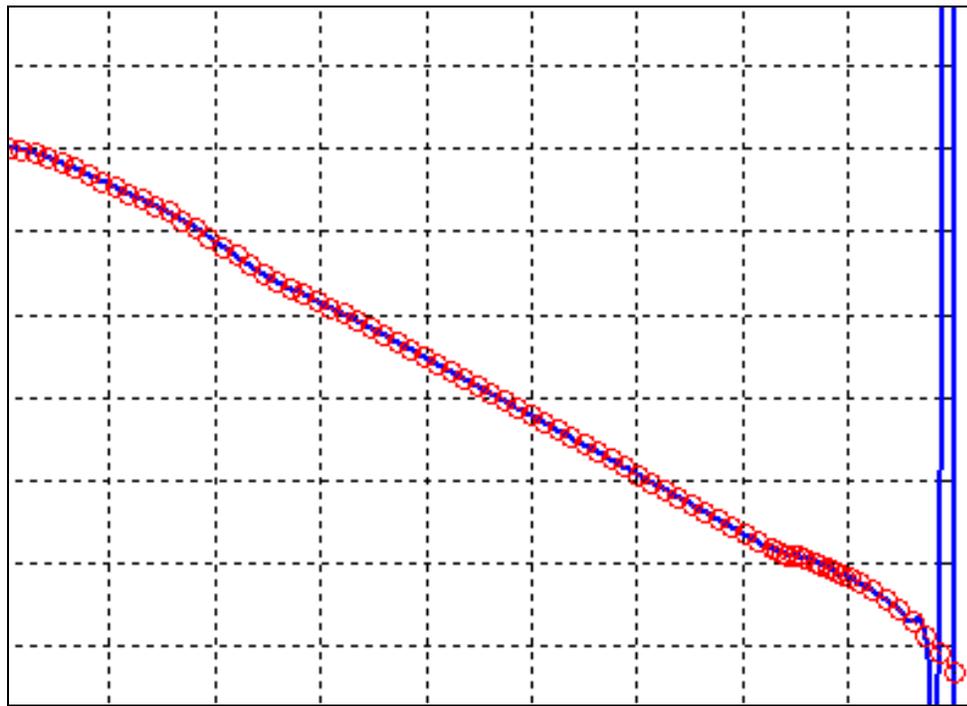
Figure 3.12 Curve-fitting divergence at tip due to excessive number of An coefficients

On the other hand, a sufficient amount of An coefficients are needed to correctly represent subtle variations in the spanloading. Since a sharp spanload variation will have high values of $(\partial\Gamma/\partial y)\,dy$, and therefore a high influence on induced drag, a certain refinement of the Fourier series is necessary to achieve good accuracy.
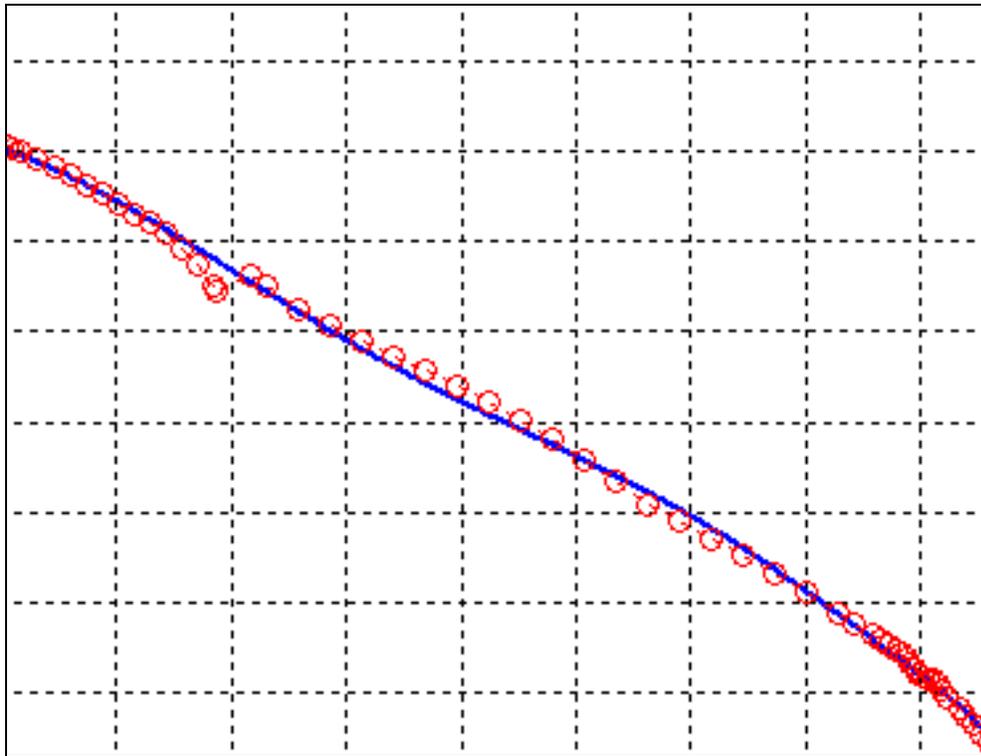
Figure 3.13 Improper assessment of a quick variation in the spanloading at engine or kink position due to insufficient number of An coefficients

After several experimentations on 6 different spanloads, it has been observed that fitting divergence starts occurring when 17-20 An coefficients are used. Also, trying to fit the same spanloads with 10 or less An coefficients results in poor accuracy or no fit at all. Therefore, it seams appropriate to use 15 An coefficients to define the lift distribution, as it is a good compromise between the accuracy of the drag calculations and the robustness of the curve-fitting.

3.2.4   Induced Drag Formulation

Now that the An coefficients that defines the lift distribution are availlable, equation (3.1) can be solved to obtain the complete induced drag of the wing.

$$Di = \rho \int_0^\pi \frac{v \sum nA_n \sin(n\theta)}{\sin(\theta)} \cdot 4sv \sum A_n \sin(n\theta) \cdot s \sin(\theta) \partial \theta$$

$$= 4\rho s^2 v^2 \int_0^\pi \sum nA_n \sin(n\theta) \cdot \sum A_n \sin(n\theta) \partial \theta \qquad (3.14)$$

and posing $S = 2s \cdot \bar{c}$:

$$Di = qSC_{D_i} = \frac{1}{2}\rho v^2 S C_{D_i} \qquad (3.15)$$

The drag coefficient in planar system can be solved:

$$C_{D_i} = \frac{2D_i}{\rho v^2 S} = \frac{8s^2}{S} \int_0^\pi \sum nA_n \sin(n\theta) \cdot \sum A_n \sin(\theta) \partial \theta \qquad (3.16)$$

The drag coefficient needs to be converted into the ESDU standards, in the non-planar coordinate system. Since the total drag remains constant, $Di = \overline{Di}$ and (3.15) is used:

$$qSC_{D_i} = q\overline{S}\overline{C}_{D_i} \qquad (3.17)$$

$$\overline{C}_{D_i} = C_{D_i} \cdot \frac{2s}{\overline{b}} \qquad (3.18)$$

where $\overline{b}$ is the ESDU reference span and $\overline{S} = \overline{b} \cdot \overline{c}$ is the ESDU reference area. The total induced drag coefficient of the wing can therefore be obtained. The only remaining step is to add a correction for the fuselage induced drag.

3.2.5 Fuselage Induced Drag Correction

Several authors have investigated the effect of the lift over the fuselage on the induced drag of a wing. Notably, Zlotnick developed a theoretical methodology to quantify the effect of the fuselage on spanload distribution. However, the major point of interest for this research relies is Multhopp's conclusions (ref. 114) obtained in 1941.

> "...*it is expedient to apply a suitable reduction factor to the total air load distribution or, what is probably better, to subtract a little from the lift over the fuselage.*"

> "*The fuselage influences the wing chiefly through a change of flow velocity in quantity and direction at each wing section. In addition, it forms a fixed boundary, for all supplementary flows induced at the wing.*" (Multhopp, 1941)

From these allegations, it seams plausible to assume that a variation of lift over the fuselage will not affect the lift distribution over the wing, since the fuselage acts as a boundary. It also means that a simple way to correct the drag coefficient of the fuselage is to remove a little lift from it. Therefore, the fuselage drag correction is represented as follows:
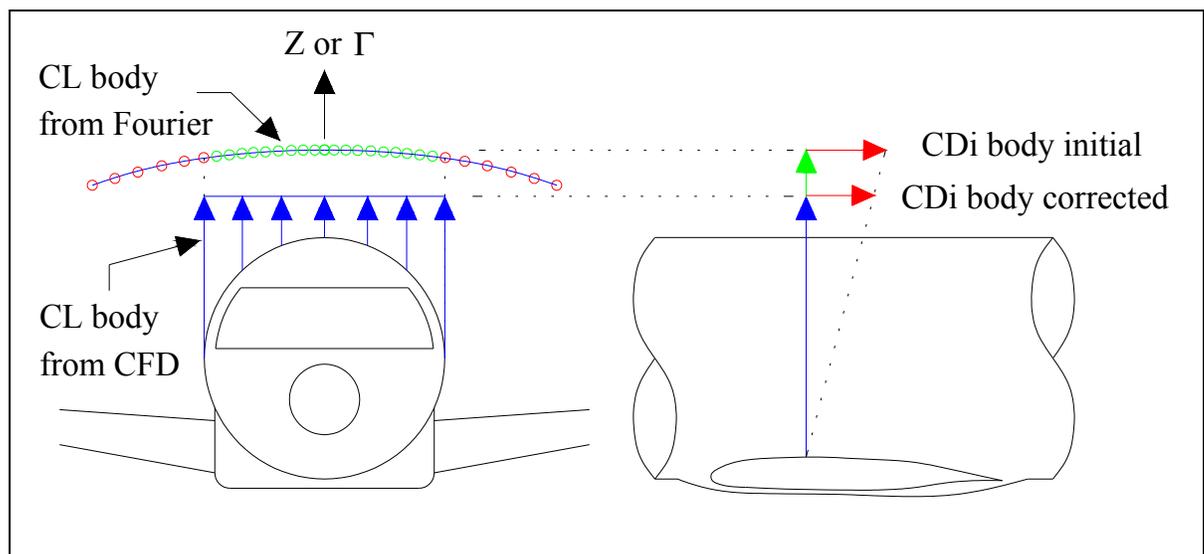
Figure 3.14 Fuselage drag correction

In the previous figure, it is showed that the real lift coefficient over the fuselage (blue) is not the same than the one predicted by the Fourier lift distribution (green). Considering the concepts brought by Multhopp, it can be assumed that the downwash angle over the fuselage will not change even if the fuselage lift coefficient is changed. Therefore, the corrected fuselage induced drag can be calculated by multiplying the ratio of the fuselage lift coefficients:

$$CDi_{body\_corrected} = CDi_{body\_LLT} \times \frac{\overline{CL}_{body\_real}}{\overline{CL}_{body\_LLT}} \tag{3.19}$$

The ESDU $\overline{CL}_{body\_LLT}$ can be obtained from the integration of the lift distribution over the fuselage. Since the lift distribution is almost flat in this region, the integration can be approximated as following:
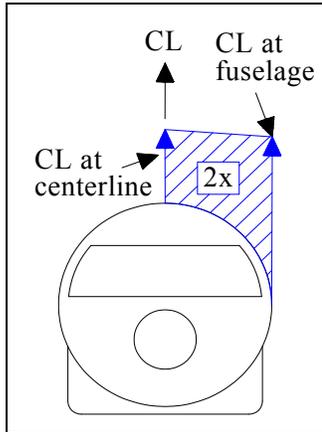
$$\overline{CL}_{Body\_LLT} = \frac{\left(CL_{centerline} + CL_{fuselage}\right)}{2} \times \frac{Diameter}{\overline{b}} \tag{3.20}$$

From the (3.8), the local $\overline{CL}$ over the fuselage is defined by:

$$\frac{\overline{CL}_s \times c}{\overline{c}}(\theta_s) = \frac{16s^2}{\overline{S}} \sum A_n \sin(n\theta_s) \tag{3.21}$$

and θ_s is the position of the centerline and fuselage in s system.

Figure 3.15 Fuselage Lift

As for the $\overline{CL}_{body\_real}$, it can be obtained from a CFD solution or from wind tunnel data as in (ref. 115). A compilation of the results showed in this last reference seem to highlight certain tendencies. For a tube-and-wing configuration with a fuselage of circular cross section having a maximum diameter of about $1/9\ \overline{b}$:

$$\overline{CL}_{Body\_real} \approx 0.52 \times CL_{WingBody} \quad \text{for low wing designs} \tag{3.22}$$

$$\overline{CL}_{Body\_real} \approx 0.65 \times CL_{WingBody} \quad \text{for high wing designs} \tag{3.23}$$

3.2.6   Total Wing-Body Induced Drag

The total induced drag coefficient for the wing-body is the summation of the corrected drag of the fuselage and the drag of the wing alone. Recalling (3.16), the drag coefficient of the wing without the fuselage is obtained by solving the integration from the fuselage to the tip. The solution of this integration is the following, written in 4 terms for clarity, where "fus" is the integration boundary θ_s in polar coordinate in the s axis system.

$$\overline{CD}_i\, wing = \frac{8s^2}{S}\left(Terme1 + Terme2 + Terme3 + Terme4\right) \times \frac{2s}{b} \tag{3.24}$$

$$Term1 = \frac{fus \sum_n nA_n^2}{1}$$

$$Term2 = \frac{\sum_n \left(-\sin(n \cdot fus)\cos(n \cdot fus) \cdot A_n^2\right)}{1}$$

$$Term3 = \frac{\sum_{n,m}\left[\left((n-m)\sin\left((n+m)fus\right) \cdot nm\right)\right]}{1(n-m)}$$

$$Term4 = \frac{\sum_{n,m}\left[\left((n+m)\sin\left((n-m)fus\right) \cdot nm\right)\right]}{1(n-m)} \tag{3.25}$$

$$fus = \cos^{-1}\left(\frac{-Diameter}{s}\right) \tag{3.26}$$

and "Diameter" is the fuselage diameter. Note that n and m = 1,3,5… and $n \neq m$. Therefore, for term 3 and 4, it is convenient to define n and m in a triangular matrix form:

$$n \begin{bmatrix} - & \square & \square & \square \\ - & - & \square & \square \\ - & - & - & \square \\ - & - & - & - \end{bmatrix}$$
$$m$$

By replacing the value of "Diameter" by 0 in (3.26), the drag coefficient of the full lift distribution is obtained. Consequently, the uncorrected induced drag coefficient of the fuselage is:

$$\overline{CD}i_{body\_LLT} = \overline{CD}i_{wing\_body} - \overline{CD}i_{wing} \tag{3.27}$$

By applying (3.20), the fuselage lift coefficient is obtained and the corrected fuselage drag coefficient can be obtained from (3.19). Finally, the total corrected induced drag coefficient of the wing-body is:

$$\overline{CD}i_{wing\_body} = \overline{CD}i_{body\_corrected} + \overline{CD}i_{wing} \tag{3.28}$$

The induced drag of an elliptical spanload of equivalent lift is used as a reference to compute the Oswald efficiency factor "e".

$$\overline{CD}i_{elliptical} = \frac{\overline{CL}}{\pi\,\overline{AR}} \tag{3.29}$$

and the Oswald efficiency factor is:

$$e = \frac{\overline{CD}i_{wing\_body}}{\overline{CD}i_{elliptical}} \tag{3.30}$$

This concludes the calculation of the induced drag of a single non-planar wing with correction for the fuselage.

3.3 Full Aircraft Induced Drag

To compute the induced drag of any three lifting surfaces configuration, we simply apply the multiplane equation (2.52) and substitute the main wing drag by its value:

$$Di_{Triplane} = \frac{L_1^2}{\pi q b_1^2} + \frac{2L_1 L_2 \sigma_{12}}{\pi q b_1 b_2} + Di_{wing\_body} + \frac{2L_3 L_2 \sigma_{32}}{\pi q b_3 b_2} + \frac{L_3^2}{\pi q b_3^2} + \frac{2L_1 L_3 \sigma_{13}}{\pi q b_1 b_3} \qquad (3.31)$$

As in chapter 3, indices 1 and 3 respectively represent the canard and the horizontal stabilizer, as indices 2 refers to the main wing. The canard is displayed in pale blue in the figures. The σ factors are calculated according to the theory of chapter 2.7, allowing for individualization of each lifting surface's drag and their mutual drag coefficients. The following figure illustrates, in the s coordinate system, a specified spanload distribution over a wing with winglets (L_2 = 0.55) that has been unfolded to a planar surface, a lifting canard (L_1 = 0.0275, b_1 = 0.20s, h_1 = 0.09s), a downlifting stabilizer (L_3 = -0.055, b_1 = 0.31s, h_1 = 0.15s) and the system's equivalent elliptical spanload of span $\overline{b}$.
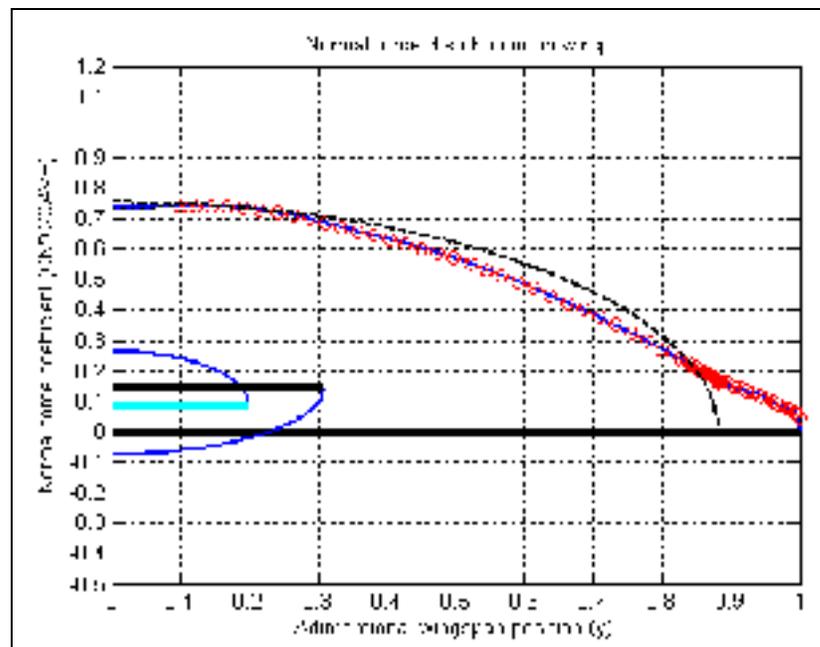
Figure 3.16 Example: Lift distributions of a 3 lifting surfaces configuration

3.4   Minimum Drag Spanloading

The minimum induced drag lift distribution is obtained following Laurendeau's method. The use of equation (2.53) returns the An Fourier coefficients defining the optimal lift distribution adimensionalized in relation to A1, which determines the total area under the spanload curve. The following figure illustrates the minimum induced drag spanloading for the same aircraft configuration defined in the preceding example, with the red line representing the real lift coefficient over the fuselage.
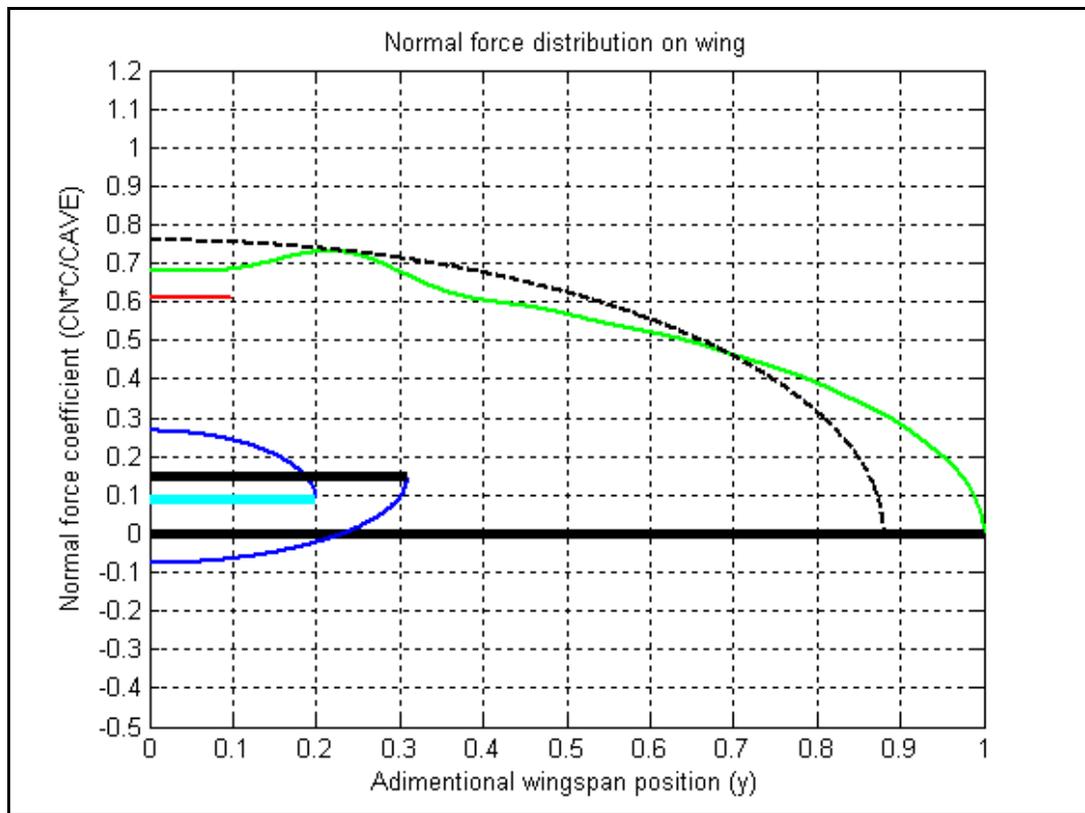
Figure 3.17 Ideal lift distribution of a given 3 lifting surfaces configuration

Once again, we evoke the question of the number of An coefficients to use to have proper representation of the spanload. At first, it seams convenient for programming reasons to use the same amount of An coefficients as for the curve-fitting method. However, as the gap between two lifting surfaces is reduced toward zero, the ideal spanload over the wing tends to show very sharp variations which cannot be properly assessed with only 15 An factors.
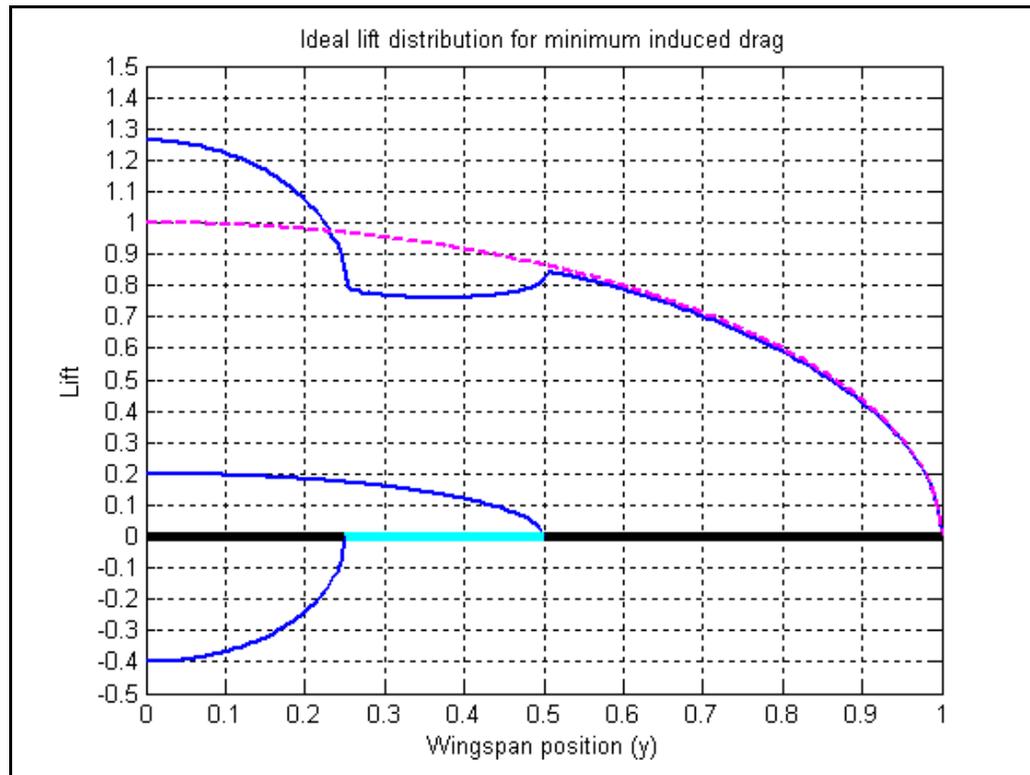
Figure 3.18 Ideal lift distribution for a three surfaces configuration with no gap

In the last figure, 100 An coefficients were required to properly represent the ideal lift distribution. I must underline once again the importance of properly assessing the number of Fourier coefficients to use, as it is of primary importance to the accuracy of the drag calculations and the robustness of the code. In references such as (ref. 105) and (ref. 26), drag results and spanload distributions are published but the number of An coefficients is not mentioned. By comparing results obtained from 4 and 100 An coefficients with figure 4.3.3 from page 73 of (ref. 108), we can observe that this aspect must not be overlooked.
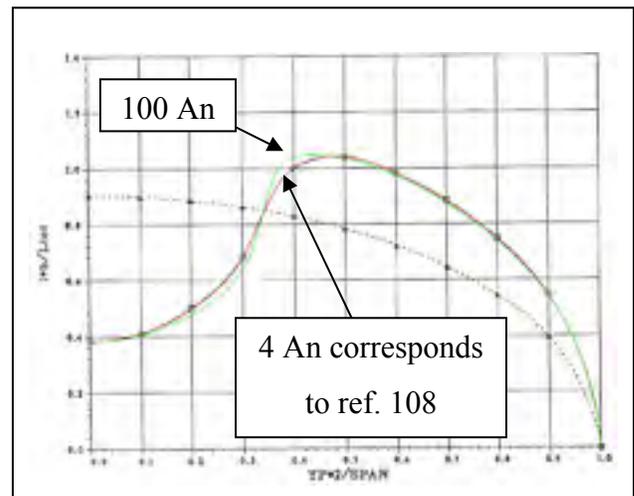
Figure 3.19 Ideal spanload error

The A1 coefficient is particular, since it defines the area under the spanload curve. In a classical planar wing without consideration for the fuselage lift or winglets, the lift of the wing is directly proportional to A1 with equation (2.28). However, in this situation, we have 2 planar lifting surfaces, a non-planar main wing and a specified lift over the fuselage. Therefore, the A1 coefficient needs to be properly scaled so that the total lift coefficient of the aircraft meets the requirement. The total lift coefficient of the aircraft is defined as following:

$$\overline{CL}_{Aircraft} = \overline{CL}_{Wing} + \overline{CL}_{Body\_real} + \overline{CL}_{Stabilizert} + \overline{CL}_{Canard} \tag{3.32}$$

Considering that the wing is non-planar, the lift over a given wing section i is the vertical component of the normal force in relation with its local dihedral angle δ_i, which is obtained from trigonometry using the data from the spanload sheet.

$$\frac{Cl_i \times c}{\overline{c}} = \frac{Cn_i \times c}{\overline{c}} \times \cos(\delta_i) \tag{3.33}$$

$$\delta_i = \tan^{-1}\left(\frac{Cn_{i+1} - Cn_i}{Z_{i+1} - Z_i} \right) \tag{3.34}$$

and Z(y) represent the height of the wing due to its dihedral at a given spanwise coordinate in the η coordinate system. It is believed that a proper mathematical representation of Z(y) would allow for an exact analytical solution of the lift coefficient. However, since such equation is not available, the A1 factor is computed numerically to meet the CL requirement.

CHAPITRE 4

RESULTS AND VALIDATION

4.1 Validation Methodology

The LLT induced drag code was first validated by comparing with Laurendeau's results, without taking into account the fuselage, dihedral and winglets. This first test proves that LLT results are in concordance with Laurendeau's results, which reduces the eventuality of an implementation error in the calculation of the interference factors.

The second test is meant to validate the induced drag calculation for a single lifting surface with dihedral, winglets and fuselage. Several spanload distributions were analysed with a Bombardier in-house code named "CDI". This software reads the same spanload sheets than LLT and makes use of both Multhopp (ref. 114) and Non-Linear Vortex Sheets (ref. 19) methods to compute the induced drag of a single wing with a correction for the fuselage. Therefore, CDI returns 2 results of induced drag. CDI has been validated in the past and constitutes a reliable source of comparison for the induced drag of a single lifting surface with fuselage, dihedral and winglets.

The results from LLT were then compared with CFD for a DLR-F4 wing-body configuration. The code used is called FANSC; it is a structured multi-block finite volume Navier-Stokes solver developed by Bombardier. Detailed information about this code is available in (ref. 83).

4.2   Comparison with Laurendeau's Results

The following figure compares LLT induced drag results with Laurendeau's results taken from figure 4.2.1 of reference (ref. 108). The markers in the graph represent the validation data, while the colored lines show LLT results. The total aircraft CL is kept constant for all cases.
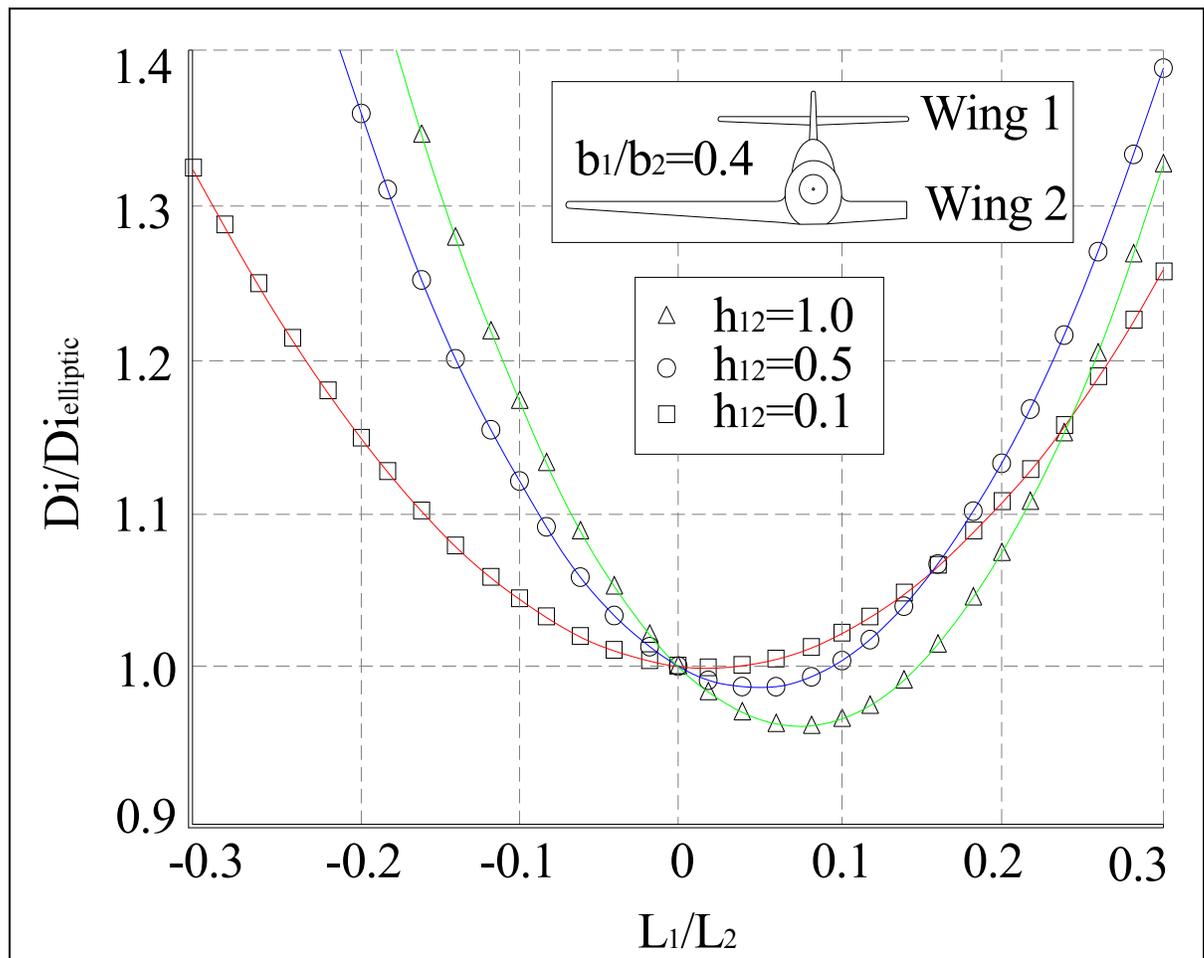
Figure 4.1 Comparison with Laurendeau's figure 4.2.1

It seems quite obvious that LLT results are perfectly matching the validation data. Therefore, it can be considered that the implementation of both codes give identical results. In this analysis, four An Fourier coefficients were used to compute the σ and σ^* factors required for minimum induced drag calculation.

4.3   Comparison with CDI Software

The following figure illustrates the six spanload cases used for validation with CDI.

Case 1		Total CL = 0.45 Body CL = 0.04542	Ref Area = Ref Span =	Proprietary Information
Case 2	Proprietary Information	Total CL = 0.55 Body CL = 0.07605	Ref Area = Ref Span =	Proprietary Information
Case 3		Total CL = 0.50 Body CL = 0.05395	Ref Area = Ref Span =	Proprietary Information
Case 4	Proprietary Information	Total CL = 0.55 Body CL = 0.07941	Ref Area = Ref Span =	Proprietary Information
Case 5		Total CL = 0.55 Body CL = 0.04805	Ref Area = Ref Span =	Proprietary Information
Case 6	Proprietary Information	Total CL = 0.55 Body CL = 0.07611	Ref Area = Ref Span =	Proprietary Information

Figure 4.2 Reference spanload distributions used for validation with CDI

Each one of these spanload distributions was obtained from a Navier-Stokes CFD solution for wing-body-winglets configurations. Every point of the raw spanload data corresponds to a cut plane directly taken from the CFD solution. It is important to mention that none of these spanloadings correspond to an actual "out-of-the-factory" Bombardier aircraft. After running both CDI and LLT codes for all of the six configurations, the following drag coefficients were obtained for wing-body-winglets configurations (Y axis confidential and removed).
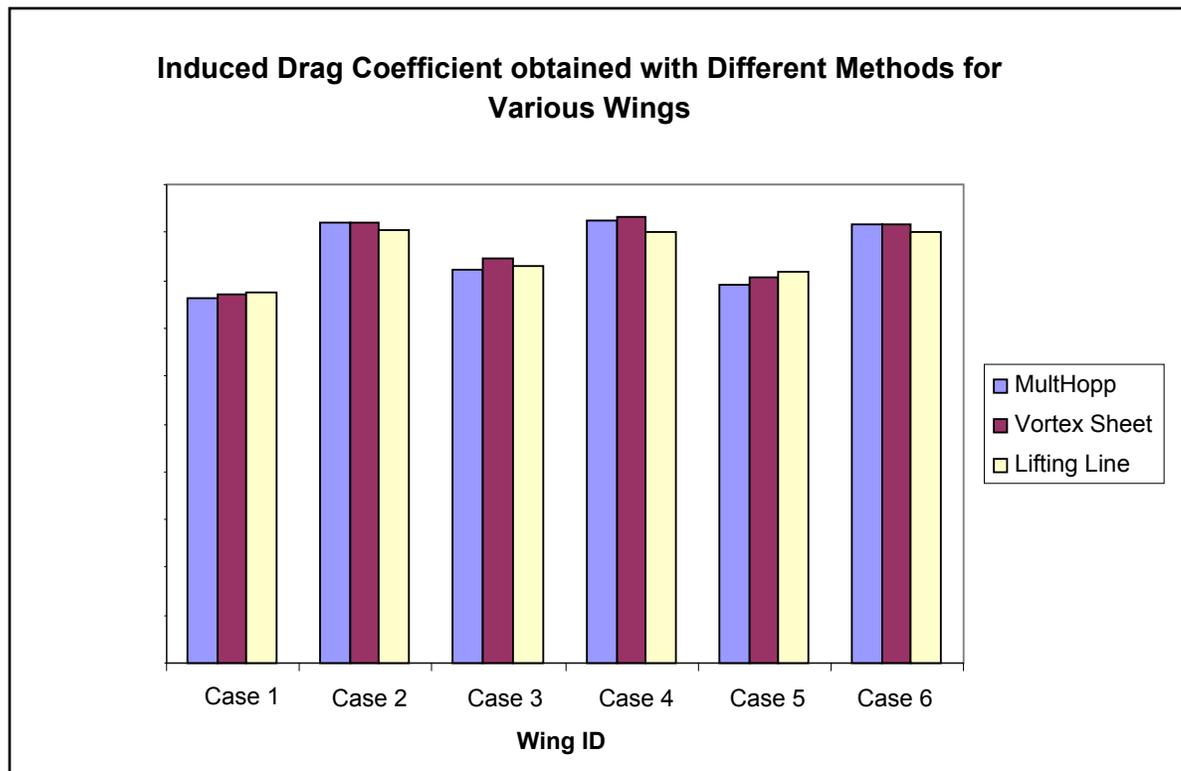
Figure 4.3 Results from CDI and LLT for a single wing with winglets and fuselage

The results for all three methods usually differ one from each other of about one to two drag counts, which is excellent for rapid computation tools. A private communication with Eric Laurendeau allowed discussion of these results. The conclusion was that it would actually be difficult to say which method is the most accurate. However, a simple observation is obtained from these test cases: LLT shows good accuracy for the calculation of the induced drag of wing-body-winglets aircraft configurations, with a precision of about two drag counts.

4.4   Comparison with FANSC

The name "FANSC" stands for "Full Aircraft Navier-Stokes code". It is a structured multi-block finite volume solver which was developed in house at Bombardier Aerospace under a multi-year defense-industry joint research program. Reference (ref. 83) contains more information about the code's flow solver, acceleration techniques, boundary conditions and turbulence models.

In the scope of this work, FANSC was used to compute aerodynamic flow on a DLR-F4 wing-body configuration. All required dimensions and geometry definition for the DLR-F4 test case is available in reference (ref. 50). The results obtained from these simulations provided two validation methods for the LLT software.

1. FANSC has a built-in induced drag calculation module, which provides a direct comparison source to validate LLT;
2. It will be shown that pressure drag results obtained from Euler simulations can also provide a proper source of validation to compute the induced drag of an aircraft. This method could prove useful to decompose the CFD drag results of a more complex, more complete aircraft configuration in order to isolate the lift induced drag.

Before starting any comparative analysis with LLT, FANSC's results for the DLR-F4 wing-body configuration were compared with wind-tunnel data coming from three different tunnels: NLR, ONERA and DRA. Walters documents the accuracy of these tunnels in reference (ref. 78). The following figure represents the drag polars coming from all three wind-tunnels, a FANSC Navier-Stokes solution and a FANSC Euler solution, on which a zero-lift drag coefficient (CDo) of 0.0175 has been added. The flow condition is the following: a Mach number of 0.600 and a Reynolds number of 3.0 E6.
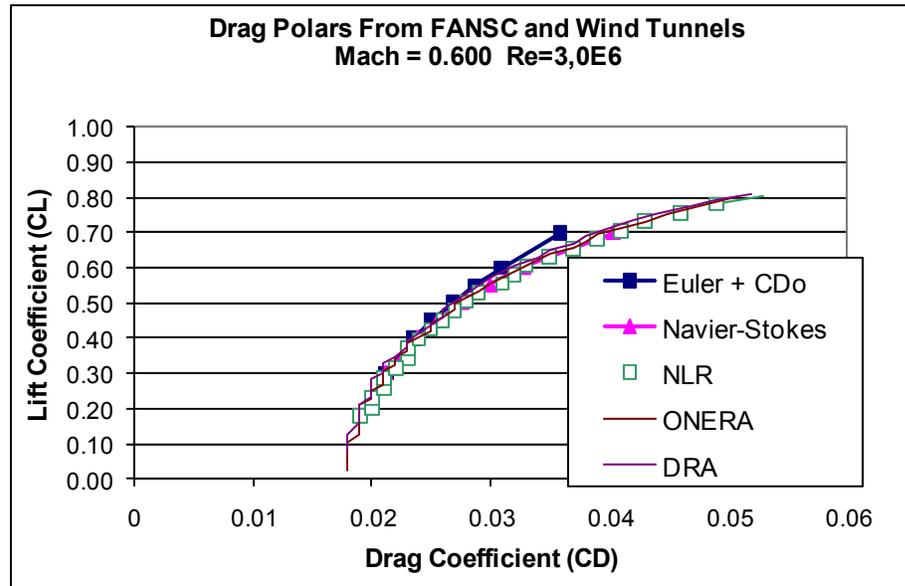
Figure 4.4 Drag polars for DLR-F4. Results from FANSC, NLR, ONERA and DRA

One can observe that both Navier-Stokes and Euler results are concordant with the wind-tunnel data for lift coefficients between 0.3 and 0.55. However, for CL's over 0.55 the Euler solution tends to underestimate the drag. This may be caused by the appearance of small shockwaves at higher CLs or to some boundary layer separation which Euler solutions cannot model. A close-up of the wing root in the Navier-Stokes solution confirms this hypothesis.
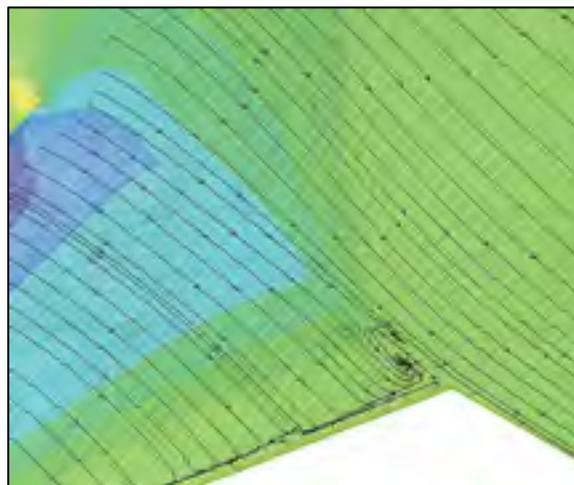
Figure 4.5 Flow Separation at root

The following figures represent the meshes used for the Euler simulations and the resulting pressure plot.
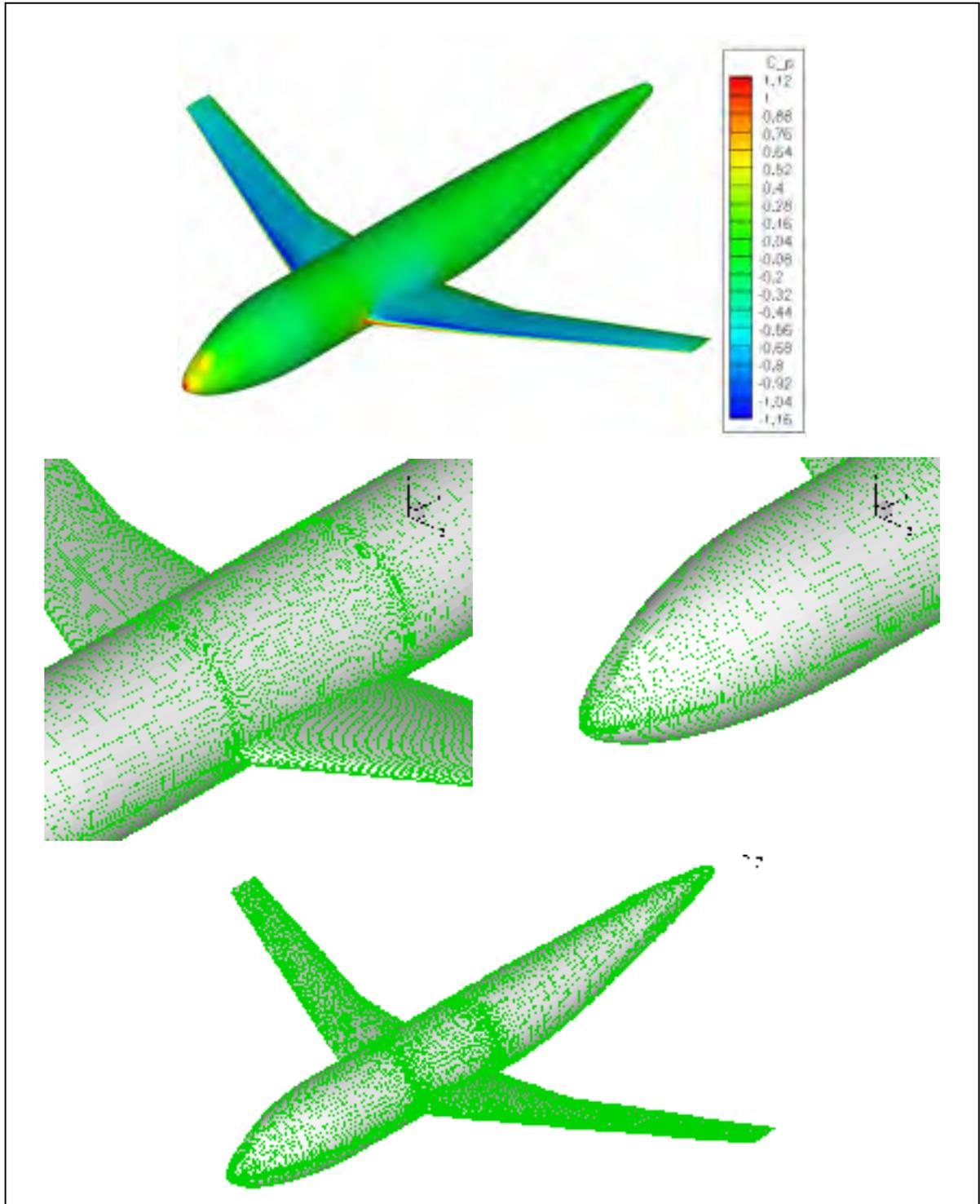
Figure 4.6 DLR-F4: Pressure plot and meshes used for FANSC Euler simulations

The following figures represent the meshes used for the Navier-Stokes simulations and the resulting pressure plot.
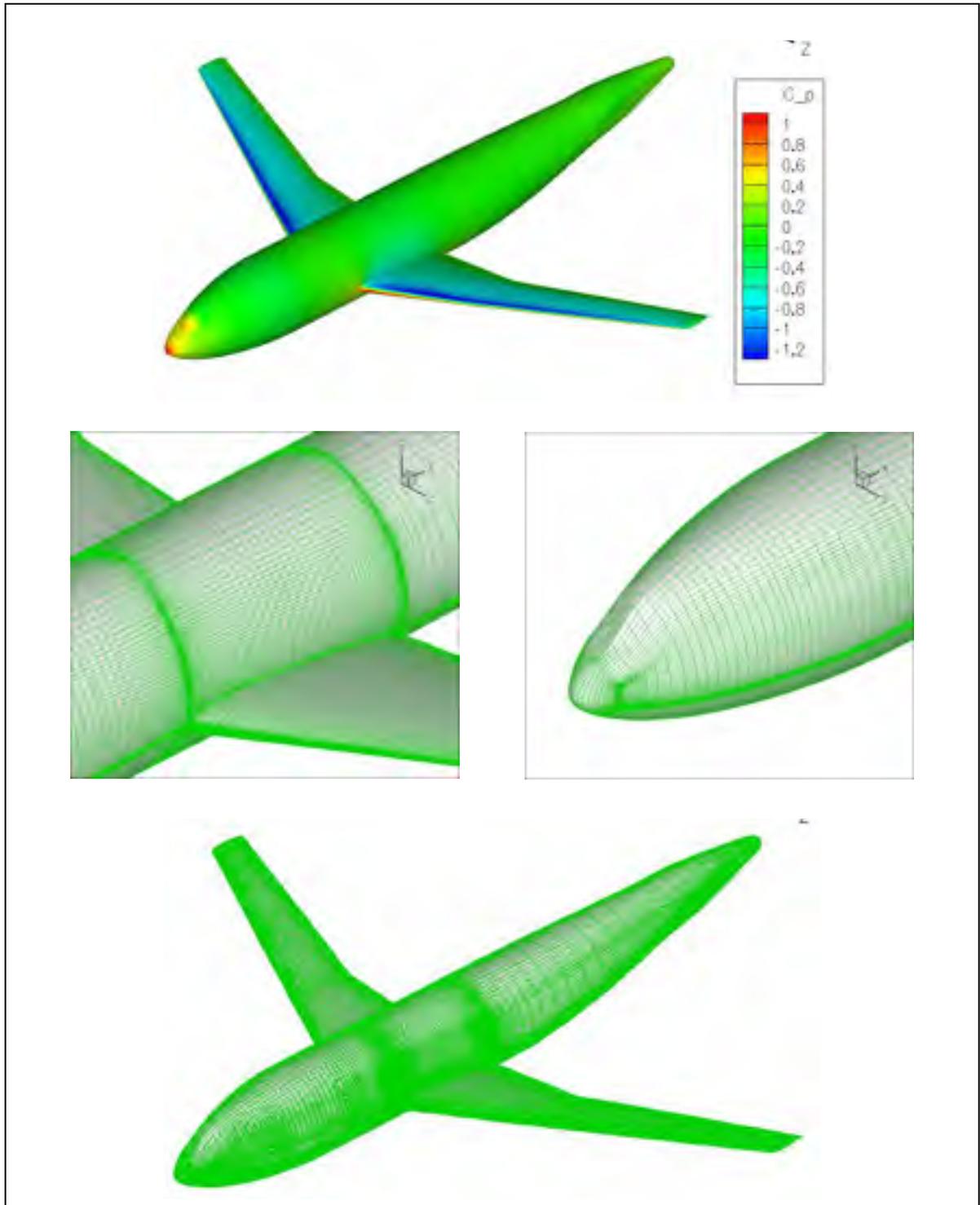
Figure 4.7 DLR-F4 : Pressure plot and meshes used for Navier-Stokes simulations

As a last step before presenting the results, a method to obtain the Oswald efficiency factor "e" from a drag polar of pressure drag coefficients is presented. The objective of this approach consist in minimizing computational cost, since if the induced drag efficiency of an aircraft can be obtained from Euler simulations instead of Navier-Stokes, valuable computational time will be saved as an Euler solution can be obtained in a few minutes, while it takes several hours for Navier-Stokes. One could also mention the fact that creating a mesh for Euler simulation purpose is much simpler than creating a Navier-Stokes mesh. The following figure shows the drag polars obtained from FANSC Euler and Navier-Stokes analysis of the DLR-F4 configuration. Of course, since Euler simulation is non-viscous, a portion of the pressure and friction drag does not appear in the results, which explains the offset separating both polars. However, it can be observed that both polars follow the same path as the lift coefficient increases. In other words, even if the absolute value of CDp is different from Euler to Navier-Stokes solutions, the variation of CDp in function of the variation of CL is very similar for both computational methods.
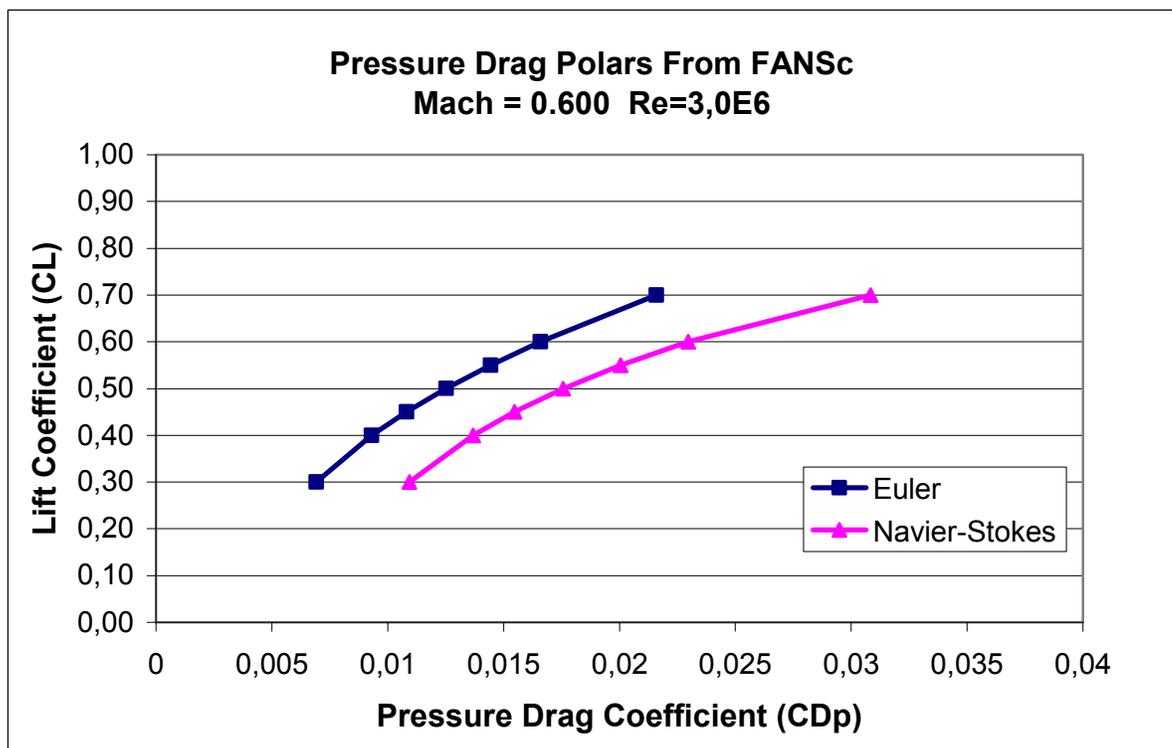
Figure 4.8 DLR-F4 pressure drag polars from Euler and Navier-Stokes solutions

Starting from this observation, the following assumptions are made:

1. Assuming that the airflow is attached all over the aircraft (mostly);
2. Assuming that there is no shockwave;
3. Assuming that the Oswald factor "e" does not change for small variations of the CL.

In these conditions, for a given lift coefficient, the pressure drag coefficient is defined by:

$$\overline{CD}p = \overline{CD}p_{aircraft} + \overline{CD}i = \overline{CD}p_{aircraft} + \frac{\overline{CL}^2}{\pi e \overline{AR}} \qquad (4.1)$$

If conditions 1 and 2 are respected, one can pose:

$$\frac{\delta \overline{CD}p}{\delta \overline{CL}} = \frac{\delta \overline{CD}i}{\delta \overline{CL}} \qquad (4.2)$$

This equation means that if assumptions 1 and 2 are valid, the variation in pressure drag is equal to the variation of induced drag when the CL changes. Adding assumption 3 to this latest statement, the Oswald factor "e" can be solved by using two points on the drag polar.

$$\overline{CD}p_2 - \overline{CD}p_1 = \frac{\overline{CL_2}^2}{\pi e \overline{AR}} - \frac{\overline{CL_1}^2}{\pi e \overline{AR}} \qquad (4.3)$$

$$e = \frac{\overline{CL_1}^2 - \overline{CL_2}^2}{\pi \overline{AR}\left(\overline{CD}p_1 - \overline{CD}p_2\right)} \qquad (4.4)$$

Of course, the drag polars should be computed at a Mach number sufficiently low to insure that no shockwave will appear. In this particular case, a Mach number of 0.600 was selected. Using this approach, the induced drag is obtained from an Euler solution, saving a lot of computational time. The following figure illustrates the value of the Oswald factor "e" obtained from the CDp polars, the FANSC induced drag module and the LLT software.
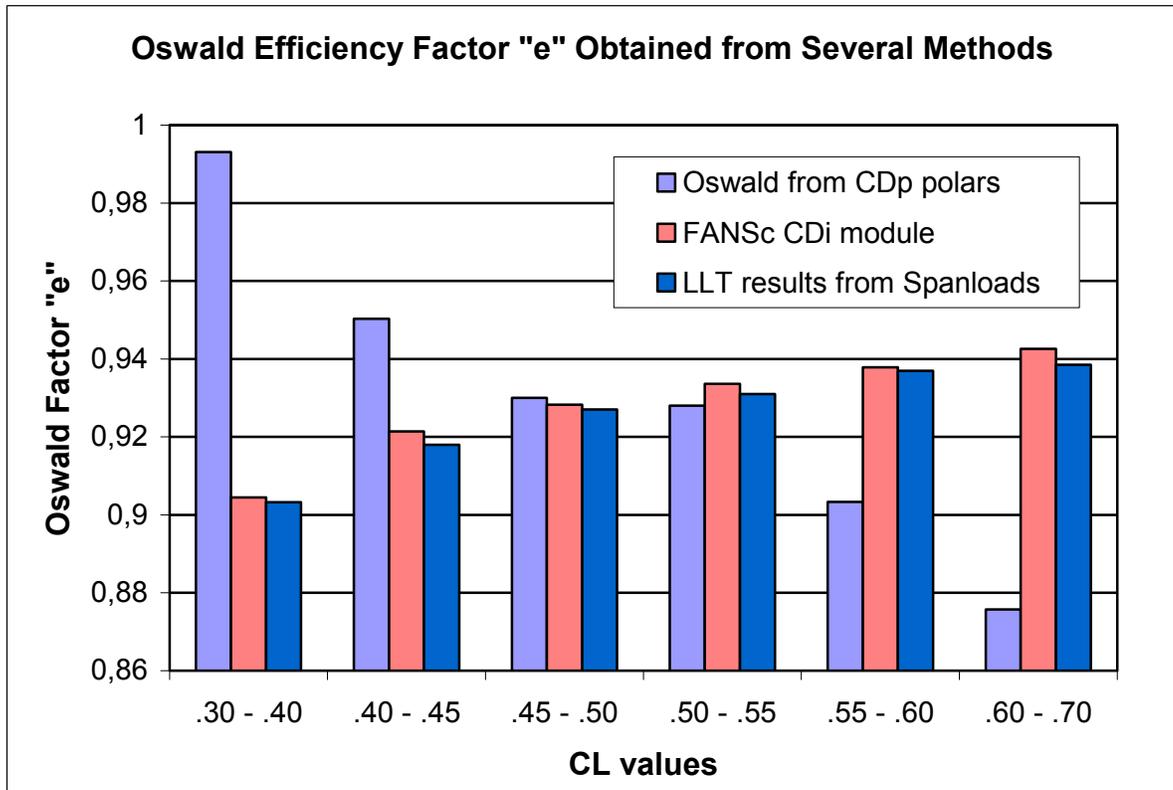
Figure 4.9 Oswald factor in function of lift coefficient obtained by several methods

The results obtained from LLT and from FANSC's induced drag module are quite consistent independently of the lift coefficient. The average error between those two codes is in the order of 0.2%. Somehow, LLT seams to compute Oswald factors that are slightly lower than the ones obtained from FANSC; a tiny variation that seems to constantly repeat itself independently of the CL. This similitude between these two codes was expected since FANSC's induced drag module also uses a lifting line approach with a correction for the fuselage. The potential sources of errors in LLT will be discussed deeper in the next chapter of this work.

Another interesting fact to observe here is the overall similarity in the results obtained from all three methods when the CL ranges from 0.45 to 0.55. Such lift coefficients correspond to the design cruise condition of the aircraft. This implies that the approach to determine the Oswald efficiency factor from pressure drag coefficient is actually quite accurate for cruise

cases. This makes sense since in cruise configuration, the airflow around the aircraft is mostly attached and the zero-lift drag coefficient of the aircraft remains mostly the same for these lift coefficients. These results seem to confirm the assumptions made before. However, further investigation should be made before jumping to conclusions.

This concludes the validation of LLT for the single lifting surface cases. Results have shown to be accurate for wing-body-winglets configurations. Nevertheless, since induced drag results are available from LLT for multiple lifting surfaces configurations, it is deemed necessary to try to compare those numbers with the ones obtained by various authors. Even if this exercise does not constitute a solid validation of the method, it can still provide interesting information about the soundness of its results.

4.5   Multiple Lifting Surfaces: Comparison with Various Authors

Without disposing of CFD or wind-tunnel data, a robust validation of LLT for the induced drag of multiple lifting surfaces is very difficult. Even if it has been show that LLT gives similar results than Laurendeau, Kroo and CDI, it does not validate the methodology for the drag results of more than one wing. Other authors such as Grasmeyer (ref. 60), Blackwell (ref. 99), Lamar (ref. 61), Henderson (ref. 102) and Löbert (ref. 72) have all published various methodologies for induced drag calculation, but none of them can constitute a solid comparison source since some of these methods analyze only one wing at the time, others don't consider the fuselage or the winglets, or simply their methods are based on a variation of the lifting-line theory, which would directly result in very similar results than LLT. Feistal (ref. 82) have shown by experiments on a wing-canard combination (without fuselage) that the Prandtl-Munk theory overestimates the total induced-drag by about 10% for such configuration, finding supported analytically by Kroo in ref (ref. 26). However, since the lift distribution over the wing was not published, LLT cannot be used to confirm their results. Since the purpose of a validation consists in demonstrating the true robustness on an approach, only by comparing with solid data can LLT's results be evaluated.

A potential validation approach could consist in comparing LLT to CFD or wind-tunnel data obtained from literature. In order to perform a proper comparison, the data would have to include:

1. Solutions for one, two and three lifting surfaces configurations with fuselage;
2. The drag polar for a Mach number where no shockwaves can appear;
3. The measurement of the lift over the fuselage;
4. The lift distribution over all lifting surfaces.

Using this data, the induced drag of the test model could be computed from the drag polar. Using the methodology presented in the previous section of this work. LLT would then compute the induced drag using the lift distribution over the wing, and using the relative lift

fraction over the canard, stabilizer and fuselage, the induced drag of the whole aircraft would be obtained and compared with source data. An effort has been deployed to find such data source. Notably, Ostowari (ref. 20) did wind-tunnel testing for a two and three lifting surfaces Learjet at transonic speeds. However, the spanload distribution is not published by the author, which does not allow LLT to compute proper induced drag values.

Another publication coming from Sacco and Lanari (Piaggio Aero Industries, ref. 11) contained wind-tunnel data for the Piaggio P-180 Avanti aircraft, a three lifting surfaces light business jet. While the lift distribution over the wing is available in their work, it did not include either the drag polar for the whole aircraft or the induced drag.

Finally, the reference (ref. 57) from Piperni contains both the spanload distribution and the drag polar obtained from CFD. However, the simulations were made at a high-cruise speed of Mach 0.80. At such speeds, shockwaves might appear at various places on the aircraft, which renders the methodology to obtain the Oswald factor from the drag polar unusable.

Considering the absence of comparative data to validate LLT's drag calculations for multiple lifting surfaces configurations, it was decided that such study would be left for someone else to work upon. However, an interesting investigation that can be done consist in comparing LLT's ideal lift distribution obtained from Laurendeau's method with the ideal spanloading obtained from other authors.

The minimum induced drag spanloading computed from LLT is not necessarily the best spanload distribution for the overall performances of an aircraft. This subject was first brought forward by Prandtl in 1932 as discussed in the literature review (ref. 35). The best aircraft design is the one that maximizes performances for a given mission. To achieve such results, the designer has to make some trade-offs between various disciplines. The problem with the minimum induced drag spanloading is that it distributes a large amount of the loads near the tip of the wing; loads that induce a significant bending moment at the root of the wing resulting in increased structural weight. As discussed in chapter 2 of this work, a

compromise has to be made between wing weight and spanloading to maximize the overall performance of the design. In order to obtain LLT's ideal spanload for a conventional configuration, the test case 3 (figure 4.2) was used since this spanload distribution is optimized for a 0.309 span downlifting tail. In order to estimate the downforce applied by the tail, the latest was iterated until the area under the ideal lift curve equaled the one under the input spanload. The following figure illustrates the total aircraft spanload distribution.
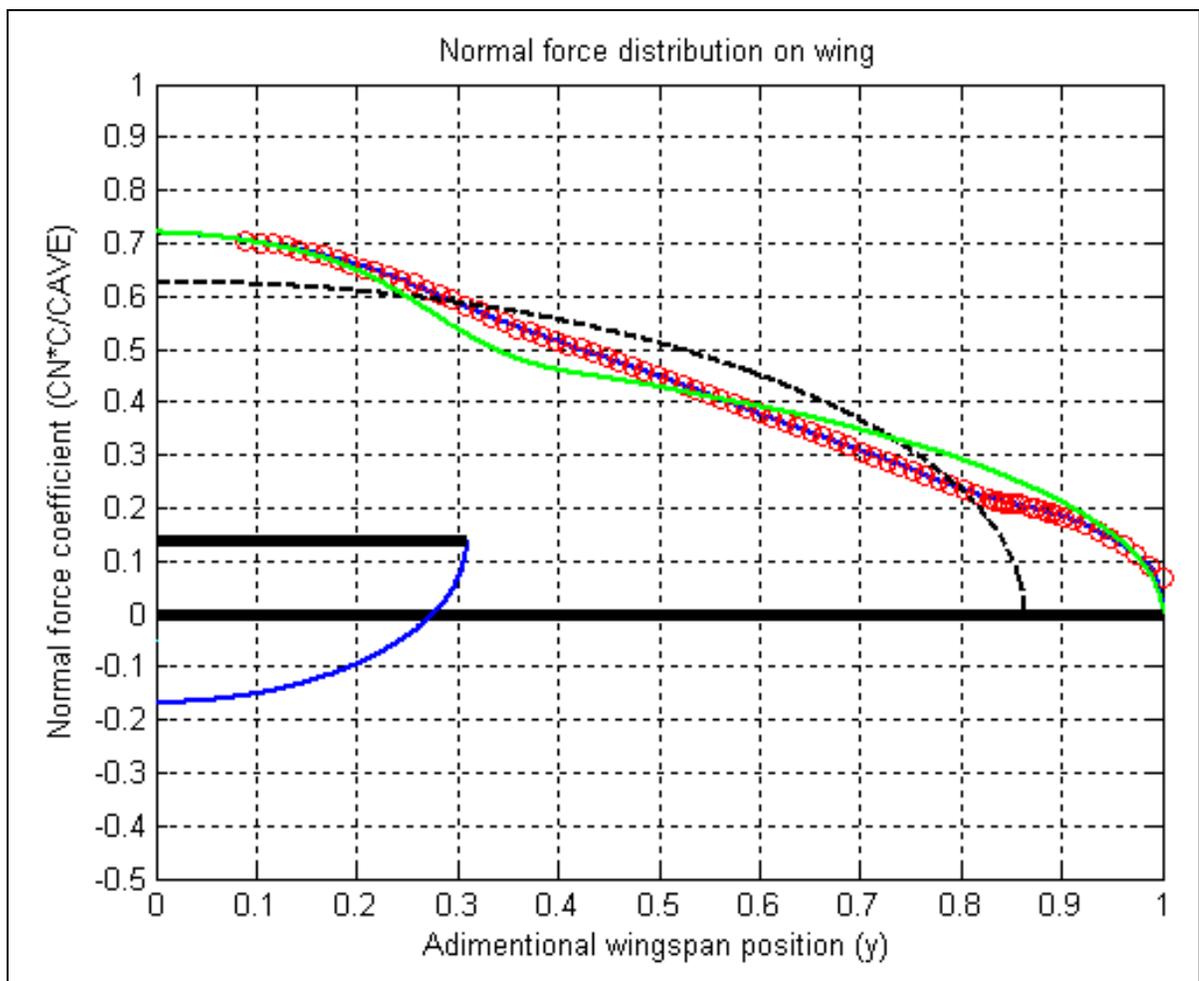
Figure 4.10 Wing and tail spanloadings representing the Case 3 aircraft

An example of the LLT outputs for this full-aircraft analysis is available in Annex I.

As a next step, the ideal lift distribution obtained from LLT is compared with the ones published by various authors. With the exception of the elliptical lift distribution, all the spanloads represented in the following figure have been scaled properly so that the total area under each curve is the same. This allows for a quick visual comparison between authors, but it does not mean that all wing represented here have the same lift coefficient, since some of them have dihedral and winglets while others are planar.
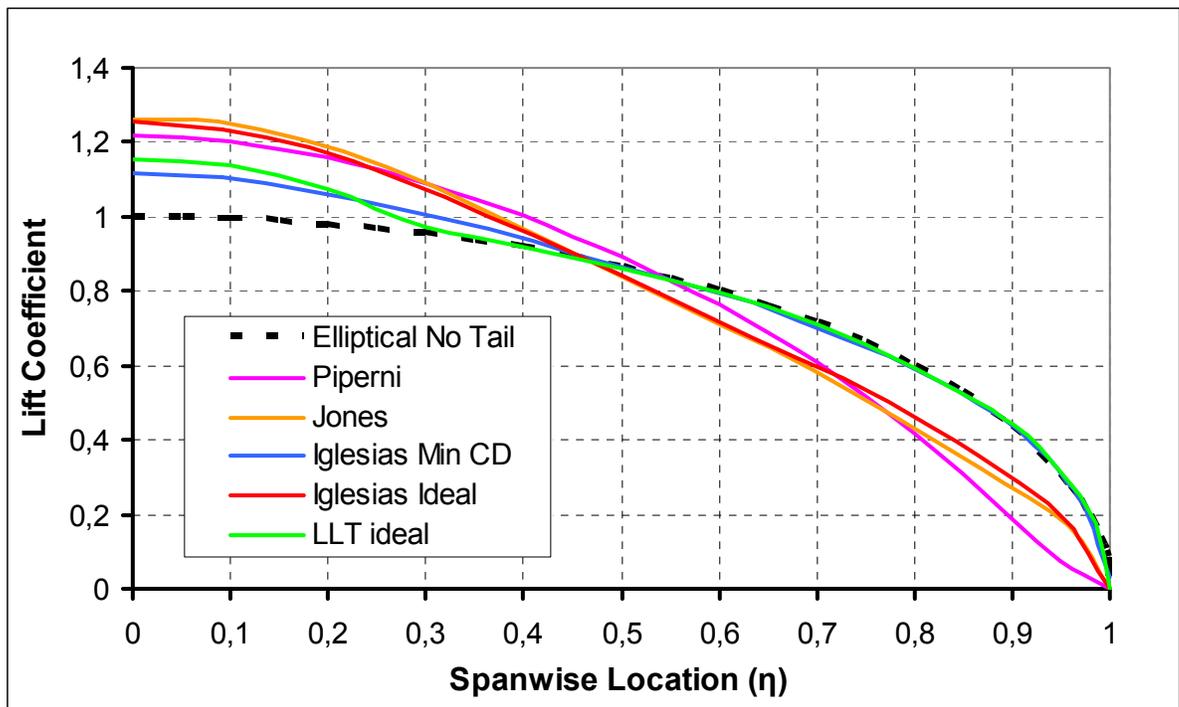
Figure 4.11 Ideal spanload distributions from various authors

The references relating to these spanloads are the following:

- Iglesias and Mason: Reference 109 (2001, p. 7)
- Piperni: Reference 57 (2007, p. 14)
- Jones: Reference 101 (1950, p. 14)

Observing these curves, it is interesting to see that LLT's minimum drag spanload is very similar to the one obtained by Iglesias and Mason. Both these spanloads tend to follow an elliptical lift distribution until they get close to the fuselage, where the interference with the tail becomes influent.

As of the three other curves, they tend to show a reduced loading near the tip to decrease wing weight, resulting in a more triangular spanload shape. As discussed before, such design compromise results in an aircraft weight reduction that justifies the increase in induced drag. The development of a methodology to convert LLT's minimum drag spanloading into a more realistic triangular distribution could constitute an interesting research subject in the future.

This concludes the validation of the LLT code, at least for what concerns this work.

CHAPITRE 5

DISCUSSION

5.1 Sources of Errors for LLT Induced Drag Calculation

Several factors may affect the accuracy of LLT's induced drag calculation. In order to keep this section relatively lightweight for the reader, sources of errors are discussed in a straightforward manner. For the few points that require additional development, subsections are added after this one to refine the discussion:

1. The lifting line theory on which LLT bases its induced drag calculation is a planar method on the physical point of view. Even if non-planar wings can be analyzed by LLT, the method remains planar. Several authors have developed non-planar methods to refine the lifting line theory, but as the comparison with CDI showed, the influence of vortex roll-up on the induced drag calculation is minimal. Section 5.2 assesses this subject more deeply, but it seems apparent that the variation in results related to such approach is beneath calculation incertitude showed in figure 4.3.

2. When calculating induced drag from a CFD Euler drag polar, the Mach number must be selected so that no shockwaves appear. Section 5.3 shows that any Mach number between 0.30 and 0.6 can result in similar pressure and induced drag computation.

3. When spanload data is imported for drag analysis, LLT adds dummy data to complete the definition of the spanload and curve-fits the data points using a least-square approach. The number of An Fourier coefficients influences the quality of the curve-fitting, especially at the tip, and therefore influences the drag results. Throughout this work, 15 An factors were used. Section 5.4 shows graphically why such number allows achieving appropriate accuracy while insuring fit robustness.

4. As demonstrated in chapter 3, the curve-fitting is never perfect. This induces an error on the lift coefficient of the fitted Fourier series lift distribution, since the area under the fitted curve slightly differs from the lift coefficient obtained from CFD. There is also a possibility that the Euler solution for pressure drag differs from the Navier-Stokes solution. It is showed in section 5.5 that the CL and CDp errors induce very small variation on the calculated induced drag coefficient.

5. The spanload data, as precise as it may be, comes from cut planes from a CFD solution. Therefore, it is not information-relevant to create a cut plane at the exact tip coordinate of the CFD model. Several methods to create the missing tip data have been tested in this research, which results in an imperfect location of the exact wingtip location. This problem has been assessed in a previous section of this work, but it might be the source of the fact that LLT gives smaller results than FANSC. If FANSC uses the last spanload data point as being the tip location, LLT will inevitably have a slightly longer span for the drag computation. Longer spans, even if it is only a fraction of an inch will result in a lesser induced drag calculation.

6. In the case of a multiple lifting surfaces configuration, one must keep in mind that the lift distribution over the canard and the stabilizer is considered elliptical, which might not be the case for a real aircraft. However, only an exhaustive validation of LLT for multi-surfaces cases could allow quantifying this error on the overall induced drag.

7. The method proposed in this work does not include any compensation for the effect of the fuselage on the canard and stabilizer. Once again, only a complete validation could determine if such assumption would constitute a significant source of error.

8. In the test case 5 (4.2) a special error occurs: the ideal lift distribution generates more drag than the initial spanload data, which makes no sense! This error is caused by the fuselage drag correction and is discussed is section 5.6.

5.2   Influence of the Vortex Roll-Up in Induced Drag Calculation

The following authors have all invested efforts in the use of non-planar techniques for the computation of induced drag. Their conclusions are concordant one from each other: vortex roll-up has a very small influence on the induced drag coefficient of a given wing. Validation with CDI code also confirmed this fact. A suggestion for additional research is made concerning the vortex model used by LLT. It could be interesting to investigate the use of a different vortex model in the lifting line theory. Instead of using Biot-Savart vortices, Kaufmann (ref. 58), Rankine (ref. 7) or Hallock-Burnham (ref. 7) vortices could be used. This could allow removing the singularities at the tip of each wing currently present with the use of Biot-Savart. The following authors used vortex roll-up and achieved conclusions:

- Kroo (ref. 18) proposes to compute induced drag with non-planar and deformed wakes using a lifting surface method. He concludes that the wake deformation has little effect on the induced drag of a single element wing, but introduces first order corrections to the induced drag of a multi-element lifting system. While lifting line theory predicts minimal induced drag with an elliptical wing planform, lifting surfaces does not. The real ideal wing is slightly more loaded to the tip, which results into a 1-2% drag reduction compared to the elliptical distribution.

- Eppler (ref. 19) proposes to replace the free single vortices of a numerical lifting line by a vortex sheet model similar to CDI code. He obtains results of induced drag 1.3% smaller when including vortex roll-up to a theoretically ideal elliptical solution obtained by the classical lifting line theory. However, Eppler does not extend its study to the interaction between multiple lifting surfaces.

- Mason (ref. 29) uses two different wake models on a close-couple slightly-staggered canard-wing fighter configuration and observes that the vortex roll-up can locally influence the induced velocities by an order of 10-20%. However, he concludes that vortex roll-up is not a critical element in the design process because the downwash fields are not very different for the two wake models, and the calculated value of the drag only varies by a few percent. This agrees with Kroo and Eppler's results.

5.3   **Influence of the Mach Number on the Pressure and Induced Drag Coefficients**

In order to investigate the influence of the Mach number on the induced drag and pressure drag computations, FANSC Euler simulations were performed for the DLR-F4 wing-body configuration at Mach numbers varying from 0.10 to 0.85. FANSC's induced drag module was used to compute the induced drag coefficients. Pressure drag coefficients were also plotted to show that Mach numbers between 0.30 and 0.60 resulted in CDp values that can be assumed safe to compute the Oswald efficiency factor. However, these results are valid for the DLR-F4 configuration. At Mach = 0.60, it could be possible to observe shockwaves on a different aircraft design. What's important to remember from this test is that lower Mach number in Euler solutions does not influence the Oswald factor calculation.
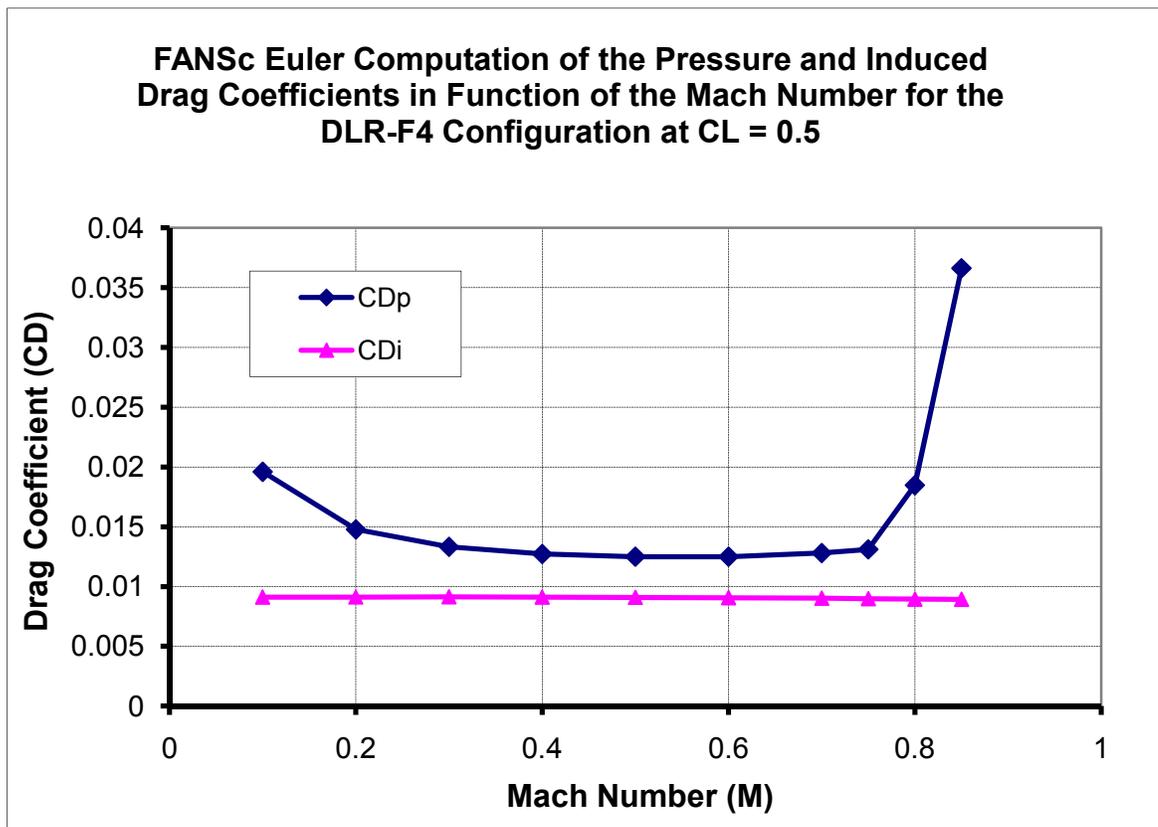
Figure 5.1 Pressure and Induced Drag Coefficients in Function of Mach Number

5.4 **Influence of the Number of An Coefficients on Induced Drag Calculation**

It has been mentioned several times in this research that the number of An Fourier coefficients play a significant role in the quality of the curve-fitting and the precision of the ideal lift distribution shape. If too few An factors are used, the shape of the minimum drag spanload is poorly represented (see figure 3.19) and the induced drag calculation of an input spanload looses accuracy. The more An factors are used, the more accurate the curve-fitting is, resulting in better drag calculation precision. However, if too many An coefficients are used, the curve-fitting loses its robustness and divergence of the drag result is observed. The following figure shows that induced drag results are robust between 12 and 17 An Fourier coefficients. Therefore, 15 coefficients were used throughout this work, since it seems to be a good compromise between accuracy and robustness. In the following figure, diverging results are not showed since they would exceed by far the graphic limits.
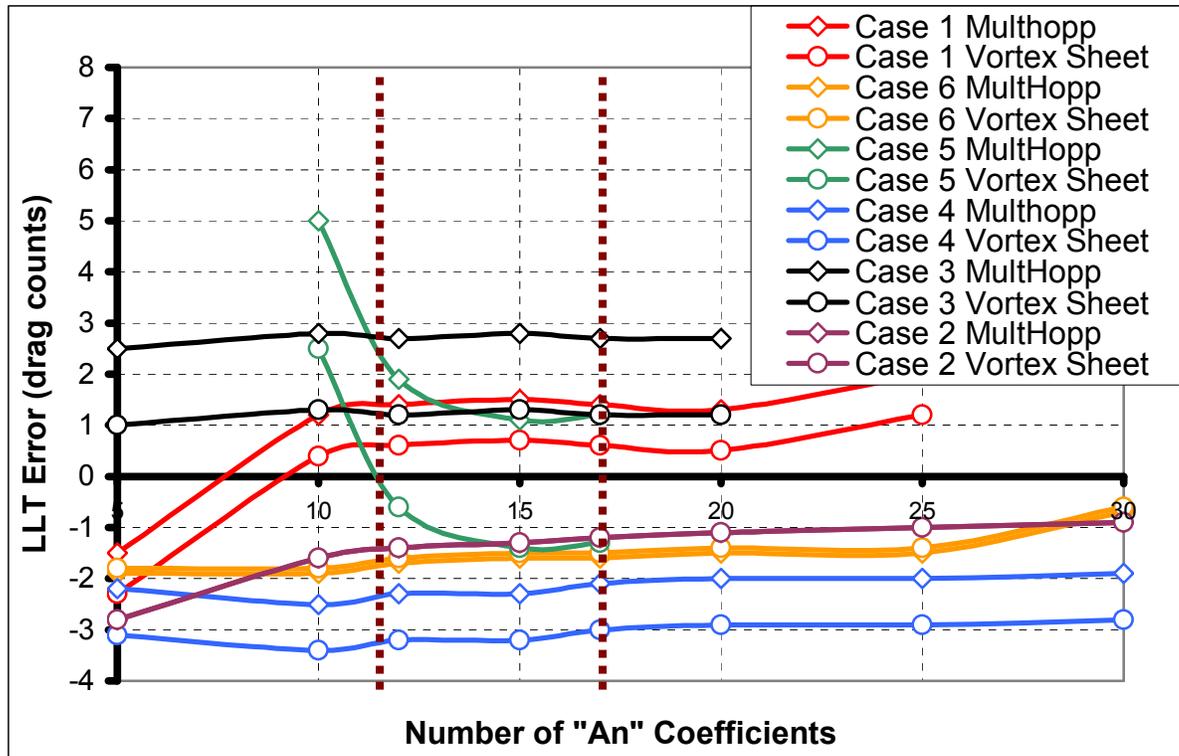
Figure 5.2 Influence of the Number of An Fourier Factors on LLT Accuracy

5.5   Influence of the CL and CDp Errors on Induced Drag Calculation

The following figure is a copy of Figure 4.9 with two added data sources: one representing a CL error of +0.0001 and the other one a CDp error of +1 drag count. The sensitivity of the Oswald factor to such error is barely visible on the figure. Therefore, in order to induce a significant error on the induced drag results, the CL error from the curve-fitting or the CDp error from Euler CFD results would have to be quite significant. On the six test cases used before for validation, the average curve-fitting induced error on the CL is on the order of 0.002, which results in a CDi error varying between more or less 1 drag count, changing from one case to another. For the CDp, the Euler solution seems to be consistent with Navier-Stokes solutions for cruise lift coefficients as shown on Figure 4.3, considering attached flow.
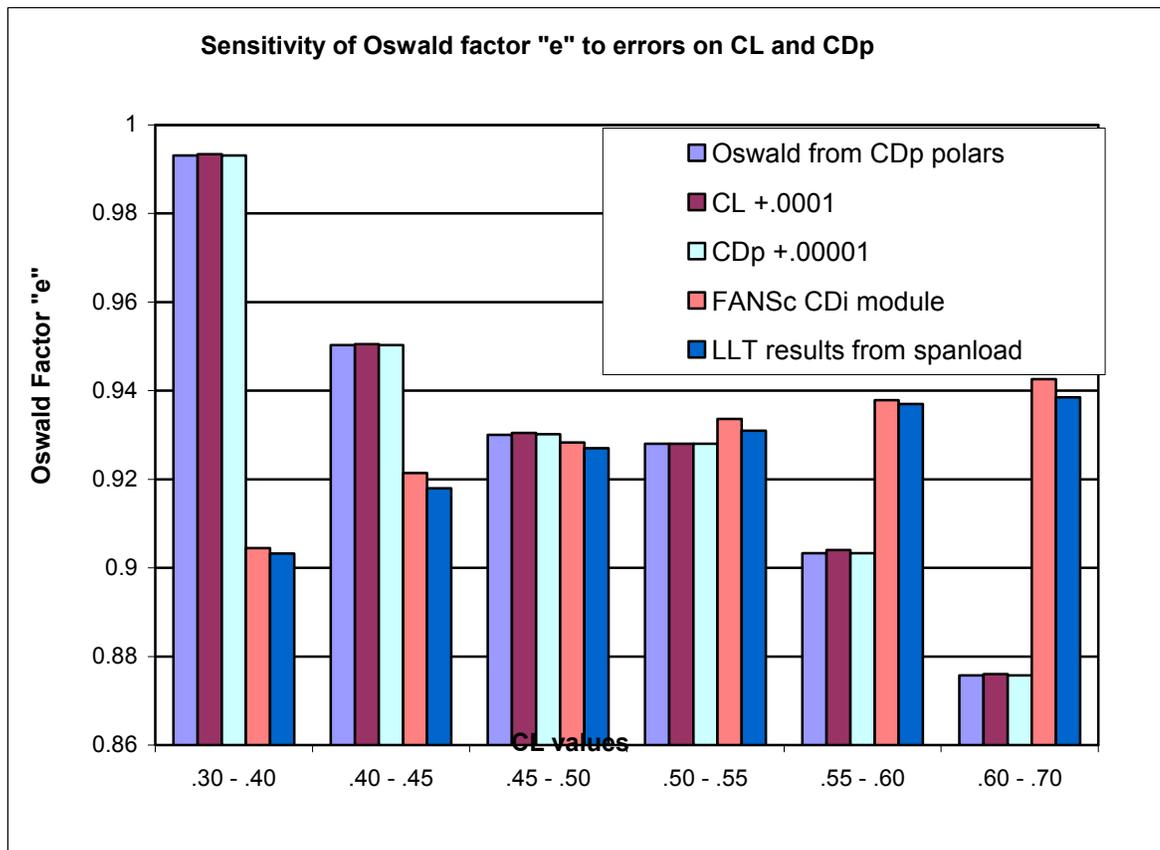
Figure 5.3 Sensitivity of the Oswald Factor to CL and CDp Errors

5.6   Potential Major Error Related to Fuselage Drag Correction

The Case 5 test spanload is particular in its shape: it has a very steep lift increase close to the fuselage. Since a sharp variation of the spanload profile will have high values of $(\partial\Gamma/\partial y)\,dy$ this particular region of the Case 5 wing generates a large amount of lift, lift variation, and therefore a large amount of induced drag according to the lifting-line theory. However, most of this drag is removed when the fuselage correction is applied. What happens with the minimum induced drag calculation for this case is that its spanload shape mostly follows an elliptical profile, resulting in a much smaller lift coefficient close to the fuselage. The application of the fuselage drag correction therefore results in a small drag removal for the ideal spanload. Looking at the overall situation, it seems that the fuselage drag correction removes so much drag to the Case 5 wing that its total induced drag is smaller than the one obtained from the ideal spanload for the same lift coefficient. Of course, if the fuselage drag correction is not applied to the drag calculation, this nonsense situation does not occur. This might show a potential flaw in the actual fuselage correction methodology. LLT has an option that allows the user to activate or deactivate the fuselage drag correction functionnality.

It can be concluded that for for certain shapes of spanload distribution, the fuselage induced drag correction might not be applicable when the circulation gradiant is very large in proximity of the fuselage. Yet, such ambiguity in the fuselage drag correction could be corrected by CFD, by including additional correction factors for special spanload cases. More research could be made on this fuselage induced drag correction. A good support to this statement is supported by a simple question: how could such method be applied to a blended-wing-body design?

CONCLUSION

Throughout this research about the induced drag calculation of multiple lifting surfaces aircrafts, it has been shown that a lifting line approach can give accurate drag results for a wing-body-winglet configuration. However, a complete validation of the induced drag of multiple lifting surfaces could not be achieved since proper comparative data was not available according to author's knowledge and resources. Nevertheless, it remains interesting to see how a 90 year old theory, once properly corrected, can achieve results similar to the ones obtained from today's CFD tools. Several conclusions can be obtained from this work:

1. The lifting line theory can be used to obtain proper calculation of the induced drag of a wing-body-winglet aircraft configuration within more or less 2 drag counts of precision over other methods. Such precision is achievable for realistic aircraft configurations with dihedral and fuselage, even if the methodology is planar and does not account for vortex roll-up, as long as a proper correction is imposed over the fuselage region;

2. The fuselage drag correction approach used in this research seemed to work properly and allows for suitable induced drag calculation for standard spanload distributions. However, when the spanloading shows a steep lift increase near the fuselage, the validity of the correction methodology is questionable;

3. The approach to obtaining Oswald efficiency factor from Euler CFD results shows good results when the flow is attached over the aircraft. Such methodology can therefore be considered an interesting approach for further work on induced drag since it allows for much simpler CFD solutions to be used as validation sources;

4. When using curve-fitting of Fourier series to represent a lift distribution over a wing, one should consider using 15 "An" Fourier coefficients (up to A_{15}) to insure fit robustness while conserving results accuracy. Special care must be taken to properly assess the wingtip region distribution since it has been shown to cause major problems in the implementation;

5. Laurendeau's equations to determine the minimum induced drag lift distribution over the wing shows to be robust as long as certain constraints are respected by the user;

6. The minimum induced drag spanload distribution over the wing is properly obtained according to Laurendeau's methodology, though it does not represent a realistic spanloading for a multi-disciplinary optimized wing design;

7. A software like LLT can give a designer a preliminary induced drag calculation of a new design without the need and cost of extensive CFD solutions. However, the complete induced drag results of two and three lifting surfaces configurations have not been validated in this work.

It is the author's belief that an interesting research project could be made using the software developed in this work. First, an in-depth validation of the induced drag of multiple lifting surfaces aircraft configuration is still required to insure the validity of LLT's results. Such validation could be made by running Euler simulations on various 2 and 3 lifting surfaces designs. The Oswald efficiency factor could then be obtained using the methodology presented in chapter 4.4.

Once validated, it could be interesting to integrate a correction factor to Laurendeau's methodology so that the minimum induced drag lift distribution obtained from LLT resembles more to the ones used on real aircrafts. To achieve this, a possible approach could be to modify the A_3 Fourier coefficient of the lift distribution in order to remove some lift near the tip region and add some closer to the fuselage. It would be interesting to study the induced drag of 2 and 3 lifting surfaces configurations using more triangular spanloading over the wing. Adding a third lifting surface to a conventional design could allow removing some load at the wing root, giving new opportunities to the designers. As the cost of fuel increases, designers have to explore several new design ideas to reduce drag and fuel consumption; this might just be one of them. With the current aerospace workforce aging rapidly and gradually passing-on the knowledge to a new generation of engineers, it seems more and more important to teach young designers to keep an open mind about these potential new solutions.

ANNEXE I

LLT OUTPUTS FOR CASE 6 WING-BODY-WINGLET-TAIL AIRCRAFT

****

LLT: INDUCED DRAG ANALYSIS

****

Written by Antoine Moreau

Advanced Aerodynamics Dept.

May 2008

AIRCRAFT CONFIGURATION SUMMARY (FRACTIONS OF WING SPAN)

			WING	CANARD	STAB.
SURFACE CONSIDERED?			----	NO	YES
FLOATING?			----	NO	NO
SPAN	b	=	----	0.000	Confidential
HEIGHT FROM WING	WL	=	----	----	Confidential

REALSPAN / REFSPAN :   bs/b   =   Confidential

INPUT SPANLOAD :   case6.spanload

LIFT COEFFICIENTS (BASED ON RFAREA)

TOTAL LIFT COEFFICIENT	CLTOT	=	Confidential
CANARD LIFT COEFFICIENT	CLC	=	Confidential
WING-BODY LIFT COEFFICIENT	CLWB	=	Confidential
STABILIZER LIFT COEFFICIENT	CLS	=	Confidential
CFD BODY LIFT COEFFICIENT	CLBOD	=	Confidential

INDUCED DRAG COEFFICIENTS (BASED ON RFAREA)

			INPUT	IDEAL
TOTAL CDI (LIFTING LINE THEORY)	CDIND	=	Confidential	Confidential
OSWALD FACTOR (BASED ON REF. AR)	e	=	Confidential	Confidential
CANARD CDI	CDINDC	=	Confidential	Confidential
WING-WINGLET CDI	CDINDW	=	Confidential	Confidential
STABILIZER CDI	CDINDS	=	Confidential	Confidential
BODY CDI (CORRECTED)	CDINDB	=	Confidential	Confidential
CORRECTION FOR BODY CDI	DCDINDB	=	Confidential	Confidential
CANARD-WING MUTUAL DRAG	CDINDCW	=	Confidential	Confidential
WING-STABILIZER MUTUAL DRAG	CDINDCW	=	Confidential	Confidential
CANARD-STABILIZER MUTUAL DRAG	CDINDCW	=	Confidential	Confidential

INPUT SPANLOAD An			IDEAL SPANLOAD An		
A1	=	Confidential	A1	=	Confidential
A3	=	Confidential	A3	=	Confidential
A5	=	Confidential	A5	=	Confidential
A7	=	Confidential	A7	=	Confidential
A9	=	Confidential	A9	=	Confidential
A11	=	Confidential	A11	=	Confidential
A13	=	Confidential	A13	=	Confidential
A15	=	Confidential	A15	=	Confidential

BIBLIOGRAPHY

1

Torenbeek, E. 2005. «Introductory Overview of Innovative Civil Transport Aircraft Configurations ». von Karman Institute for Fluid Dynamics, Lecture Series 2005-2006, June, 12 p.

2

McMasters, J.H. 2005. «A U.S. Perspective on Future Commercial Airliner Design». von Karman Institute for Fluid Dynamics, Lecture Series 2005-2006, June, 50 p.

3

Richter, H. and S. Menczykalski. 2005. «Civil Propulsion of the Future». von Karman Institute for Fluid Dynamics, Lecture Series 2005-2006, June, 38 p.

4

Green, J.E. 2005. «Greener by Design». von Karman Institute for Fluid Dynamics, Lecture Series 2005-2006, June, 50 p.

5

Slingerland, R. 2005. «Aircraft With LH2 Propulsion». von Karman Institute for Fluid Dynamics, Lecture Series 2005-2006, June, 47 p.

6

Liebeck, R.H. 2005. «Design of the Blended-Wing-Body Subsonic Transport». von Karman Institute for Fluid Dynamics, Lecture Series 2005-2006, June, 28 p.

7

Martinez-Val, R. and E. Pérez. 2005. «Medium Size Flying Wings». von Karman Institute for Fluid Dynamics, Lecture Series 2005-2006, June, 71 p.

8

Bolsunovski, A.L., N.P. Buzoverya, B.I. Gurevich, V.E. Denisov and O.V. Sonin. 2005. «Flying Wing- Problems and Decisions». von Karman Institute for Fluid Dynamics, Lecture Series 2005-2006, June, 15 p.

9

Frediani, A. 2005. «The Prandtl Wing». von Karman Institute for Fluid Dynamics, Lecture Series 2005-2006, June, 23 p.

10

Kroo, I. 2005. «Nonplanar Wing Concepts for Increased Aircraft Efficiency». von Karman Institute for Fluid Dynamics, Lecture Series 2005-2006, June, 29 p.

11

Sacco, G. and C. Lanari. 2005. «The Three Lifting Surface Configuration Concept and Lessons Learned From the Piaggio P180». von Karman Institute for Fluid Dynamics, Lecture Series 2005-2006, June, 40 p.

12

Friend, M.G. and C.P. Nelson. 2005. «From Concept to Market Reality : A Case Study of the Sonic Cruiser». von Karman Institute for Fluid Dynamics, Lecture Series 2005-2006, June, 9p.

13

Aronstein, D.C. 2005. «Supersonic Business Jets and Sonic Boom Reduction». von Karman Institute for Fluid Dynamics, Lecture Series 2005-2006, June, 44 p.

14

Cicalè, M., E. Bianchi, C. Monteggia, A. Saporiti and A. Campanile. 2005. «The ERICA Tiltrotor Concept». von Karman Institute for Fluid Dynamics, Lecture Series 2005-2006, June, 47 p.

15

Kroo, I. 2005. «Unconventional Configurations for Efficient Supersonic Flight». von Karman Institute for Fluid Dynamics, Lecture Series 2005-2006, June, 25 p.

16

Frota, J. and Y. Vigneron. 2005. «Airbus Future Projects Approach to New Aircraft Concepts and R & T». von Karman Institute for Fluid Dynamics, Lecture Series 2005-2006, June, 22 p.

17

Argüelles, P., M. Bischoff, P. Busquin, B.A.C. Droste, Sir Richard Evans, W. Kröll, J-L.Lagardère, A. Lina, J. Lumsden, D. Ranque, S. Rasmussen, P. Reutlinger, Sir Ralph Robins, H. Terho and A. Wittlöv. 2001. «European Aeronautics: A Vision for 2020». Report of the Group of Personalities, ISBN 92-894-0559-7, January, 28 p.

18

Kroo, I. and S.C. Smith. 1990. «The Computation of Induced Drag with Nonplanar and Deformed Wakes ». SAE Technical Paper Series, SAE 901933, 9 p.

19

Eppler, R. and S. Schmid-Göller. 1989. «A Method to Calculate the Influence of Vortex Roll-Up on the Induced Drag of Wings». Notes on Numerical Fluid Mechanics, Vol. 25, Vieweg Verlag, 14 p.

20

Ostowari, C. and D. Naik. 1986. «An Experimental Study of the Lift, Drag and Static Longitudinal Stability for a Three Lifting Surfaces Configuration». AIAA paper 1986-398, January, 12 p.

21

Strohmeyer, D., R. Seubert, W. Heinze, C. Oersterheld and L. Fornasier. 2000. «Three Surface Aircraft – A Concept for Future Transport Aircraft». AIAA paper 2000-566, January, 12 p.

22

Rhodes, M.D. and B.P. Selberg. 1984. «Benefits of dual wings over single wings for high-performance business airplanes». Journal of Aircraft, Vol.21, noº2, p.116-127.

23

Rokhsaz, K. and B.P. Selberg. 1989. «Three-Surface Aircraft – Optimum vs Typical». Journal of Aircraft, vol.26, noº8 (August), p.699-704.

24

Selberg, B.P. and K. Rokhsaz. 1986. «Aerodynamic Tradeoff of Conventional, Canard and Trisurface Aircraft Systems», Journal of Aircraft, Vol.23, noº10 (October), p.768-774.

25

Kroo, I.M. and T. McGeer. 1983. «A Fundamental Comparison of Canard and Conventional Configurations». Journal of Aircraft, Vol. 20, noº11 (November), p.983-992.

26

Kroo, I.M. 1982. «Minimum Induced Drag of Canard Configurations». Journal of Aircraft, Vol.19, noº9 (September), p.792-794.

27

Kendall, E.R. 1985. «The Theoretical Minimum Induced Drag of Three Surfaces Airplanes in Trim». Journal of Aircraft, Vol. 22 (October), 8 p.

28

Laitone, E.V. 1980. « Prandtl's Biplane Theory Applied to Canard and Tandem Aircraft ». Journal of Aircraft, Vol. 17 (April), 5 p.

29

Mason, W.H. 1982. «Wing-Canard Aerodynamics at Transonic Speeds--Fundamental Considerations on Minimum Drag Spanloads». AIAA 20th Aerospace Sciences Meeting, Orlando (Florida), AIAA paper 82-0097, January 11-14, 9 p.

30

Kendall, E.R. 1984. «The Aerodynamics of Three-Surface Airplanes». AIAA paper 1984-2508, 7 p.

31

Wakayama, S. and I.M. Kroo. 1990. «A Method for Lifting Surface Design Using Nonlinear Optimization», AIAA paper 1990-3290, September, 10 p.

32

Kroo, I. 1984. «A General Approach to Multiple Lifting Surfaces and Analysis», AIAA paper 1984-2507, 7 p.

33

Laitone, E.V. 1978. «Positive Tail Loads for Minimum Induced Drag of Subsonic Aircraft». Journal of Aircraft, Vol.15, noº12 (December), p.837-842.

34

Lundry, J.L. 1967. «Minimum Swept-Wing induced Drag with Constraints on Lift and Pitching Moment». Journal of Aircraft, Vol.4, noº1 (January), p.73-74.

35

Bowers, A.H. 2006. «On the Minimum Induced Drag of Wings». Slides of the conference presented at the Soaring Valley Soaring Club, January 21st, 28 p.

36

Wakayama, S. and I. Kroo. 1994. «Subsonic Wing Design Using Multidisciplinary Optimization». Proceedings of the 5th AIAA/USAF/NASA/ISSMO Symposium on Multidisciplinary Analysis and Optimization , AIAA paper 1994-4409, September, 11 p.

37

Jing, S. Z. Binqian and Y. Guangjun. «Concept Investigation of "W" Tailless Configuration». AIAA paper 2005-4602, 8 p.

38

Binqian, Z. and B. Laschka. 2002. «Several Ways to Control the Flow Separation at the Root Part of Forward-Swept Wing (FSW)». Aerodynamik Technische University Muenchen, A3-51-56.

39

Rhodes, M.D. and B.P. Selberg. 1982. «Dual Wing, Swept Forward Swept Rearward Wing, and Single Wing Design Optimization for High Performance Business Airplanes». ICAS-82-1.4.2, 16 p.

40

Van Dam, C.P. 1987. «Induced Drag Characteristics of Crescent-Moon Shaped-Wings». Journal of Aircraft, Vol. 24, noº2, 5 p.

41

Jong, T. and R. Slingerland. 2003. «Analysis of the Twin-Fuselage Configuration and its H-Cabin Derivative». AIAA's 3rd Annual Aviation Technology, Integration, and Operations (ATIO) Forum, AIAA paper 2003-6811, Denver, Colorado, November 17-19, 10 p.

42

Hamel, P. G. 2005. «Birth of Sweepback: Related Research at Luftfahrtforschungsanstalt - Germany». Journal of Aircraft, Vol. 42, noº4 (July), 13 p.

43

Lombardi, G., M.V. Salvetti and A. Talamelli. 1997. «Shock-Wave/Boundary-Layer Interaction in Transonic Flow Around a Forward-Swept Wing». AIAA paper 1997-1838, 10 p.

44

Haftka, R.T., B. Grossman, P.J. Kao, D.M. Polen and J.S. Sobieski. 2001. «Integrated Aerodynamic-Structural Design of a Forward-Swept Transport Wing». Slides of a Presentation to Virginia Polytechnic Institute (March), 19 p.

45

Redeker, G. and G. Wichmann. 1988. «Forward Sweep – A Favorable Concept for a Laminar Flow Wing». AIAA paper 88-4418, 11p.

46

Smith, P.R. and A.J. Srokowski. 1983. «High Aspect Ratio Forward Sweep for Transport Aircraft». AIAA paper 1983-1832, 16p.

47

Krone Jr, N.J. 1980. «Forward Swept Wing Design». Proceedings, AIAA paper 1980-3047, 3p.

48

Uhuad, G.C., T.M. Weeks and R. Large. 1983. «Wind Tunnel Investigation of the Transonic Characteristics of a Forward Swept Wing». Journal of Aircraft, Vol.20, noº3, p.195-202.

49

Palmer, R. 1994. « Techno-Economic Requirement for Composite Aircraft Components ». Douglas Aircraft Company's Internal Document, 36 p.

50
AGARD. 1994. « A Selection of Experimental Test Cases for the Validation of CFD Tools », AGARD-AR-303, Vol.2, 24 p.

51
McMaster, J.H. and R.M. Cummings. 2004. «From Farther, Faster Higher to Leaner, Meaner, Greener – Further Directions in Airplane Design». Journal of Aircraft, Vol.41, noº1 (January), p.51-61.

52
McMaster, J.H. and R.M. Cummings. 2002. «Airplane Design – Past, Present and Future». Journal of Aircraft, Vol.39, noº1 (January), p.10-17.

53
Stengel, R. 2006. «Evolution of Transport Aircraft – 1970s to Tomorrow». MAE 331, 4 p.

54
McMaster, J.H. 2005. «Reflections on the Future of Aeronautics – An Early 21st Century Perspective». AIAA paper 2005-0004 (January), 23 p.

55
Diez M. and U. Iemma. 2007. «Robust Optimization of Aircraft Life-Cycle Costs Including the Cost of Community Noise». AIAA paper 2007-3668, 8 p.

56
Brodersen, O., M. Rakowitz, S. Amant, P. Larrieu, D. Destarac and M. Sutcliffe. 2005. «Airbus, ONERA, and DLR Results from the Second AIAA Drag Prediction Workshop». Journal of Aircraft, Vol. 42, noº4 (July), 9 p.

57
Piperni, P., M. Abdo and F. Kafyeke. 2007. «Preliminary Aerostructural Optimization of a Large Business Jet». Journal of Aircraft, Vol. 44, noº5 (September), 17 p.

58
Sitaraman, J. and J.D. Baeder. 2004. «Computational-Fluid-Dynamics-Based Enhanced Indicial Aerodynamic Models». Journal of Aircraft, Vol.41, noº4 (July), 13 p.

59
Gebbie, D.A., M.F. Reeder, C. Tyler, V. Fonov and J. Crafton. 2007. «Lift and Drag Characteristics of a Blended-Wing Body Aircraft». Journal of Aircraft, Vol.44, noº5 (September), 13 p.

60

Grasmeyer, J. 1997. «A Discrete Vortex Method for Calculating the Minimum Induced Drag and Optimum Load Distribution for Aircraft Configurations with Noncoplanar Surfaces». Virginia Polytechnic Institute, VPI-AOE-242 (January), 39 p.

61

Lamar, J.E. 1976. «Minimum Trim Drag Design for Interfering Lifting Surfaces Using Vortex-Lattice Methodology». NASA Langley Research Center, 23 p.

62

Smith, S.C. and I. Kroo. 1990. «A Closer Look at the Induced Drag Characteristics of Crescent-Shaped Wings». AIAA paper 90-3063 (August), 10 p.

63

Xueqiang, L., L. Qui, C. Jianzhong and W. Yizhao. 2007. «Aerodynamic Characteristic Research for Box-Wing Aircraft». Journal of Nanjing University of Aeronautics & Astronautics, Vol.39, noº6 (December), 4 p.

64

Lombardi, G. 1993. «Experimental Study on the Aerodynamic Effect of a Forward Sweep Angle». Journal of Aircraft, Vol. 30, noº5 (September), 7 p.

65

Klein, Armin, Viswanathan and Sathy. 1975. «Approximate Solution for Minimum Induced Drag of Wings with a Given Structural Weight». Journal of Aircraft, Vol.12, noº2 (February), 3 p.

66

Butler, G.F. 1983. «An Analytical Study of the Induced Drag of Canard-Wing-Tail Aircraft Configurations with Various Level of Static Stability». Aeronautical Journal of the Royal Aeronautical Society (October), 8 p.

67

Binqian, Z. and B. Laschka. 1993. «Effect of Canard Wing Positions on Aerodynamic Characteristics of Swept-Forward Wing». Foreign Aerospace and Technology Center, AD-A262 373 (March), 14 p.

68

Lange, R.H., J.F. Cahill, E.S. Bradley, R.R. Eudaily, C.M. Jenness and D.G. MacWilkinson. 1974. «Feasibility Study of the Transonic Biplane Concept for Transport Aircraft Application». NASA-CR-132462, 128 p.

69

Joslin, R.D. 1998. «Aircraft Laminar Flow Control». Annual Review of Fluid Mechanics, Vol.30, Annual Reviews Inc., Palo Alto, California, 29 p.

70

Binqian, Z. and B. Laschka. 1989. «On Forward-Swept Wing's Aerodynamic Characteristics». Northwestern Polytechnical University, Vol.7 (July), 8 p.

71

Burns, B.R.A. 1983. «Were the Wrights right?». Air Int., Vol.25, noº6 (December), 11 p.

72

Löbert, G. 1981. «Spanwise Lift Distribution of Forward and Aft-Swept Wings in Comparison to the Optimum Distribution Form». Journal of Aircraft, Vol.18 (June), 3 p.

73

Sliwa, S.M. 1980. «Impact of Longitudinal Flying Qualities Upon the Design of a Transport with Active Controls». AIAA paper 80-1570, 9 p.

74

McMasters, J.H. and R.M. Cummings. 2002. «Airplane Design as a Social Activity: Emerging Trends in the Aerospace Industry». AIAA paper 2002-0516 (January), 23 p.

75

Hertel, J. and M. Albers. 1993. «The Impact of Engine and Aircraft Design Interrelations on DOC and its Application to Engine Design Optimization». AIAA paper 93-3930, 7 p.

76

Torenbeek, E. 1991. «Aerodynamic Performance of Wing-Body Configurations and the Flying Wing». SAE General, Corporate, and Regional Aviation Meeting and Exposition, SAE Paper 911019, Wichita, Kensas (April), 6 p.

77

Jobe, C.E., R.M. Kulfan and J.D. Vachal. 1978. «Wing Planforms for Large Military Transports», AIAA paper 1978-1470 (August), 16 p.

78

Walters, R.W. 2006. «Challenges of Uncertainty Quantification for Computational Aerodynamic Applications». Slides of the presentation at NCSU ACE Workshop, May 31 – June 1, 17 p.

79

Liebeck, R. 2001. «Design of Blended-Wing-Body Subsonic Transport». Journal of Aircraft, Vol.41, noº1, 16 p.

80
Li, G.L., G.W. Li and J. Li. 2006. «Aerodynamics Investigation of the Joined-Wing Configuration». Kong Di Dong Li Xue Xue Bao, Vol.24, noº4, 7 p.

81
Gallman, J. 1996. «Structural Optimization for Joined-Wing Synthesis». Journal of Aircraft, Vol. 33, noº1, 10 p.

82
Feistal, T.W., V.R. Corsiglia and D.B. Levin. 1981. «Wind-Tunnel Measurements of Wing-Canard Interference and a Comparison with Various Theories». SAE Technical Paper 810575, 14 p.

83
Laurendeau, E. and J. Boudreau. 2001. «DLR-F4 Results using Bombardier Aerospace Full-Aircraft Navier-Stokes Code FANSC». Slides of the presentation at AIAA 1st Drag Prediction Workshop, Anaheim, Califirnia, June 9-10, 10 p.

84
Cheng, H.K. 1981. «Transonic Aerodynamics of Forward Swept Wings Analyzed as a Lifting-Line Problem», Journal of Applied Mathematics and Physics (ZAMP), Vol.32, 7 p.

85
Owens, D.B. 1998. «Weissinger's Model of the Nonlinear Lifting-Line Method for Aircraft Design». AIAA paper 1998-0597, 10 p.

86
Funk, J.D. and B.W. McCormick. 1991. «Simulation of Stall Departure Using a Nonlinear Lifting Line Model». AIAA paper 1991-0340, 10 p.

87
Ariyur, K.B. 2005. «Prediction of Dynamic Ground Effect Through Modified Lifting Line Theory». AIAA paper 2005-4610, 14 p.

88
Chi, X., B. Williams, R.E. Kreeger, R.G. Hindman and T.I.P. Shih. 2007. «Simulation of Finite Wings with 2-D and 3-D Ice Shapes: Modern Lifting-Line Theory versus 3-D CFD». AIAA paper 2007-504, 5 p.

89
Prandtl, L. 1921. «Application of Modern Hydrodynamics to Aeronautics». NACA TR 116, 59 p.

90

Sliwa, S.M. 1980. «Economic Evaluation of Flying Qualities Design Criteria for a Transport Configured with Relaxed Static Stability». NASA TP 1760, 27 p.

91

Sivells, J.C. and R.H. Neely. 1947. «Method of Calculating Wing Characteristics by Lifting-Line Theory Using Nonlinear Section Lift Data». NACA TN 1269, 20 p.

92

Prandtl, L. 1924. «Induced Drag of Multiplanes». NACA TN 182 (March), 22 p.

93

Munk, M.M. 1923. «The Minimum Induced Drag of Aerofoils». NACA TR 121, 16 p.

94

McCormack, G.M. and W.L. Cook. 1949. «A Study of Stall Phenomena on a 45º Swept-Forward Wing». NACA TN-1797 (January), 32 p.

95

Whitcomb, R.T. 1976. «A Design Approach and Selected Wind-Tunnel Results at High Subsonic Speeds for Wing-Tip Mounted Winglets». NACA TN D-8260 (July), 30 p.

96

Turriziani, R.V., W.A. Lovell, G.L. Martin, J.E. Price, E.E. Swanson and G.J. Washburn. 1980. «Preliminary Design Characteristics of a Subsonic Business Jet Concept Employing an Aspect Ratio 25 Strut-Braced Wing». NASA CR-159361 (October), 99 p.

97

Smith, P.M., J. DeYoung, W.A. Lovell, J.E. Price and G.F. Washburn. 1981. «A Study of High-Altitude Manned Research Aircraft Employing Strut-Braced Wings of High-Aspect Ratio». NASA CR-159262 (February), 91 p.

98

Diederich, F.W. and B. Budiansky. 1965. «Divergence of Swept Wings». NACA Report 1680 (August), 32 p.

99

Blackwell, J. A. Jr. 1976. «Numerical Method to Calculate the Induced Drag or Optimum Loading for Arbitrary Non-Planar Aircraft». NASA SP-405 N76-28167 (May), 22 p.

100
Munk, M.M. 1922. «General Biplane Theory». NACA Report 151, 48 p.

101
Jones, R.T. 1950. «The Spanwise Distribution of Lift for Minimum Induced Drag of Wings Having a Given Lift and a Given Bending Moment». NACA TN-2249 (December), 14 p.

102
Henderson, W.P. and J.K. Huffman. 1975. «Aerodynamic Characteristics of a Tandem Wing Configuration at a Mach Number of 0.30». NASA TM X-72779 (October), 11 p.

103
Jones, R.T. and T.A. Lasinski. 1980. «Effect of Winglets on the Induced Drag of Ideal Wing Shapes». NACA TM-81230 (September), 27 p.

104
Johnsson, Y., Private communication, Bombardier Aerospace inc., February 2007.

105
Laurendeau, E., Private communication, Bombardier Aerospace inc., February 2008.

106
Confidential

107
http://www.lissys.demon.co.uk/

108
Laurendeau, E. 1990. «Traînée Induite de Configurations d'Avions». École Nationale Supérieure de l'Aéronautique et de l'Espace (ENSAE), Toulouse, France (September), 109 p.

109
Iglesias, S. and W.H. Mason. 2001. «Optimum Spanloads Incorporating Wing Structural Weight». AIAA-2001-5234, Virginia Polytechnic Institute and State University, Blackburg, Virginia (October), 19p.

110
Anderson, J.D. 2006. «Fundamentals of Aerodynamics». McGraw-Hill, 4th edition, 1008 p.

111
Bertin, J.J. 2001. «Aerodynamics for Engineers». Prentice Hall, 4th edition, 600 p.

112
von Kármán, T. and J.M. Burgers. 1963. « General Aerodynamic Theory – Perfect Fluids ». Vol.2 of Aerodynamic Theory, Edited by W.F. Durand, Dover Edition, New York.

114
Multhopp, B 1942. « Aerodynamics of the Fuselage ». NACA TM-1036.

115
Jacobs, E.N. and K.E. Ward. 1935. «Interference of Wing and Fuselage from Tests of 209 Combinations in the N.A.C.A. Variable-Density Tunnel». NACA Report no.540.